Connectivity Based Characterization of Brain Function in Humans and Dogs

by

Sinan Zhao

A dissertation submitted to the Graduate Faculty of
Auburn University
in partial fulfillment of the
requirements for the Degree of
Doctor of Philosophy

Auburn, Alabama
December 16, 2017

Keywords: Functional MRI, Connectivity analysis, Awake animal imaging

Approved by

Gopikrishna Deshpande, Chair, Associate Professor of Electrical and Computer Engineering
Thomas Denney, Professor of Electrical and Computer Engineering
Jeffrey Katz, Alumni Professor of Psychology
Jennifer Robinson, Assistant Professor of Psychology

Abstract

Functional magnetic resonance imaging (fMRI) has been widely used to infer brain function in both healthy and clinical populations. Here, we propose novel approaches for connectivity based characterization in both humans and dogs. In humans, these approaches have been applied for characterizing brain network alterations in Alzheimer's disease (AD) patients. AD, which affects millions of elderly worldwide, is a neurodegenerative disorder with a long pre-morbid period such as mild cognitive impairment (MCI). Brain declines, both functional and structural, are inevitable with age. However, determining how and when the trajectories begin to deviate from healthy elderly individuals is a crucial step to effectively slow down the progression of the disease.

Using resting-state fMRI, we first estimated Betweenness Centrality (BC) and a novel nodal characterization approach called Middlemen Power (MP) from directed network that characterize information flow. The directed network were derived from the following populations: Normal Control (NC), Early MCI (EMCI), Late MCI (LMCI) and AD. Our results demonstrate that MP detected more brain regions that progressively deteriorated from NC to EMCI to LMCI to AD, as compared to BC in directed networks. Also, BC did not identify a single node from undirected networks that significantly deteriorated. This demonstrates the MP may represent a more sensitive analytic tool for characterizing biomarkers in both directed and undirected networks.

Most connectivity analyses have reported distributed decreases as well as increases in causal relationships among brain regions in MCI and AD. However, it is difficult to interpret these connectivity results because traditionally, our knowledge of brain function is anchored on regions and not connections. Therefore, we employed a novel approach for identifying focal directed

connectivity deficits in AD compared to healthy controls. Two foci were identified, locus coeruleus (LC) in the brain stem and right orbitofrontal cortex (OFC). Corresponding disrupted connectivity network associated with the foci showed that the brainstem is the critical focus of disruption in AD. Our findings suggest that fMRI studies of AD, which have been largely cortico-centric, could in future investigate the role of brain stem in AD.

Functional brain connectivity based on resting state fMRI has been shown to be correlated with human personality and behavior. In the third study, we sought to know whether capabilities and traits in dogs can be predicted from their resting state connectivity as in humans. We trained awake dogs to keep their head still inside a 3T MRI scanner while resting state fMRI data was acquired. Canine behavior was characterized by an integrated behavioral score. Functional scans and behavioral measures were acquired at three different time points (TPs). We hypothesized that the correlation between resting state FC in the dog brain and behavior measures would significantly change during their detection training process (from TP1 to TP2), and would maintain for the subsequent several months of detection work (from TP2 to TP3). To further study the resting state FC features that can predict the success of training, dogs at TP1 were divided into successful group and failure group. We observed a core brain network which showed relatively stable (with respect to time) patterns of interaction that were significantly stronger in the successful group compared to failure group and whose connectivity strength at TP1 predicted whether a given dog was eventually successful in becoming a detector dog. A second flexible peripheral network was observed whose changes in connectivity strength with detection training tracked corresponding changes in behavior. Our findings suggest that upon replication and refinement, fMRI-based resting state brain connectivity may assist in choosing dogs that are more easily trainable for performing detection tasks.

Acknowledgments

I would like to express my sincere gratitude to my advisor, Dr. Gopikrishna Deshpande, for his exceptional support throughout my Ph.D. study, great patience in reviewing and editing manuscripts, and sparkling ideas in trouble shooting when I meet problems.

I would like to thank my committee members Dr. Thomas Denney, Dr. Jefferey Katz, Dr. Jennifer Robinson, and Dr. Paul Waggoner for their kind guidance and encouragement to me both as a student in their courses and outside of it.

For the DARPA project, I would like to thank Bhavitha Ramaiahgari, Pradyumna Lanka, Andie Thompkins and Lucia Lazarowski for cooperation and great help in performing the dog fMRI experiments and visual scoring. All the IK9 members for their great patience in dog training and cooperation for the MRI scan. I would also like to thank Dr. Ronald Beyers for his guidance in operating fMRI scans and trouble shooting.

Next, I would like to thank my friends in MRI center Wenjing Yan, Yun Wang, Tuo Shi, Xinyu Zhao, Bowen Yuan, Bonian Lu, Hao Zou, Yuan Bian, Ming Li, Chenxi Hu, Ranga Deshpande and Karthik Ramakrishnan for their great help, encouragement and for the time they spent working with me.

Finally, I would like to thank my parents, my sisters and my girlfriend for their constant love, encouragement and support. I couldn’t imagine how hard life would be without their support.

Table of Contents

List of Tables

List of Figures

List of Abbreviations

Aβ	Beta-amyloid
ACC	Anterior Cingulate Cortex
AD	Alzheimer's disease
ADNI	Alzheimer's Disease Neuroimaging Initiative
Amy	Amygdala
APP	Amyloid Precursor Protein
BC	Betweenness Centrality
BOLD	Blood Oxygenation Level Dependent
Caud	Caudate
CDR	Clinical Dementia Rating
CPGC	Correlation-purged Granger Causality
CPL	Characteristic Path Length
CT	Computed Tomography
DCM	Dynamic Causal Modeling
DEC	Dynamic Effective Connectivity
dlPFC	dorsolateral prefrontal cortex
DMN	Default Mode Network
DPARSF	Data Processing Assistant for Resting-State fMRI
dHB	Deoxygenated Hemoglobin
EC	Effective Connectivity
EEG	Electroencephalograph
EM	Expectation-Maximization
FAQ	Functional Assessment Questionnaire
FC	Functional Connectivity
FE	Free Energy
fMRI	Functional Magnetic Resonance Imaging
FOC	Frontal Orbital Cortex
FWHM	full width half maximum

FPR	False Positive Rate
GRAPPA	Generalized Autocalibrating Partially Parallel Acquisitions
HCP	Human Connectome Projection
Hippo	Hippocampus
HB	Oxygenated Hemoglobin
HRF	Hemodynamic response function
ICA	Independent Components Analysis
IFG	Inferior Frontal Gyrus
IPL	Inferior Parietal Lobule
LC	Locus Coeruleus
LOC	Lateral Occipital Cortex
MEG	Magneto Encephalogram
MFG	Middle Frontal Gyrus
MMSE	Mini-mental State Examination
MNI	Montreal Neurological Institute
MOG	Middle Occipital Gyrus
MP	Middleman Power
MRI	Magnetic Resonance Imaging
MVAR	Multivariate Autoregressive
MTG	Middle Temporal Gyrus
MVAR	Multivariate Autoregressive
NE	Norepinephrine
NPI-Q	Neuropsychiatric Inventory Questionnaire
OB	Olfactory Bulb
OFC	Orbitofrontal Cortex
PCC	Posterior Cingulate Cortex
PFC	Prefrontal Cortex
PHG	Parahippocampal gyrus
RN	Reward Network
ROC	Receiver Operating Characteristic
ROI	region of Interest

RS-fMRI	Resting state fMRI
SEC	Static Effective Connectivity
SFG	Superior Frontal Gyrus
SNR	signal-to-noise ratio
SPM	Statistical Parametric Mapping
TPs	Time Points
TPR	True Positive Rate
TR	Time of Repetition
vlPFC	ventrolateral prefrontal cortex
vmPFC	ventromedial prefrontal cortex

CHAPTER 1

Introduction

Of all the objects in the universe, the human brain is the most complex organ which is capable of storing and processing information from a myriad of sensory inputs, and yet it remains very much a mystery. Over the years, neuroscientists have strived to understand the complex brain structures and tried to decipher the brain's command of all its diverse functions. However, recent advances in magnetic resonance imaging (MRI) and functional MRI (fMRI) have led to great gains in our understanding of the brain and how it functions.

1.1 Magnetic Resonance imaging (MRI)

MRI is a non-invasive technique which uses strong magnetic field and electromagnetic waves to detect images of different structures in the body without the use of damaging radiation, and thus has been widely utilized in the area of radiology, disease diagnostics, treatment monitoring as well as in medical research [1]. An MRI scanner is a large magnet that generates a strong magnetic field that is thousands of times stronger than the natural magnetic field on the earth. By making use of the nuclear magnetic resonance property of elements in the body, the images can be obtained by the MR scanner [2]. Specifically, atomic number and the atomic weight are two characteristics that are of particular interest for MR, and these two determine the third property of an atom, namely its spin. In practice, ^{1}H isotope of hydrogen is the most common to study as hydrogen is found in

abundance in the tissues that are the target of magnetic resonance imaging, and is very sensitive to the magnetic field into which the body is placed for the purpose of imaging. When the subject lies in the scanner, the hydrogen atoms, in particular, have a tendency to line up in the direction of the magnetic field, with slightly more than half going parallel and the rest going anti-parallel creating a net magnetization in the direction parallel to the magnetic field. The gradient coil can generate a gradient magnetic field so that each location has its own resonance frequency. To acquire the MR image, an additional energy need to be injected into the system, in the form of radiofrequency (RF) pulses. When the RF pulse is at the right resonance frequency, the protons absorb the energy and jump from the low energy state to high energy state. The affected protons are aligned at a uniform angle, and "tipped" away from its orientation at equilibrium and towards the transverse plane that is orthogonal to the axis of the original field. When the RF pulse is turned off, the protons release the energy and gradually return to the original state realigning to the static field. The emitted energy that is released by the protons is detected in turn by radiofrequency coils in the MR scanner to obtain the raw data matrix. By using the gradients in different directions, it enables different k-space encoding of spatial information. The data are collected in Fourier space, known as k-space in MRI/fMRI literature [3]. By using an inverse Fourier transformation, k-space information can be transformed into image domain, and the spatial information can be recovered of the body that has been scanned. Once the RF pulse is turned off, the protons start to relax. The change in the MRI signal is called relaxation and can be classified into T1 and T2 relaxation. These relaxation time varied from different protons in the different tissues in the body thus can be utilized to construct images of different contrast. Images of different contrast can reflect different biological tissues which will be helpful in distinguishing interested tissues more clearly from surrounding areas and thus have various applications. With the advantage of good image quality and good

contrast between different tissues and comparatively high resolution, the MRI technique has earned broad prevalence in brain imaging, cardiac imaging, muscles over other medical imaging technique such as computed tomography (CT) and X-rays [4].

1.2 Functional magnetic resonance imaging (fMRI)

fMRI is now a primary technique to study the human brain, and the relevant pieces of literature are growing exponentially in recent years [5], [6]. The brain itself does not store glucose which is primary source of the energy. When the brain becomes active in response to a task or stimulus, the rate of blood flow to the regions that involved in the stimulus grows. The increase in the blood flow occurs because the brain requires oxygen to metabolize glucose, thus more oxygenated blood arrives in the relevant areas. The reason why magnetic resonance enters into this field is because blood contains iron in hemoglobin molecules, which is paramagnetic. A paramagnetic material has the property that when it is placed into a strong magnetic field, the atoms in the material align themselves with the field, thereby increasing the field strength. The magnetic properties of oxygenated and deoxygenated blood are different, oxygenated hemoglobin (HB) is diamagnetic while the deoxygenated hemoglobin (dHB) is paramagnetic. Since the changes in HB will cause changes in the local magnetic field applied to the body, this will affect the measured MR signal through the Blood Oxygenation Level Dependent (BOLD) contrast effect [7]. When neuron fires, the blood flow increases to bring more glucose and oxygen (HB) to replace dHB, the increase of the HB in the flow of blood in the vessels leads to MR (magnetic resonance) signal rise. In a word, neural activity and blood flow are coupled, the increase of neural activity brings more HB and less dHB and subsequently the increase of the MR signal. Consequently, the magnetic spin-spin relaxation time T_2 and T_2^* grows, leading to an increase of intensity in T_2-weigthed and T_2^*-

weighted MR images. That's the mechanism of fMRI technique use BOLD contrast effect to obtain the picture of the activity in the brain.

The changes in the ratio of oxygenated to deoxygenated blood are measured via the hemodynamic response function (HRF). Normally there is a delay of approximately 2 seconds after the triggering of neuronal activity, as the blood need time to be delivered to the relevant area. A gradual increase in the response peaks at about 6 seconds after that. If there is no further stimulation, the HRF starts to slow decay, returning to the baseline. Often there's a dip below baseline is observed before complete recovery. It takes approximately 16 to 20 seconds to go back to baseline levels (see Fig.1.1). If the neuron keeps firing, the peak will spread to a flat plateau [5].

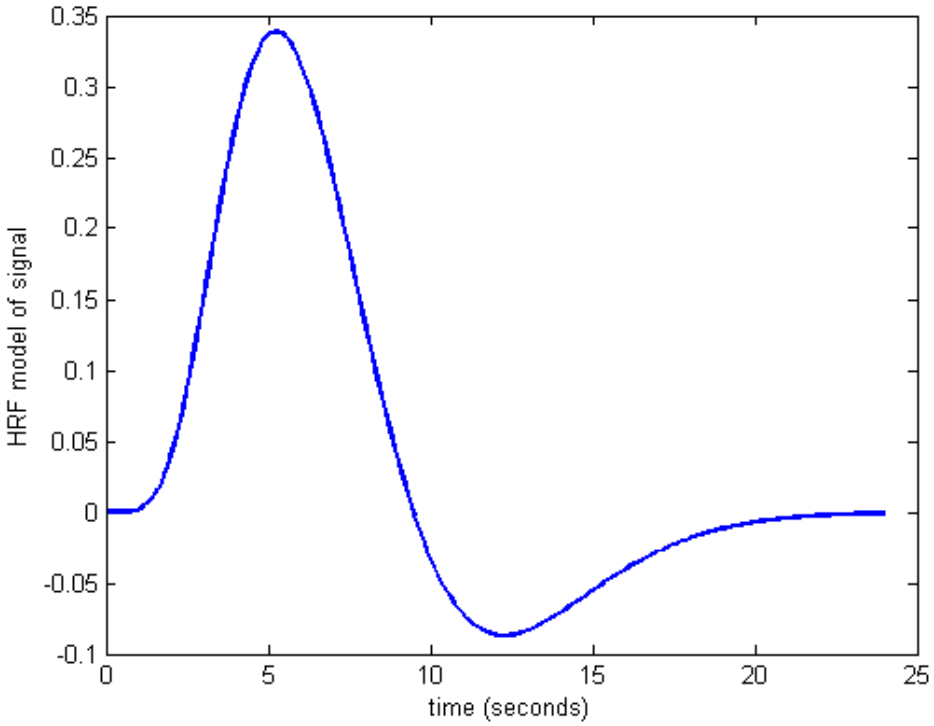

Fig.1.1 Hemodynamic response function

Functional MRI tracks functionality of the brain in time, for every time of repetition (TR), a three dimensional volume image is generated by the MRI scanner. All 3D images generated within one scanning session can be concatenated in the form of a 4D image, with time as the fourth dimension. It can be noted that the temporal resolution is of great importance to the fMRI technique, however, due to the fact that the BOLD signal has its intrinsic limitation on temporal resolution, this prevent the temporal resolution from further progressing [8]. Recently, the deconvolution technique has been proposed to solve this problem. Further explanation will be elucidated in the chapter 1.4.3. Although fMRI technique has a comparatively poor temporal resolution compare to underlying neuronal signal, its spatial resolution is relatively high compared to other imaging technique such as the electroencephalograph (EEG) and magneto encephalogram (MEG). Thus some new techniques which can improve both spatial and temporal resolutions such as simultaneous recording and analysis of EEG and fMRI have received substantial attention.

For the clinical use of the fMRI technique, physicians can use it to learn how a diseased brain is functioning, and how an invasive treatment works for a patient. They map the brain with connections between critical regions which are highly correlated with functions such as movement and sensory.

1.3 fMRI Data Preprocessing

Due to the noisiness of the data and subjects movement, the raw fMRI data cannot directly be used to the brain functionality analysis. A standard preprocessing pipeline step is needed. Normally, standard preprocessing of raw fMRI data includes slice timing correction, realignment, normalization, temporal filtering and regressing out nuisance covariates such as motion

parameters, white matter signal and cerebrospinal fluid signal, and spatial smoothing. Preprocessing usually performed using Data Processing Assistant for Resting-State fMRI (DPARSF) [9], which is based on the Statistical Parametric Mapping [10] and Resting-State fMRI Data Analysis Toolkit [11].

1.3.1 Slice Timing Correction

As mentioned earlier, a 3D volume image is obtained by the scanner for each TR. However, functional volumes are usually acquired one slice at a time with the timing evenly separated over the TR to obtain a complete 3D volume image, the whole process normally takes within a few seconds. Therefore it's incorrect to assume that all slices were captured at the same time. If the change of the timing isn't correctly accounted for, the relative stimulus and response will not match across the slices and the statistical analysis will not fit the model with accuracy. Slice timing correction aims to adjust the voxel time series so that common reference timing appears for all the voxels. The temporal adjustment is achieved by shifting the time series of values slightly forward or backward in time using the sinc-interpolation.

1.3.2 Realignment

While the slice timing correction performs alignment in the temporal domain, the realignment does it in the spatial domain. Due to the fact that subjects' movements are inevitable during the long-term scan session, the functional data acquired within a session (normally between 3 minutes to 12 minutes) cannot be perfectly matched. Therefore, the realignment of all the 3D volumes across each session are needed. The motion effect can be accounted by rigid body translations under the 6 motion parameters (3 translations and 3 rotations). Normally for each session, a

reference image is set to calculate the rigid body transformation between the reference image and other images in the same session that need to be realigned. Then the rigid body transformation is imposed on each image so that they are all aligned with each other.

1.3.3 Spatial normalization

Spatial normalization serves to convert the functional images which acquired from different subjects with different brain sizes to a standard template. This step is crucial because for most fMRI study, we need to concatenate data from different sessions and different subjects for the statistical analysis. However, different subjects have different brain size, it is impossible to perform the group-level analysis without using spatial normalization. Usually, the functional volumes are normalized to the standard template atlases such as MNI (Montreal Neurological Institute) [12].

1.3.4 Spatial smoothing

Spatial smoothing works to average the data points with their nearby voxels to produce a smoother spatial map across the image compare to the raw data. This has the effect of removing the spatial high-frequency information of the data while enhancing the low frequencies. The average is often employed by convolving the fMRI signal with a Gaussian function of a particular width. If the filter width matches the expected signal width, this process improves the signal-to-noise (SNR) ratio, but will reduce the spatial resolution of each image. Thus, a balance should be found between improving the SNR and maintaining the resolution of the functional image. In practice, for the most purpose a full width half maximum (FWHM) of the Gaussian kernel of 4mm

is suitable, but a larger FWHM may be useful if the SNR is particularly poor and the activation expected to cover a large area.

1.3.5 WM and CSF removal

In general, the BOLD signal has common source of error introduced by the physiological noise (WM and CSF). Signal changes in the WM and CSF primarily reflect the non-neural fluctuations such as scanner instability, respiration, etc. These signals are independent from BOLD signal fluctuations recorded in gray matter, and may cause the overestimation of the functional connectivity strength. Thus regressing out signals from CSF and WM may increase SNR. Usually, this can be done by averaging signals over all voxels within a WM or CSF mask for each time point, the mean WM and CSF time series are then used as temporal covariates and removed from the functional data through linear regression.

There are also some other preprocessing steps that need to be taken account of, such as temporal filtering. Temporal filtering is applied to purge signal from unwanted noise and artifacts which come from thermal noise, physiological noise from heartbeat and breathing, and magnetic field shifting, etc. Especially for resting state time series, low frequency oscillations (~ 0.01—0.1 HZ) are of great interest. However, it should be noted that band-pass filtering was not performed during preprocessing in this work, since the deconvolution method makes use of information carrying in the high frequency components[13].

1.4 Relevant Literature and Methods

1.4.1 Resting state fMRI

Functional imaging provides complementary viewpoints of the brain. In this chapter, we outline the general method in connectivity analysis, which are common to the rest of the chapters. There are mainly two ways in which fMRI can infer the brain functioning. Task fMRI asks subjects to perform certain tasks during the fMRI scan. The tasks are carefully designed to capture specific subdivision of the brain. The post analysis of task fMRI aims at identifying brain regions which are activated while performing the task as compared to a baseline condition. Task based fMRI experiment has several disadvantages that limit its application. The activation results are highly dependent on how well the patients can perform the described task. Patients with Parkinson's disease may unable to cooperate. The task effects are small thus may need longer acquisition time to improve the SNR of the measurement. Further, brain functioning relies more on the communication between regions instead of isolated activation of these regions, thus activation analysis may not further shows how the brain process while tasking. In recent years, there has been an increase in interest in the application of the alternate approach at rest, termed resting-state fMRI (RS-fMRI). Resting state data are obtained without any explicit task requirements, subjects are asked to let their mind wander and lie still in the scanner, therefore the experiment cannot be influenced by particular task demands. Brain activity is present even in the absence of external task, any brain region will have spontaneous fluctuations in BOLD signal. The functional significance of these fluctuations was first found from one part of the motor cortex that were temporally correlated with other network functioning the same as motor cortex, even when the subject at rest. Literatures of resting state studies have reported sub-networks that are strongly functionally linked during rest, which referred to as the resting-state networks [14], [15]. These sub-networks are anatomically separated, but with brain regions that are functionally linked that show an ongoing functional connectivity during rest. Among these sub-networks, the default mode

network (DMN) is of special interest, which suggest to reflect a “default state” of neural activity in the brain [16]. The DMN is consist of functionally linked posterior cingulate cortex/precuneus, medial frontal and inferior parietal regions. Compared to other resting state networks, regions in the DMN have a high level of neuronal activity during resting, in contrast to the tasking performing. This makes the connectivity analysis in default mode network of special interest in examining cognitive malfunctioning in psychiatric and neurologic brain disorders.

1.4.2 Connectivity analysis in RS-fMRI

RS-fMRI technique helps to measure and examine the interrelationship between brain regions. Normally, the connectivity analysis which aims to model the interrelationship between brain regions is thought to be of two types: functional connectivity (FC) and effective connectivity (EC). FC studies the simultaneous activity between two brain regions, it can be defined as the temporal correlation between spatially neurophysiological events. EC on the other hand, studies the causal information from one region to the other, with one region being the source and the other being the destination. EC refers to the influence that one neuronal system exerts over another, at synaptic or population level. The change of the causality indicates that if the brain activity changes in one region, it will cause altered activity in another region. In this work, we employ EC to understand brain network alterations in Alzheimer’s disease (AD) patients and investigate FC correlation changes with behaviors in dogs in different data acquisition time point.

It can be noted that connectivity focus more on the relationship between two brain regions, but human brain operates interrelationship among all the regions simultaneously. Thus pairwise relationships are inadequate and incomplete to represent the ground truth. To this effect, graph-

theoretic measures derived from resting state connectivity measures have been used to identify potential biomarkers in AD patients. Among all the connectivity paths in the network, there are always some central nodes that participate in many short paths, and act as the controller of the information flow. Betweenness Centrality (BC), a local nodal characteristic which quantifies how much information may traverse the node (any given brain region) belongs to one of those critical node measures. We study the alterations in critical nodes in AD patients and its two preliminary stage groups.

1.4.3 Deconvolution

An important role that should not be ignored is that the fMRI is an indirect measure of neural activity which can be modeled as the convolution of the hemodynamic response function $h(t)$ and underlying neural response $s(t)$ which are driven by the external stimulus from performing task (see Fig.1.2).

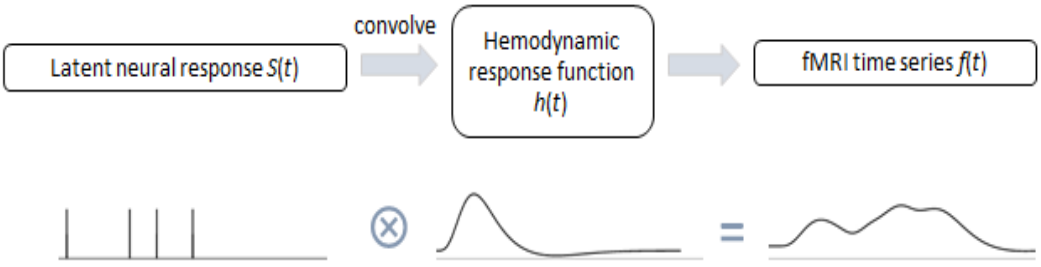

Fig.1.2 Hemodynamic model

The HRF is the impulse response which governs the relationship between underlying neural response and the acquired fMRI signal. Since the fMRI data acquisition happens between the neurons firing and the change of HB in blood that changes the signal, the signal itself is not

faithfully represent the hidden neural activity. Moreover, it has been proved that the HRF vary across different subjects and also among different regions in the same subject. Given the fact that the fMRI signal can be influenced by variability of the HRF instead of the underlying neural response, studies have shown that the causal relationship obtained from the raw fMRI time series can be confounded by the factor [17], [18]. Therefore, performing deconvolution is an alternative way to overcome this problem.

Since both the voxel-specific HRF and underlying neural responses are unknown and only can be estimated from the observed fMRI data, the deconvolution must be blind. To date, many deconvolution method have been proposed [19]–[21], in this study, we performed method demonstrated by Wu et al [13] to remove non-neural variability of the HRF and estimate latent neural response. Specifically, the resting-state fMRI data was considered as spontaneous event-related, and those events can be detected by picking up the comparatively large amplitude of BOLD signal fluctuations. The HRF of each voxel was reconstructed by fitting them with a double gamma function and two time derivatives. Finally, signals at the neural level can be recovered by Wiener deconvolution using the corresponding HRF. Many previous literatures have performed this deconvolution method, and it has been proved that deconvolution improves the estimation of effective connectivity [20], [22] .

1.4.4 This work in relation to prior literature

While most studies performed Betweenness Centrality of functional connectivity as an indicator of node's centrality in a network. A Previous study have shown that centrality measures do not necessarily identify some important critical nodes even though their removal might cause

the functional deterioration of the whole network [24]. With the combination of effective/functional connectivity, and a novel critical node identification method in directed networks named Middleman Power, we test the hypothesis that MP is superior to BC from both directed and undirected networks.

There has been considerable work on studying the biomarkers of Alzheimer's disease and its preliminary stage such as mild cognitive impairment. However, none of the studies have utilized dynamic connectivity information in characterizing the disorders. Dynamic connectivity has been shown to have better predictive ability than static connectivity. [25][25][25]Recent work suggests that connectivity varies over time, and the temporal variability of connectivity is sensitive to human behavior in health and disease [25]. In this study, we used a novel framework to identify the foci that affected most by the disease with the combination of Effective connectivity and dynamic effective connectivity, we believe that this work provide a unique insight of view into the brain alterations in the AD studies. While connectivity analysis provide valuable information on the biomarkers of the disease based on brain network alterations, it is difficult to interpret these connectivity results because traditionally, our knowledge of brain function is anchored on regions (activations and morphometric changes) and not connections. From an interventional standpoint, it is easier to functionally modulate the activity of regions (using brain stimulation, neurofeedback, etc.) rather than connections. Further, we assume that most abnormalities are usually characterized by certain sources (foci), the impairments affect neural signaling along pathways associated with the diseased regions. By identifying the source could leave better understanding to the rest of the abnormal effects. Moreover, traditional connectivity simply assumed to be stationary over time, and only one value of connectivity can be obtained from the whole scan. However, the state of human brain

changes every moment, with such a static formulation seems intuitively incomplete. Considered that dynamic fluctuation of connectivity cannot be captured by using this approach, and such change carries biological information [26]. Recent work suggests that connectivity varies over time, and the temporal variability of connectivity is sensitive to human behavior in health and disease [25]. In addition to studying the conventional static effective connectivity (SEC), we also estimated dynamic effective connectivity (DEC) from the resting state fMRI data acquired from AD group and NC group.

Functional brain connectivity based on resting state functional magnetic resonance imaging (fMRI) has been shown to be correlated with human personality and behavior. In this study, we sought to know whether capabilities and traits in dogs can be predicted from their resting state connectivity as in humans. We trained awake dogs to keep their head still inside a 3T MRI scanner while resting state fMRI data was acquired. Canine behavior was characterized by an integrated behavioral score capturing their hunting, retrieving, and environmental soundness. Functional scans and behavioral measures were acquired at three different time points (TPs). The first time point (TP1) was prior to the dogs entering formal working detector dog training. The second time point (TP2) was soon after formal detector dog training. The third time point (TP3) was three month's post detector dog training while the dogs were engaged in a program of maintenance training for detection work. We hypothesized that the correlation between resting state FC in the dog brain and behavior measures would significantly change during their detection training process (from TP1 to TP2), and would maintain for the subsequent several months of detection work (from TP2 to TP3). To further study the resting state FC features that can predict the success of training, dogs at TP1 were divided into successful group and failure group. Moreover, we

identified the homologous areas by comparing the connectivity fingerprints of regions between humans and dogs. Despite the lack of abundant literature into the neural basis of behaviors of dogs and their trainability, projecting dog brain regions identified here onto the human brain, and evaluating similar literature in humans may help us better understand the evolutionary role of brain-behavior relationships. This comparative evaluation is particularly relevant for dogs since they are a rare species which has socially co-evolved with humans for thousands of years.

1.5 Organization of the Dissertation

The first chapter gives a short introduction of relevant background knowledge, briefly elucidating the MRI, fMRI and its preprocessing pipelines. The other chapters are organized as follows. Chapters 2 and 3 are connectivity based characterization of resting state fMRI in Alzheimer's disease patients. Chapter 2 presents the using of nodal characteristics to identify brain based biomarkers that progressively deteriorate from healthy status to mild cognitive impairment to Alzheimer's disease. Chapter 3 presents the identification of disease foci which affect most by the Alzheimer's disease. Chapter 4 presents resting state functional connectivity analysis in dogs. Chapter 5 provides concluding remarks on this work and Chapter 6 lists peer-viewed publications.

CHAPTER 2

Deterioration from Healthy to Mild Cognitive Impairment and Alzheimer's Disease Mirrored in Corresponding Loss of Centrality in Directed Brain Networks

2.1 Introduction

Alzheimer's disease (AD) is a neurodegenerative disorder that affects millions of individuals worldwide [27]. The disease is initially characterized by memory loss, and then cognitive decline and incapacity as the disease progresses. In order to accelerate discovery of the neurobiological basis of AD, Alzheimer's Disease Neuroimaging Initiative (ADNI) was conceived in 2000, aiming to characterize biomarkers of AD and study the progression from normal cognition to dementia [28], [29]. Mild cognitive impairment (MCI) presents as a transition period between normal aging and AD. Evidence regarding the pathologic basis of MCI has demonstrated characteristics similar to those seen in AD patients such as amyloid-β, neurofibrillary tangles, etc. [30]. It is estimated that half of the MCI patients will convert to AD patients in three to five years [31]. Therefore, studies employing both healthy, MCI and AD populations may help us to better understand the dynamic alterations in brain structure and function with the deterioration of the disease [32], [33]. Also, it is important to identify brain-based biomarkers that progressively deteriorate from healthy status to MCI to AD.

Resting state functional magnetic resonance imaging (RS-fMRI) is a promising method that can non-invasively characterize distributed brain networks [34], [35]. RS-fMRI has been widely used to study the inter-regional functional connectivity between healthy and disease populations, especially for detecting connectivity abnormalities in AD and MCI [36]. Studies have found that AD is associated with alteration of connectivity among different brain regions [37], [38]. Specifically, it has been shown that AD patients have decreased hippocampal connectivity with prefrontal lobe and posterior cingulate cortex [39], [40]. Further, connectivity alterations in AD patients' brain have been shown to occur in medial frontal, medial parietal and posterior cingulate cortex, and those regions also have a high resting-state metabolism and are part of the "default mode network" [41]. Huang et al. [42] found that compared with control subjects, AD patients had decreases in the amount of inter-regional connectivity, especially in the hippocampus, weaker between-lobe connectivity and between-hemisphere connectivity. In contrast, MCI patients had increased between-lobe connectivity between the occipital and frontal lobes compared with control subjects. Reduced resting-state functional connectivity [43] has been found in the default-mode network of MCI patients. Some of the connectivity changes in MCI have been postulated to be a compensatory response to the onset of AD-like pathologies in the brain.

Recently, the combination of RS-fMRI and graph theoretical analysis has revealed the topological organization of human whole-brain functional networks. For example, the healthy brain has been shown to exhibit small-world characteristics [44], [45]. Using graph theoretical analysis of AD/MCI patients and healthy populations can lead to better understanding of the differences in the topology of brain networks as well as the relationship between brain connectivity and the disease processes [37], [46]. Previous studies have found widespread reduction in node

degree (a measure of connection density) in MCI compared to healthy controls, suggesting that graph-based analyses might potentially be used in the determination of biomarkers for pathological aging [47]. For example, decrease in local clustering coefficient (specifically, in the hippocampus) and increased characteristic path length (CPL) in AD compared to normal controls has been demonstrated [37], [48]. Decreased long-distance connectivity of the frontal and caudal brain regions had been found in AD compare to controls [49]. Moreover, Betweenness Centrality (BC), a local nodal characteristic which quantifies how much information may traverse the node (any given brain region), was shown to be lower in certain brain regions in both AD and MCI compared to healthy controls [50].

We identify two shortcomings in previous studies employing graph-theoretic complex network analysis of resting state brain networks. First, it is noteworthy that previous studies have not investigated whether complex network measures obtained from brain networks mirror neuropathological deterioration from NC to MCI to AD. This is important because such metrics could signal a neurodegenerative course which is different from normal aging at early stages of the disease when intervention is more likely to be successful. Second, previous reports have found promise in BC [50], but have utilized BC calculated from undirected networks that characterize synchronization rather than information flow, which is better characterized using directed networks. It is to be noted that both synchronization and information flow are prevalent mechanisms by which brain regions interact with each other. Besides, even though Betweenness Centrality can determine the importance of a particular node in a network, it tends to over-inflate the power of nodes [24] as will be explained in the next section.

In this study, we estimated BC from directed networks derived from the application of Granger causality [51]–[58] to resting state fMRI data acquired from the following populations: Normal Control, Early MCI, Late MCI and AD. We used an additional metric called Middlemen Power (MP) which not only characterizes information flow through a node as in BC, but also estimates the power of the node in terms of its criticality for information flow in the entire network [24]. We hypothesized that BC and MP of brain regions should progressively decrease from NC to EMCI to LMCI to AD and sought to identify such brain regions.

2.2 Materials and Methods

2.2.1 Subjects

Data used in this study were obtained from ADNI database (http://www.loni.ucla.edu/ADNI). The ADNI is a multisite, longitudinal observational study of clinical, imaging, genetic and bio-specimen biomarkers through healthy elders to MCI to dementia or AD. Over 800 adults, aged 55 – 90 years, have been recruited from over 50 sites across USA and Canada to be followed for two or three years.

Resting state fMRI data from 35 control subjects, 34 EMCI, 34 LMCI and 29 Alzheimer's disease patients were obtained through ADNI-2 from the database. The participants in this study were recruited between 2011 and 2013 through ADNI-2 protocol, and we selected subjects who had completed both the 3D MPRAGE and resting state fMRI data scans in the same visit. We manually discarded 2 LMCI patients from the group so that the ages of four groups are statistically the same. Subjects were tested with Neuropsychiatric Inventory Questionnaire (NPI-Q), Mini-mental State Examination (MMSE), Functional Assessment Questionnaire (FAQ), as well as Global Clinical Dementia Rating (Global CDR) (Table.2.1). Functional MRI data were acquired

using a T_2^*-weighted single shot echo-planar imaging (EPI) sequence on 3.0 Tesla Philips MR scanners with 48 slices, slice thickness = 3.3mm, repetition time (TR) = 3000 ms, echo time (TE) = 30 ms, flip angle (FA) = 80 degrees, field of view (FOV): RL = 212, AP = 198.75mm, FH = 159 mm, voxel size: RL = 3.3125 mm, AP = 3.3125 mm and 140 temporal volumes in each run. Anatomical images were acquired using magnetization-prepared rapid gradient echo (MPRAGE) sequence for overlay and localization (TR = 6.8 ms, TE = 3.1 ms, voxel size: 1.11 × 1.11 × 1.2 mm^3, FA = 9 degree, FOV: RL = 204 mm, AP = 253 mm, FH = 270 mm). The data was subjected to standard resting state preprocessing pipelines using SPM8 and DPARSF toolboxes [9], [59]. Mean time series were extracted from 200 functionally homogeneous ROIs identified via spectral clustering [60]. It has been suggested that with 200 or fever ROIs, the Craddock template offers better interpretability and has been widely used in graph theory [61].

Table.2.1. Demographics and clinical findings.

	Controls	EMCI	LMCI	AD
Sex (F/M)	20 / 15	16 / 18	14 / 20	16 / 13
Age	74.5 ± 5.8	72.2 ± 5.7	71.4 ± 8.6	73.1 ± 7.35
NPI-Q	0.6 ± 1.3	2.1 ± 3.1	2.8 ± 2.5	3.0 ± 2.4
MMSE	28.8 ± 1.6	28.1 ± 1.5	27.1 ± 2.3	20.9 ± 3.9
FAQ	0.2 ± 0.8	3.3 ± 4.1	5.4 ± 6.2	16.3 ± 7.6
Global CDR	0.0 ± 0.1	0.5 ± 0.1	0.5 ± 0.1	0.8 ± 0.2

2.2.2 Connectivity Analysis

Directional brain networks were obtained from resting state fMRI data using Granger Causality [36], [62]–[67]. The principle underlying Granger Causality [68]–[71] is as follows: If using the past time series X improves the prediction of the future of time series Y, then X can be said to have a causal influence on Y (Granger, 1969). Let $X(t) = [x_1(t), x_2(t),\ldots, x_q(t)]$ be the q

selected ROI time series, then the multivariate autoregressive (MVAR) model with order *p* is given by

$$X(t) = \sum_{n=1}^{p} A(n)X(t-n) + E(t) \tag{2.1}$$

Where $A(n)$ is the model parameter, and $E(t)$ is the vector of the residual error. There are many previous studies which have used the MVAR model to estimate the causal relationship between fMRI time series from different brain regions. However, using Granger causality analysis on raw fMRI signals can be confounded by the spatial variability of the hemodynamic response [72], [73]. The spatial variability of the hemodynamic response function and its smoothing effect can be removed by blind hemodynamic deconvolution methods. Consequently, a novel blind deconvolution approach based on the detection of pseudo-events proposed by [13] was used to estimate the hemodynamic response function (HRF) and unmeasured neural variables from the observed data. Specifically, resting-state fMRI data was considered as spontaneous event-related, wherein the events were detected by picking up the comparatively large amplitude of BOLD signal fluctuations after removing other sources of noise. The HRF of each voxel was reconstructed by fitting them with a double gamma function and two time derivatives. Finally, signals at the neural level were recovered by Wiener deconvolution using the corresponding HRF. When the latent neuronal variables are input into the MVAR model (Eq.2.1) instead of raw fMRI data, we get the following equation

$$\begin{bmatrix} h_1(t) \\ h_2(t) \\ . \\ . \\ h_q(t) \end{bmatrix} = \begin{bmatrix} 0 & a_{12}(0) & ... & a_{1q}(0) \\ a_{21}(0) & 0 & & a_{2q}(0) \\ . & . & 0 & . \\ . & . & & . \\ a_{q1}(0) & a_{q2}(0) & ... & 0 \end{bmatrix} \times \begin{bmatrix} h_1(t) \\ h_2(t) \\ . \\ . \\ h_q(t) \end{bmatrix} + \sum_{n=1}^{p} \begin{bmatrix} a_{11}(n) & a_{12}(n) & ... & a_{1q}(n) \\ a_{21}(n) & a_{22}(n) & & a_{2q}(n) \\ . & . & & . \\ . & . & & . \\ a_{q1}(n) & a_{q2}(n) & ... & a_{qq}(n) \end{bmatrix} \times \begin{bmatrix} h_1(t-n) \\ h_2(t-n) \\ . \\ . \\ h_q(t-n) \end{bmatrix} + \begin{bmatrix} e_1(t) \\ e_2(t) \\ . \\ . \\ e_q(t) \end{bmatrix} \tag{2.2}$$

Where $h_q(t)$ are the hidden neural states, p is the model order estimated from the Akaike/Bayesian information criterion [36], [51], a and e are the MVAR model coefficients and errors, respectively. The instantaneous influences between time series are represented by $a(0)$ and the causal influences between time series can be inferred from $a(n)$, $n = 1 .. q$. Using $a(0)$ and $a(n)$ in the model can minimize the "leakage" of instantaneous correlation into causality [68], [72], [74], [75]. Subsequently, the correlation-purged causality (CPGC) from time series j to time series i could be obtained using the following equation

$$CPGC_{ij} = \sum_{n=1}^{p} (a_{ij})^2(\mathrm{n}) \tag{2.3}$$

The hidden neuronal response corresponding to all the 200 ROIs were first identified using deconvolution and then input into a fifth order MVAR model to obtain the causal connectivity between them. Surrogate data were obtained by randomizing the phase of the original time series and retaining their magnitude spectrum and then input into the MVAR model. This procedure was repeated 1000 times and the statistical significance of each path was obtained by comparing the CPGC value obtained from original data with the null distribution obtained from surrogate data. If region A significantly influenced region B ($p<0.05$), then the path from A to B was considered directionally connected.

2.2.3 Nodal Characteristics

Betweenness Centrality (BC) is a local nodal characteristic that quantifies how much information may traverse the node (any given brain region) and has been widely used in graph analysis [76]. To define the BC measure, let $\lambda_i(st)$ be the num paths [77] between node *s* and node *t*, passing through node *i*. Let the total number of shortest paths between node *s* and node *t* be denoted by $\lambda(st)$. Then the Betweenness Centrality in network *D* (containing nodes *s*, *t* and *i*) can be defined as

$$BC_i(D) = \sum_{s,t:s\neq i\neq t} \frac{\lambda_i(st)}{\lambda(st)} \tag{2.4}$$

Eq. 2.4 indicates that nodes with high Betweenness Centrality connect, otherwise unconnected parts of the network. However, some nodes located on the shortest paths between long distance vertices can turn out to possess rather high values of BC (due to long geodesics) that in actuality are not critical for information flow. This indicates that Betweenness Centrality is a rather good local characteristic measure, but may lose its advantages in large-scale networks. Comparatively speaking, a middleman in a network occupies a critical position that can block at least one node's information flow to another. In the extreme case, middlemen nodes might have the ability to separate the whole network into several disconnected components [24]. On the contrary, centrality measures do not necessarily identify these important critical nodes, even though, their removal might cause the functional deterioration of the whole network.

For example, consider the directed network shown in Fig.2.1 Nodes N1, N2, N3 block information flow from nodes F1, F2, F3 to other nodes respectively. If we discard node N1

(Fig.2.1, left), information flow from F1 to other nodes will be blocked. Thus, the middlemen nodes are N1, N2, and N3. The value of un-normalized Betweenness Centrality of N1, N2 and N3 are equal to 4. However, if we discard N4 (or N5) separately, it does not block the information flow from any of two nodes that originally communicate with each other (Fig.2.1, right). For non-middlemen N4, N5, their Betweenness Centrality value equal to 6. Here, the non-middlemen nodes (N4, N5) have higher Betweenness Centrality value compared to actual middlemen (N1, N2, N3) because betweenness is counted on geodesics, and the geodesics between given nodes have equal weight. This example illustrates that BC tends to exaggerate the power of some non-middlemen nodes and thus may not necessarily accurately measure the 'power' of middlemen nodes (Table.2.2).

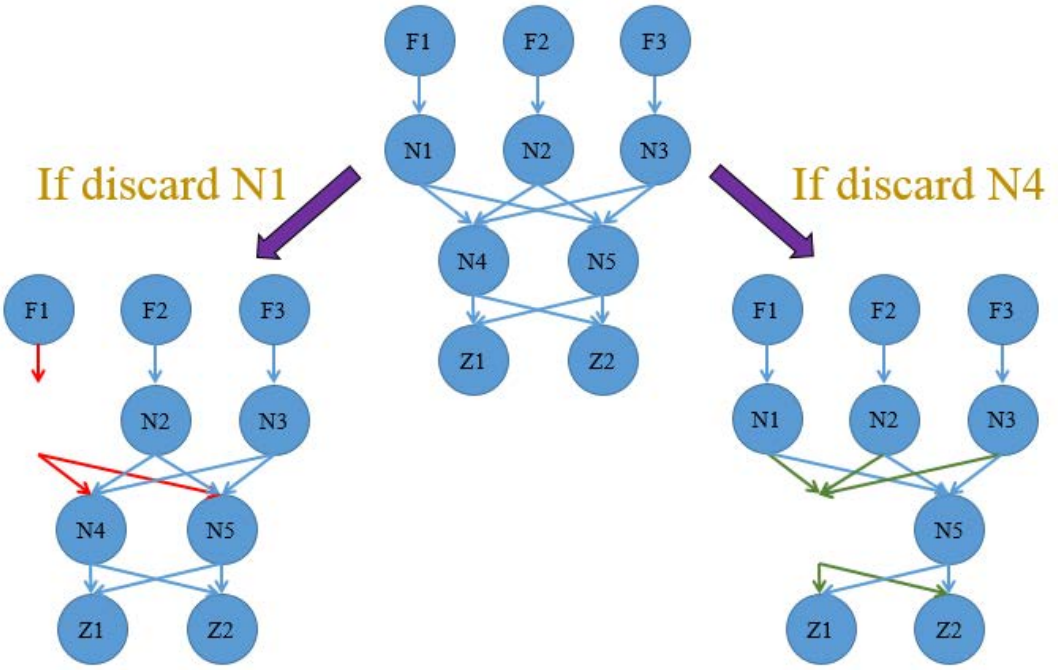

Fig.2.1 An example illustrating the concept of Middleman Power and its superiority over Betweenness Centrality

Table.2.2 The value of un-normalized Betweenness Centrality and Middlemen Power for the directed network in Fig.2.1

	Betweenness Centrality	Middlemen Power
N1	4	4
N2	4	4
N3	4	4
N4	6	0
N5	6	0

The brokerage position of middlemen in directed networks allows them to be highly extractive to both directly and indirectly connected nodes. The brokerage of node *i* in network *D* can be defined as

$$b_i(D) = \sum_{j \in N} \#S_j(D) - \sum_{j \neq i} \#S_j(D - i) - \#S_i(D) - \#P_i(D) \tag{2.5}$$

Where *N* is the set of all nodes in *D*, *i* denotes an arbitrary node belong to set *N*. Node *j* is the successor of node *i* and node *i* is called the predecessor of *j* if there is at least one node that adjacent to the path from *i* to *j*. Symbol # denotes the number of instances which satisfy the expression being referred to. For example, $\#S_j(D)$ is the number of successors of node *j* in network D. The maximal potential brokerage in network *D* is defined as

$$B^{'}(D) = \sum_{i \in N} [\#S_i(D) - \#s_i(D)] \tag{3.6}$$

Where $s_i(D)$ are all of the direct successors of i in D. By normalizing a node's brokerage score, the Middleman Power of a node can be defined as

$$v_i(D) = \frac{b_i(D)}{\max\{B'(D), 1\}} \tag{2.7}$$

Eq. 2.7 indicates that if a middleman node breaks all potential opportunity in the network, in other words disconnects connections between all the other nodes due to its removal (such as the removal of the center node of a star shaped network), then the middleman node has a network power of 1.

2.2.4 Statistical Analysis

The directional connectivity matrices obtained using the MVAR model were binarized with a threshold $p<0.05$. Betweenness Centrality and Middleman Power measures were calculated from the binarized matrices. BC [76] and MP [24] were obtained for each node from the directed networks. Six one-sided t-tests using BC and MP measures were performed (NC > EMCI, NC > LMCI, NC > AD, EMCI > LMCI, EMCI > AD, LMCI > AD), to find common nodes among all the six comparisons in order to identify brain regions in which BC and MP decreased progressively from NC to EMCI to LMCI and AD.

Besides, to test the BC measures for undirected networks (as MP is not defined for undirected networks), conventional functional connectivity, and associated p-values were derived from each group. This was done by calculating Pearson's correlation coefficients between each pair of 200 fMRI time series representing those ROIs. Similar to the effective connectivity, the functional

connectivity matrices were binarized at a threshold of $p<0.05$, and BC measures were calculated for each subject. Six one-sided t-tests were also performed to find the common nodes as described before.

2.2.5 Behavioral Relevance of Nodal Characteristics

In order to determine the behavioral relevance of nodal characteristics, we correlated both Middlemen Power and Betweenness Centrality of ROIs (which satisfied our hypotheses as stated above) with clinical variables (scores of NPI-Q, MMSE, FAQ and Global CDR) using the entire subject sample.

2.3 Results

Middlemen power of Left Orbitofrontal Cortex (L OFC) and Lateral Occipital Cortex (LOC) progressively decreased from NC to EMCI to LMCI to AD (Fig.2.2). These two regions are displayed (Fig.2.3) on a brain surface using BrainNet Viewer software (www.nitrc.org/projects/bnv/), which is a graphical interface visualization tool [78]. BC obtained from directional brain networks was able to identify only the LOC and not L OFC (Fig.2.4).

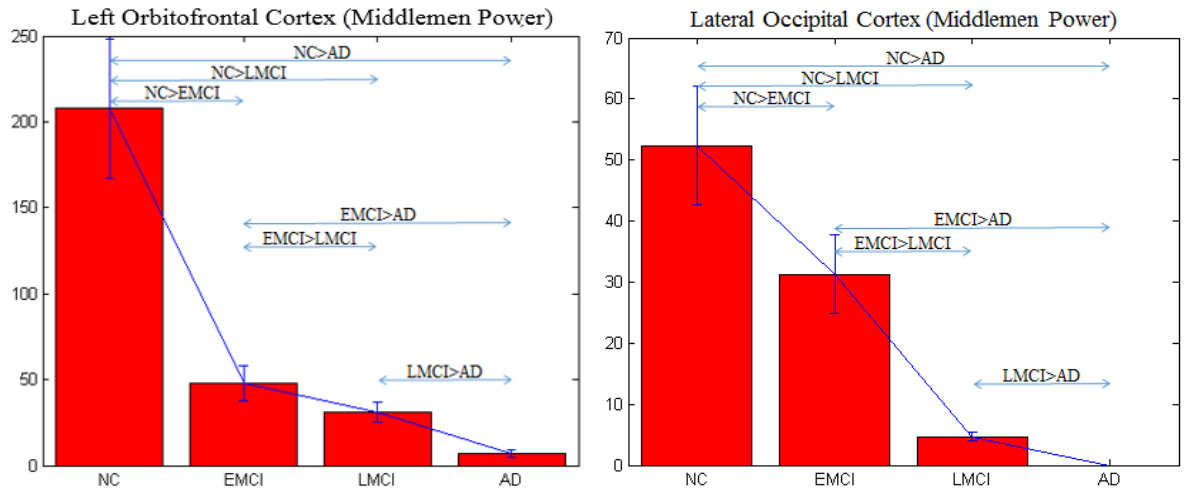

Fig.2.2 Middlemen Power of Left Orbitofrontal Cortex and Lateral Occipital Cortex, which were significantly different between the groups and deteriorated from NC to EMCI to LMCI to AD

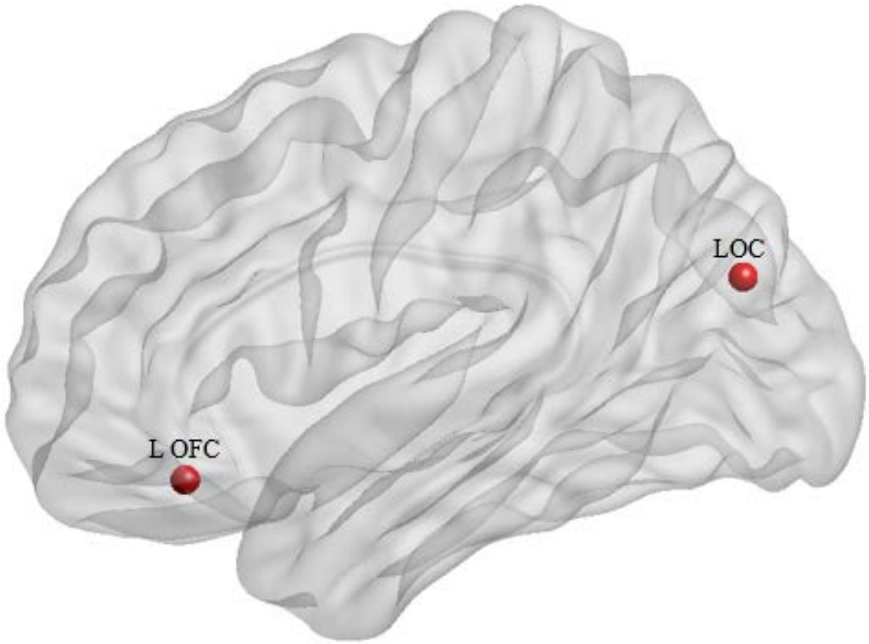

Fig.2.3 The location of two ROIs in the brain whose power progressively decreased with the deterioration of disease. L OFC: Left orbitofrontal cortex, LOC: lateral occipital cortex

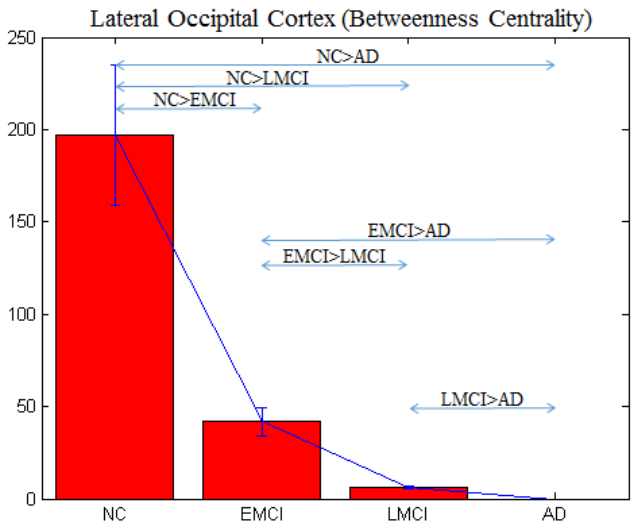

Fig.2.4 Betweenness Centrality of Lateral Occipital Cortex obtained from directional networks, which was significantly different between the groups and deteriorated from NC to EMCI to LMCI to AD

Betweenness Centrality estimated from undirected networks obtained from each subject using conventional functional connectivity did not identify a single node which was significant in the six t-tests mentioned above. To be more specific, we gradually relaxed the p-value threshold in all tests and tried to find the node that was common among all the six comparisons. It was not until the p-value threshold was 0.25, that the first node, Cuneal Cortex (Fig.2.5) was identified. Obviously, it is not statistically significant. This demonstrates the superiority of Middlemen Power over Betweenness Centrality obtained from both directed and undirected networks.

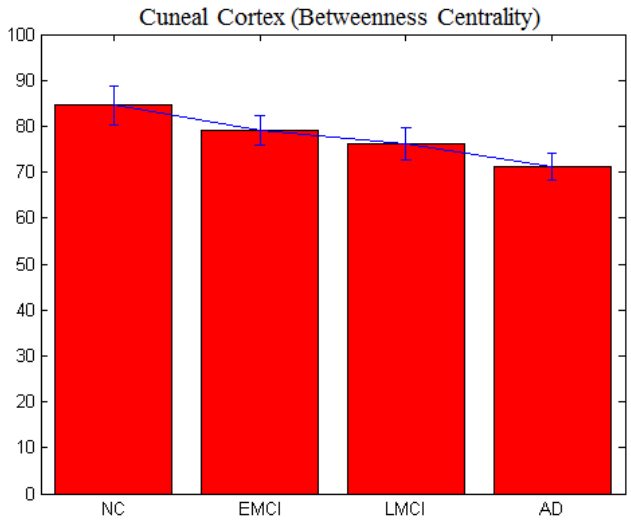

Fig.2.5 Betweenness Centrality of Cuneal Cortex obtained from undirected networks, which was not significantly different between the groups

Middlemen power of L OFC and LOC, and Betweenness Centrality of LOC (all of which were estimated from directed networks) which progressively decreased from NC to EMCI to LMCI to AD correlated significantly with behavioral measures across the entire subject sample, thus highlighting their relevance to the underlying neuropathology (Tables.2.3 and 2.4). It is noteworthy that MMSE is highest in controls and lowest in AD while the opposite is true for the other three measures. Therefore, it makes sense that MMSE was positively correlated with nodal characteristics while the other three behavioral measures were negatively correlated with nodal characteristics. The correlations with behavior were also stronger for middlemen power as compared to betweenness centrality.

Table.2.3 Correlation value (R) and corresponding p-value for the correlation of behavioral

measures with Middlemen Power of L OFC and LOC

Behavioral Measures	L Orbitofrontal Cortex		Lateral Occipital Cortex	
	R	p-value	R	p-value
NPI-Q	-0.34	6.32×10^{-04}	-0.38	1.49×10^{-04}
MMSE	0.41	3.297×10^{-05}	0.38	1.41×10^{-04}
FAQ	-0.48	8.97×10^{-07}	-0.46	2.45×10^{-06}
Global CDR	-0.79	2.16×10^{-21}	-0.83	1.33×10^{-25}

Table.2.4 Correlation value (R) and corresponding p-value for the correlation of behavioral measures with Betweenness Centrality of LOC

Behavioral Measures	Lateral Occipital Cortex	
	R	p-value
NPI-Q	-0.24	1.86×10^{-02}
MMSE	0.34	1.52×10^{-03}
FAQ	-0.36	3.81×10^{-04}
Global CDR	-0.45	3.11×10^{-06}

2.4 Discussion

We applied correlation-purged Granger causality to latent neural signals estimated from blind hemodynamic deconvolution of fMRI to obtain measures of directional influence across 200 brain regions covering the entire brain. We estimated BC and MP from directed networks from the following populations: Normal Control, Early MCI, Late MCI and AD. Our major findings were as follows. MP of two brain regions, Lateral Occipital Cortex and Left Orbitofrontal Cortex that significantly decreased with the deterioration of the disease were identified while Betweenness Centrality only found Lateral Occipital Cortex. In addition, no significant node was found in

undirected networks using Betweenness Centrality. The Middlemen Power of LOC and L OFC, and Betweenness Centrality of LOC also correlated significantly with behavioral scores, indicating their relevance to underlying pathology. Our results provide evidence that, for identifying imaging markers of deterioration from NC to MCI to DC, (i) Middlemen Power is a better local nodal characteristic compared to BC and, (ii) Directed networks seem to be more sensitive than undirected networks .

Our results are in agreement with previous functional network studies. The orbitofrontal cortex is damaged conspicuously in AD, and from the view of neurofibrillary tangle (NFT) pathology, AD cases have been shown to have pathology in orbitofrontal cortex and distinct patterns of NFT while control cases had no appreciable pathology other than an occasional NFT and diffused plaque [79]. The Orbitofrontal Cortex plays crucial roles in cognitive processing of decision-making [80] and age-related cognitive decline was shown to mirror neurodegenerative changes in this region [81]. On the other hand, LOC has also been previously noted in AD-related brain imaging studies. For example, it has been reported that with the deterioration of the disease, LOC showed a faster rate of atrophy in AD compared to MCI and NC [82]. Yao et al. found that the functional connectivity between LOC the left amygdala decreased in EMCI compared to LMCI, indicating that the decrease in memory ability was related to such connectivity changes [83]. Some previous studies have also found increased functional connectivities in MCI/AD which were attributed as compensatory mechanisms for losses in cognitive functionality [84], [85]. There hasn’t been more direct and expansive evidence for this alternative model. Therefore, we hypothesized that BC/MP of a few brain regions should progressively decrease with the

deterioration of the disease. The deterioration hypothesis is a more mainstream view with wider acceptability since it has roots in molecular/cellular level events in AD as discussed below.

Beta-amyloid (Aβ) shows a high degree of spatial overlap with default mode network [86] and recent work has detected a linear relationship between amyloid deposition and functional connectivity derangement [87]. The Aβ is the critical initiating event in AD, starting with the aberrant clearance of Aβ-peptides followed by consecutive peptide aggregation and disruption of neural activity [88]. Thal et al analyzed whole brain regions Aβ deposition to clarify whether there are differences in the expansion of Aβ-pathology between clinically proven AD cases and healthy population [89] and their results showed that occipital cortex and frontal cortex were severely affected by the Amyloid deposition with the deterioration of the disease. These results by Thal et al are in concordance with our findings. Taken together, the decreasing of MP/BC is supported by deterioration in Aβ deposition with progression of disease. Given that estimating Aβ deposition requires a PET scan which is more invasive and expensive than an MRI scan, our results highlight the possibility of using the graph-theoretic characterization of directional brain networks obtained from resting state fMRI for tracking neurodegeneration.

Some other regions have also been reported to be crucial to AD pathology [37], [90]–[92]. In fact, we also identified cingulate gyrus, hippocampus and middle temporal gyrus in the comparison of (NC>EMCI, NC>AD, EMCI>AD) using MP. This is in accordance with previous studies [37], [90]–[92]. However, these regions were not identified among all 6 comparisons (NC > EMCI, NC > LMCI, NC > AD, EMCI > LMCI, EMCI > AD, LMCI > AD). Considering that we were

primarily interested in brain regions that progressively deteriorated from NC to EMCI to LMCI to AD, we did not emphasize these results in this report.

2.5 Conclusion

In conclusion, our results showed that the MP detected more brain regions that progressively deteriorated from NC to EMCI to LMCI to AD, as compared to BC in directed networks. Also, BC did not identify a single node from undirected networks that significantly deteriorated. This demonstrates the superiority of MP over BC in both directed and undirected networks, and could serve as a potential biomarker for progressive deterioration from NC to MCI to AD.

2.6 Acknowledgements

The work described in this paper was supported by a grant from the National Natural Science Foundation of China (61473196). The authors also acknowledge support from the Auburn University MRI Research Center. The funders had no role in study design, data collection and analysis, decision to publish, or preparation of the manuscript.

CHAPTER 3

Investigating Focal Connectivity Deficits in Alzheimer's Disease using Directional Brain Networks Derived from Resting-State fMRI

3.1 Introduction

Alzheimer's disease (AD) is a progressive neurodegenerative disorder with a long pre-morbid asymptomatic period [93] which affects millions of elderly individuals worldwide [27]. The disease is initially characterized by the presence of neuronal and synaptic loss, β-amyloid (Aβ) production which results in the formation of intracellular neurofibrillary tangles and senile plaques [94], thereby resulting in memory loss, cognitive decline, etc. Structural and functional decline are inevitable with age and the existing treatment options for AD are highly limited. Therefore, determining neural aberrations underlying AD are an important step in addressing this challenge.

Resting-state functional magnetic resonance imaging (RS-fMRI) is a promising neuroimaging technique that can non-invasively characterize underlying brain networks. This technology has been widely used to identify biomarkers of AD based on brain network alterations [38], [95], [96]. Seed-based approaches [97], independent components analysis (ICA) based approaches [98] and graph theory [99] have been the three primary methods used in the study of resting-state functional connectivity (FC) in the brain. The seed-based approach involves predefining a region of interest (ROI) and extracting the BOLD signal from it; then a map of FC is obtained by calculating the

cross-correlation between the time series extracted from the seed ROI and all other voxels in the brain. Previous studies in AD employing seed-based FC revealed decreased connectivity between the posterior cingulate cortex seed and regions spread across the whole brain in subjects with AD compared to healthy aging, with the Default Mode Network (DMN) being the most affected system [100], [101]. Rather than define prior seeds, the ICA approach is model-free, which identifies independent components or co-activation networks throughout the brain. [102] examined the components corresponding to the DMN for AD patients, and found significantly decreased FC in the posterior DMN and increased connectivity in ventral and anterior DMN in the AD group. Graph theoretic analysis is typically performed using FC matrices, revealing the topological properties and organization of the underlying brain network. For example, [91] found that AD impacted the clustering coefficient and modularity in resting-state networks before the onset of the symptoms, suggesting that there might be a network-level pathology even in the preclinical stage. In summary, a profile of decreased connectivity has been consistently observed in AD.

However, most of the existing works on connectivity analyses have relied on FC or co-activation patterns, the literature on directed or effective connectivity (EC) patterns in AD is comparatively limited (more on this in the next paragraph). It is noteworthy that synchronization and causality in fMRI time series both represent distinct mechanisms in the brain [103], hence investigating EC aberrations in AD deserves attention. Motivated by this, we employed EC modeling to investigate aberrations in causal relationships between brain regions in AD. EC is often obtained using either of the two popular approaches, Granger causality (GC) [72], [104], [105] and dynamic causal modeling (DCM) [106]. DCM is highly dependent on prior assumptions concerning the underlying connectomic architecture and is therefore not generally considered

suitable for analyses of large graphs. On the other hand, GC is a data-driven approach that does not need a predefined model [57], [62]–[64], [66], [107], [108]. Recent developments have demonstrated that GC is a viable technique for obtaining EC networks from fMRI data [109], [110]. Therefore, in this study, we used a GC-based analysis framework. Strictly speaking, GC measures directed functional connectivity because it does not appeal to an underlying model of causal influences. In other words, GC tests for temporal precedence, thereby endowing functional connectivity with a direction. However, to emphasize the distinction between directed and non-directed connectivity, we will refer to our GC measures as effective connectivity (see [111] for further discuss on this issue).

There have been several studies investigating EC-related aberrations in AD [112]–[115]. These studies have reported distributed increases as well as decreases in directed relationships among brain regions in AD compared to healthy controls. However, these studies performing conventional GC analysis assume connectivity to be stationary over time, wherein only one connectivity value is obtained from the whole scan [68]–[70], [75], [116], [117]. However, connectivity, specifically the non-directed FC, has been shown to be non-stationary across time [26], [118]. Recent works suggests that connectivity varies over time, and that the temporal variability of connectivity is sensitive to human behavior in health and disease [25], [119]–[121]. Therefore, in addition to studying the conventional static effective connectivity (SEC), we also estimated dynamic effective connectivity (DEC) [52]–[56] from the resting-state fMRI data acquired from participants with AD as well as healthy controls (HC).

Traditionally, univariate statistical tests are performed for analyzing connectivity differences in population studies. Based on the statistical score, connectivity paths that differ from HC are ascertained. However, it is not straightforward to interpret such connectivity results, because traditionally our knowledge of brain functioning relies more on region-based properties (activations and morphometric changes) than connectivities. Further, from an interventional standpoint, it is easier to modulate the activity of brain regions (using brain stimulation, neurofeedback, etc.) rather than connections. With these viewpoints, Venkataraman et al. [122] recently introduced a technique for identification of focal regions of functional disruption based on non-directed FC differences between populations. In this work, we extend this technique for identifying focal regions of disruption based on static as well as dynamic directed/effective connectivity aberrations in AD compared to HC.

We constructed brain networks using strength (SEC) and temporal variability (variance of DEC [vDEC]). After certain modifications to the connectivity measures, we fed them into the foci-identification model to obtain disrupted foci. The foci obtained independently from SEC and vDEC networks were then overlapped (intersection) to identify the common foci which exhibited impairments in both static and time-varying EC. Reduced temporal variance in dynamic connectivity is often associated with psychiatric disorders [121], [123], and a relatively low variability of connectivity has been associated with poor behavioral performance in healthy individuals [25]. Recall that a profile of decreased static connectivity has been consistently found in AD as discussed above. Taken together, we hypothesized that AD is characterized by dysfunctional disease foci, and that these foci are associated with connectivity paths that exhibit lower strength (SEC) as well as lower variability (vDEC) of effective connectivity.

3.2 Materials and Methods

3.2.1 Participants

Data used in this study were obtained from the ADNI database (http://www.loni.ucla.edu/ADNI). Resting state fMRI data of 30 participants diagnosed with Alzheimer's disease (AD), along with 39 matched healthy controls (HC) were obtained through ADNI-2 cohort. Participants in this study were recruited between 2011 and 2013 through the ADNI-2 protocol, and we selected participants who had completed both 3D MPRAGE and resting-state fMRI data. Functional MRI data were obtained from a 3.0 Tesla Philips MR scanner with repetition time (TR) = 3000 ms, echo time (TE) = 30 ms, flip angle (FA) = 80 degrees, field of view (FOV): RL (right-left) = 212, AP (anterior-posterior) = 198.75mm, FH (foot-head) = 159 mm, voxel size: RL = 3.3125 mm, AP = 3.3125 mm, slices = 48, thickness = 3.3125mm. 140 temporal volumes were acquired for each participant in a single scanning session. All data available from the ADNI database was acquired in accordance with the recommendations of local IRBs with written informed consent from all subjects. All subjects gave written informed consent in accordance with the Declaration of Helsinki. The protocol was approved by local IRBs. More specific information can be obtained from the ADNI website (http://www.loni.ucla.edu/ADNI). The data was subjected to a standard resting-state preprocessing pipeline using SPM12 [59] and DPARSF toolboxes [9], including slice timing correction, realignment & motion correction, normalization to MNI space, and spatial smoothing with a Gaussian kernel of $4 \times 4 \times 4$ mm^3 full width at half maximum (FWHM). Six rotation and translation parameters were first tested individually. Except rotation in Y axis ($P < 0.05$), there were no significant differences between the groups ($P > 0.05$). Then, all the six head motion parameters were aggregated into a single

metric (i.e. framewise displacement), and no significant differences in framewise were found between the groups ($P > 0.05$). Nuisance variables such as the mean white matter signal, mean cerebrospinal fluid signal, and six head motion parameters were regressed out of the BOLD time series. It should be noted that band-pass filtering was not performed during pre-processing since it will likely impact deconvolution. Mean time series were extracted from 200 functionally homogeneous ROIs identified via spectral clustering [60].

3.2.2 Connectivity analysis

Static effective connectivity (SEC) was obtained using Granger causality (GC) analysis. However, before GC analysis is performed, it is necessary to acknowledge the impact of hemodynamic response function (HRF) on connectivity modeling, which is known to vary across different regions within a participant, as well as vary across participants [124]. Previous studies have shown that results obtained by using GC analysis on HRF-corrupted fMRI data can be confounded by the variability of the HRF [18], [125]. Hence, a blind deconvolution technique, proposed by Wu et al. [13], was employed to minimize the non-neural variability of the HRF and estimate the latent neuronal time series from the observed fMRI data. In brief, the resting-state data was modeled as spontaneous event-related data [126], and the HRF of each voxel was estimated by Wiener deconvolution [127]. The estimated neural time series were then used in further GC analysis.

The underlying concept of GC is that a directed causal influence from time series X to time series Y can be inferred if the past values of time series X improves the prediction of the present and future values of time series Y [104]. Let q time series $X(t) = [x_1(t), x_2(t),\ldots,x_q(t)]$ be the latent neural time series obtained after HRF deconvolution of selected ROI fMRI time series, with q

being 200 ROIs in this study. Then the multivariate autoregressive (MVAR) model with order *p* is given by

$$X(t) = A(1)X(t-1) + A(2)X(t-2) + \cdots + A(p)X(t-p) + E(t) \tag{3.1}$$

Where $A(1)\ldots A(p)$ are the model parameters, and $E(t)$ is the vector of the residual error.

To remove the zero-lag correlation effect (i.e. ignore co-activations), the time series were input into a modified multivariate autoregressive model which included the zero-lag term used by Deshpande et al. [51] shown as follows:

$$X(t) = A'(0)X(t) + A'(1)X(t-1) + \cdots + A'(p)X(t-p) + E(t) \tag{3.2}$$

The diagonal elements of $A'(0)$ were set to zero, to model only the instantaneous cross-correlation rather than zero-lag auto-correlation. The off-diagonal elements of $A'(0)$ corresponded to the zero-lag cross-correlation [51]. It is to be noted that the coefficients in Eq. 3.1 $A(1)$, … $A(p)$ would not be the same as $A'(1)$ … $A'(p)$ as in Eq. 3.2, because the modified zero-lag term affects other coefficients since it removes the zero-lag cross correlation effects from them. Accordingly, the correlation-purged granger causality (CPGC) from time series *i* to time series *j* was obtained using the following equation

$$CPGC_{ij} = \sum_{n=1}^{p} (a'_{ij})^2(n) \tag{3.3}$$

Where a'_{ij} are the elements of A'. It is well-known that the coupling among brain areas is time-varying and context-sensitive. Indeed, the most interesting parameters of dynamic causal models are the fluctuations in effective connectivity (induced by experimental manipulations or time). In recent years, the functional connectivity (resting state) community has dubbed these fluctuations in coupling as "dynamic functional connectivity". In our work, we characterised dynamic effective connectivity using a temporally adaptive modified MVAR model:

$$X(t) = A'(0,t)X(t) + A'(1,t)X(t-1) + \cdots + A'(p,t)X(t-p) + E(t) \tag{3.4}$$

In this model, the coefficients $A'(p)$ were allowed to vary over time, thus 'dynamically' estimating EC.

The parameters $A'(n,t)$, $n = 0,\ldots,p$ were estimated in a Kalman filter framework using variable parameter regression [128], [129]. The Kalman filtering is a recursive process, where new information is added when it arrives. Thus, estimates taken from early steps are less reliable compared to later ones. A forgetting factor (FF) is introduced to circumvent this problem by taking recent past Kalman filter estimates into account during current estimation in order to control smoothness and enhance stability. The forgetting factor was determined by minimizing the variance of estimated error energy [130] and was found to be equal to one in our study. In brief, Kalman filtering treats the underlying MVAR coefficients as slowly fluctuating states. This enables the estimation of time varying directed connectivity that was used for subsequent modelling at the between-subject level. The DGC is estimated as:

$$DGC_{ij}(t) = \sum_{n=1}^{p} (a'_{ij}(n,t))^2 \quad (3.5)$$

Where DGC_{ij} (t) is the dynamic Granger causality value from time series *i* to time series *j* at time point *t*. Given that the neural delays of interest are of the order of a TR or less [65], and that previous literature supports using a first order model to capture most relevant causal information [71], we employed a first order model for estimating both SEC and DEC in this work.

3.2.3 Identification of Disease Foci

Connectivity studies often report aberrations in functional connections between brain regions. While this is useful, it does not provide a comprehensive characterization of the underlying connectomics. First, it is likely that several aberrations in connectivity are the after-effects arising from disruptions in certain focal brain regions. Second, our knowledge about brain functioning is centered on functions of regions rather than connections. Therefore, it is advantageous to identify certain focal regions of disruption using connectivity data. Thus in this study, we sought to identify diseased foci in AD. A recent study introduced a novel technique for the identification of disease foci [122] based on non-directed FC differences between populations. Here we generalise this technique to the identification of diseased foci from effective connectivity as well as dynamic connectivity data.

The model proposed by Venkataraman et al. considers the connectivity measure (C^M_{ij} for HC group and P^M_{ij} for the AD group) as a noisy observation of the latent connectivity (C^L_{ij} for HC group and P^L_{ij} for the AD group). The model is illustrated in Fig.3.1 and consists of several parts.

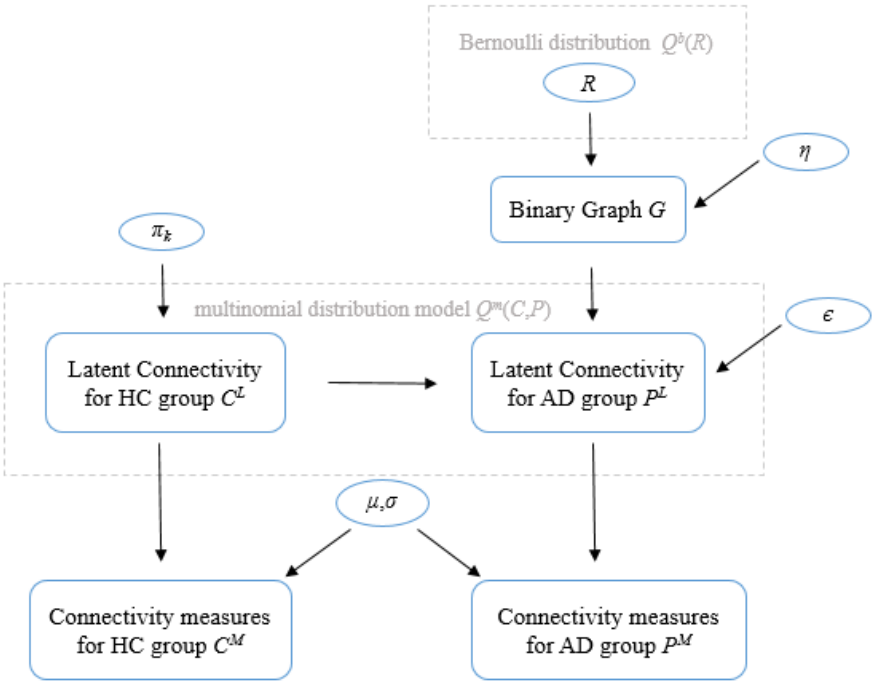

Fig.3.2 General model of the Foci identification technique. Parameters in circles indicate random variables. Please refer to the text for a description of the variables.

The first part defines a binary indicator vector that selects disrupted regions, and a binary graph characterizes corresponding abnormal connectivity. Let N be the total number of regions in the brain being considered. The model assumes a the random variable $R = [R_1,\ldots,R_N]$ is a binary vector (i.e. brain regions are either healthy with R_i=0 or disrupted with R_i = 1, where i=1 .. N indicates the state of each region in the brain. Elements of R follow an independent, identically distributed (i.i.d.) Bernoulli distribution model $Q^b(R)$ where $Q(\cdot)$ denotes the posterior distribution and superscript b indicates a Bernoulli distribution. Then, an underlying binary graph G which characterizes the network of abnormal connectivity can be defined as follows: a connection between two healthy regions is always healthy with probability equal to 1, a connection between two disrupted regions is always abnormal with probability equal to 1, and a connection between a

healthy region and a disrupted region is abnormal with probability η. The second part specifies the latent connectivity for controls (C^L) as a tri-state variable from a multinomial distribution with parameter π_k (k denotes three different states), positive connectivity with probability π_1, little or no functional connection (0) with probability π_0, and negative connectivity with probability π_{-1}. Given the binary graph G and latent connectivity for controls C^L, the tri-state latent connectivity of the AD population can be defined. Specifically, the latent connectivity from the control group C^L_{ij} equals to P^L_{ij} with probably ϵ if the binary graph connection between regions i and j is abnormal, C^L_{ij} equals to P^L_{ij} with probably 1 - ϵ if the connection between regions i and j is healthy. The third part characterizes the observed connectivity measures C^M_{ij} and P^M_{ij} as Gaussian random variables whose mean and variance (μ and σ) depend on the value of C^L_{ij} and $P^L_{ij.}$ Then, the joint likelihood of all configurations of latent connections between regions can be modeled as an 9-state multinomial distribution model $Q^m(C, P)$ (superscript m denotes that $Q(\cdot)$ is a multinomial distribution).

The model in Venkataraman et al [122] was applied in the case of functional connectivity, i.e. the Pearson's correlation coefficient between regions. However, EC is not a bounded measure, a small number of outliers is to be expected. In our EC data, we found a small portion of connectivity values which were greater than 1 or less than -1 (0.3%), wherein these outliers indicate stronger causal information flow between regions. To maintain the importance of those stronger effective connections and minimize its negative impact on model evaluation, inverse Fisher transformation was used to render the EC values as a bounded measure within [-1 1]. For the variance of dynamic EC, the latent tri-states of variance of connectivity vF_{ij} can be considered as follows: little variability or stationary connection, modest variability and strong variability. It is to be noted that

static FC is direction-less, hence only the upper or lower triangle of the symmetric connectivity matrices were needed to fit the model in Venkataraman et al. However, in our case, both SEC and vDEC are directed with asymmetric connectivity matrices, and hence the whole matrices were used in the model. Taken together, these modifications permitted the model to be applied to both static and dynamic EC.

After initiating the prior parameters (such as the Bernoulli prior for binary state vector R, prior for latent connectivity for controls π_k, etc) for the model, a variational expectation maximization (EM) algorithm [131] was adopted for estimating the latent connectivity and model parameters from the observed connectivity measures (C^M and P^M). Technically, we inverted the (between subject) model of disconnection using variational Bayes. This scheme is formally similar to an EM algorithm that uses a variational update for all the factors of an approximate posterior. These included an approximate posterior distribution over model parameters (π_k, η, ϵ, μ and σ), latent connectivity for both groups of subjects ($Q^m(C, P)$) and regional pathology ($Q^b(R)$). In brief, this variational scheme optimises the sufficient statistics of each marginal distribution or density with respect to variational free energy (FE), under the expected values of the remaining factors. The variational EM alternates between updating the latent posterior distribution and estimating the nonrandom model parameters. Convergence was based on the relative change in free energy of the model of less than 10^{-4} between consecutive iterations. Disrupted focal regions and latent abnormal connectivity would then be identified from the posterior probabilities for each region and each connection. Fig.3.2 illustrates the flow chart of the algorithm.

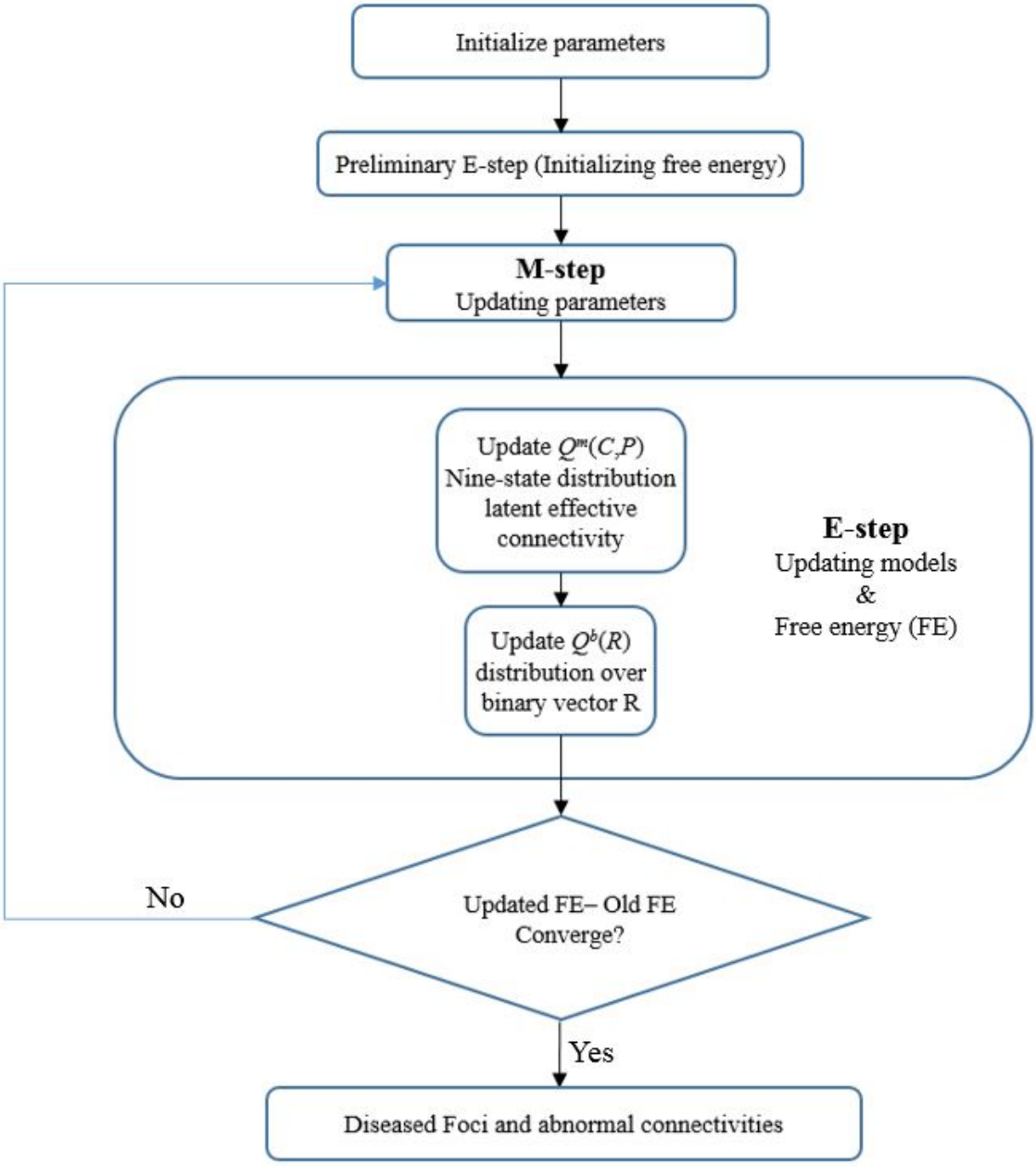

Fig.3.2 A flow chart of the Foci identification technique. The foci-identification technique posits that the latent connectivities can be stochastically generated from a distribution mode, and that the observed connectivity data are a noisy measurement of the latent unmeasured connectivity. Latent variables of the model were randomly initialized, and the variational EM algorithm was used to obtain the posterior distribution Q (both the nine-state distribution of latent functional connectivity

and distribution over binary vector R) and model parameters to minimize the variational free energy. Then the disrupted foci and corresponding dysfunctional connections can be identified.

The significance of the resulting foci was estimated using nonparametric permutation tests. Specifically, the group label of each participant was randomly permuted for 1000 times. For each permutation, we fit the data to the model and obtained the posterior probability of disrupted foci for each region. This provided an empirical null distribution from which the p-value of the significance was obtained. The method also identified the affected connections associated with the disrupted foci. Among such connections, we retained those that were also in accordance with our hypothesis (paths exhibit lower SEC, as well as lower vDEC of effective connectivity in AD compared to healthy controls with a threshold of $p < 0.05$).

3.3 Results

We identified two disrupted foci which were common to both SEC and vDEC networks: 1) Locus Coeruleus (LC) in the Brainstem (p-value = 0.003 for SEC and 0.006 for vDEC), 2) Right orbitofrontal cortex or R OFC (p-value = 0.007 for SEC and 0.002 for vDEC). Disrupted connectivity paths associated with these foci exhibited higher strength and larger temporal variability in HC as compared to AD (in accordance with our hypothesis). Furthermore, they exhibited a unique pattern of disrupted connectivity – those associated with the LC in the brain stem emanated from it, while connectivity paths associated with R OFC converged onto it (Fig.3.3).

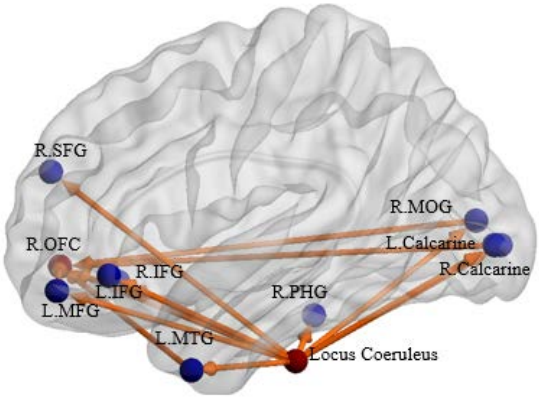

(a)

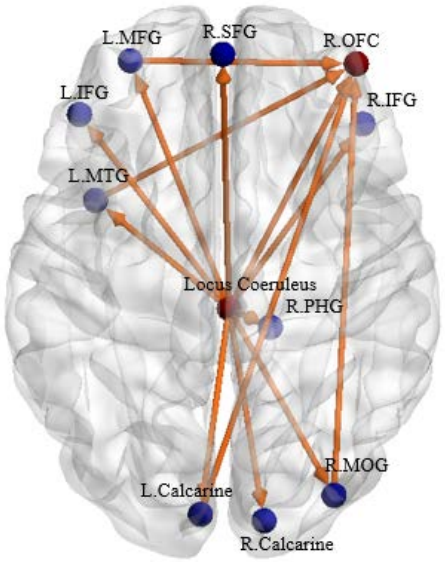

(b)

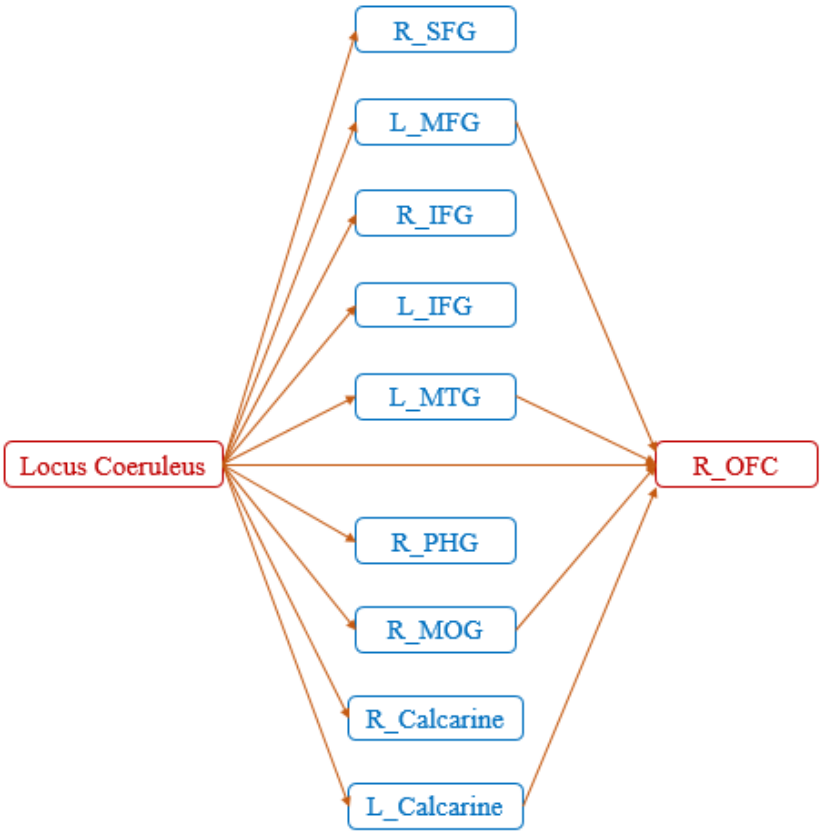

(c)

Fig.3.3 Sagittal view (a) and axial view (b) of the disease foci and corresponding disrupted

connections. Regions in red are the identified affected foci, located in Locus Coeruleus and Right orbitofrontal cortex. Regions in blue are the non-foci regions that were connected from/to the disease foci. A schematic of the identified network is also shown for better visualization of the network architecture (c). The expansions for the abbreviations are as follows: SFG = superior frontal gyrus, MFG = middle frontal gyrus, IFG = inferior frontal gyrus, MTG = middle temporal gyrus, PHG = parahippocampal gyrus, MOG = middle occipital gyrus, OFC = orbitofrontal cortex

Five of the ten connectivity paths emanating from the LC resulted in connectivity paths terminating in the R OFC, with four of these five paths being indirect pathways via the L MFG, L MTG, R MOG and L Calcarine, and one path being a direct connection from LC to R OFC. All connectivity paths exhibited lower SEC and lower vDEC in AD compared to HC.

Further clarity on the corresponding aberrant connectomic network was obtained by partitioning the network into four unique subnetworks (Fig.3.4): a) LC-PFC working memory system, b) LC-PHG emotional memory system, c) LC-visual cortex sensory system, and d) LC-MTG language system. Note that this partitioning is based on different functions performed by the locus coeruleus – norepinephrine system and is not based on any analytical strategy. Taken together, the disruption of these networks likely leads to working memory deficits, difficulties in processing emotional memories, and several other symptoms commonly observed in those with AD. The relevance of these subnetworks to AD pathology are discussed in detail in the next section.

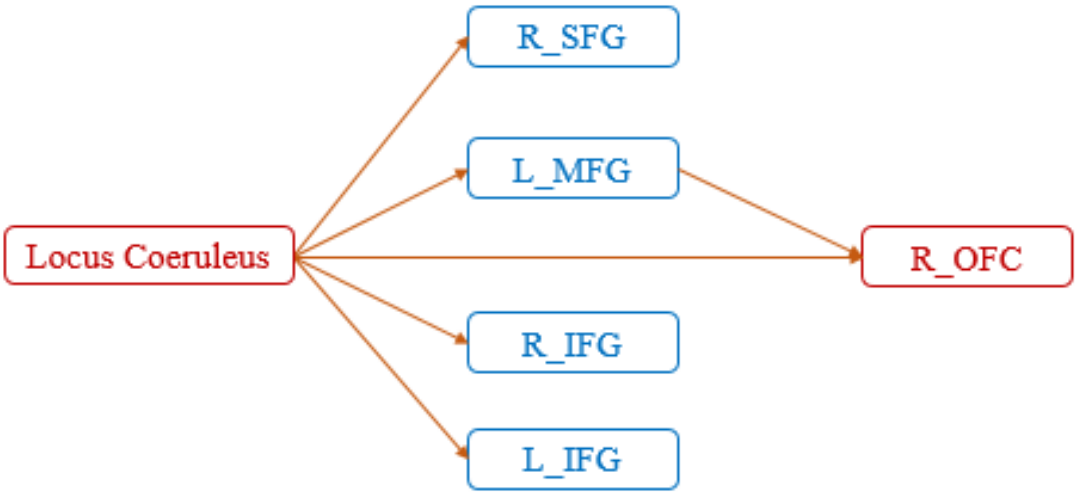
R_SFG
L_MFG
Locus Coeruleus
R_OFC
R_IFG
L_IFG

(a)


Locus Coeruleus
R_PHG

(b)

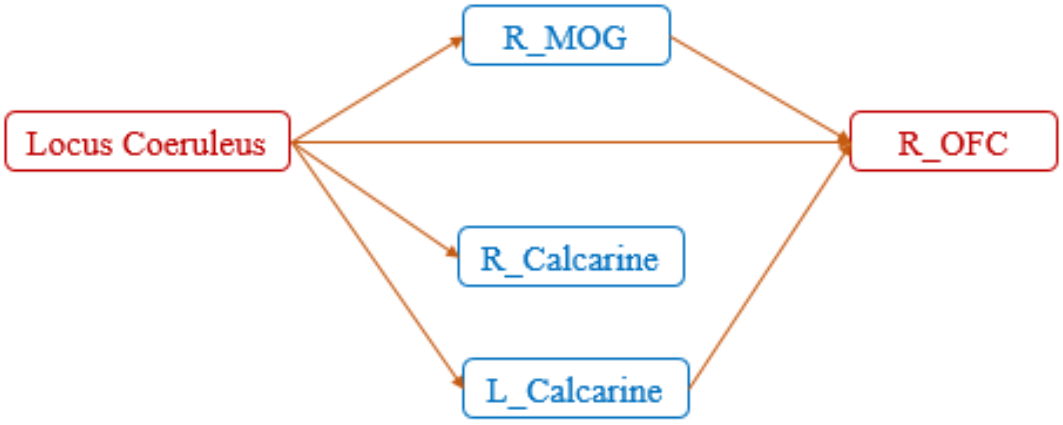
R_MOG
Locus Coeruleus
R_OFC
R_Calcarine
L_Calcarine

(c)

(d)

Fig.3.4 Disrupted networks associated with the diseased foci, showing the entire network partitioned into four unique subnetworks: a) LC-PFC working memory system, b) LC-PHG emotional memory system, c) LC-visual sensory system, and d) LC-MTG language system. Abbreviations: SFG = superior frontal gyrus, MFG = middle frontal gyrus, IFG = inferior frontal gyrus, MTG = middle temporal gyrus, PHG = parahippocampal gyrus, MOG = middle occipital gyrus, OFC = orbitofrontal cortex.

3.4 Discussion

In this study, we estimated static and dynamic measures of directed influences between 200 ROIs covering the entire brain in both AD and HC participants taken from the ADNI database. SEC and vDEC connectivity data were fed into a probabilistic model to identify regions with focal connectivity deficits in AD, with the hypothesis that connections associated with those regions would be weaker in strength and lower in temporal variability (i.e. rigid) in AD. We identified two such foci, brain stem and orbitofrontal cortex, which were affected significantly by the disease. The aberrant connections emanating from LC suggested a widespread dysregulation originating from the brainstem, part of which terminated into the other focus (orbitofrontal cortex).

Interestingly, all connectivity paths corresponded with the directed influence of the LC (in the brain stem) on mostly cortical (and few sub-cortical) regions. This corroborates with previous

studies that have shown progressive damage [132] in the brain stem during early periods of AD. Further, LC in the brain stem is the largest repository of Norepinephrine (NE) in the human brain [133]. Noradrenergic neurons in LC have projections to several parts of the brain including olfactory, limbic, prefrontal and other cortical regions [134], [135]. NE is known to suppress neuroinflammation [23]. This purported role has been hypothesized to be a protective factor against AD. In fact, Heneka et al., 2010 showed that NE stimulation of mouse microglia suppressed Aβ-induced cytokine and chemokine production and increased microglial migration and phagocytosis of Aβ. Induced degeneration of the brain stem increased the expression of inflammatory mediators in amyloid precursor protein (APP)-transgenic mice and resulted in elevated Aβ deposition. [137] suggesting that the decrease of NE in the brainstem facilitates the inflammatory reaction of microglial cells in AD and impairs microglial migration and phagocytosis, thereby contributing to reduced Aβ clearance. The Aβ is the critical initiating event in AD, starting with the aberrant clearance of Aβ-peptides followed by consecutive peptide aggregation and disruption of neural activity [88]. Moreover, a post-mortem study has found significant volume decreases in the LC during AD progression, highlighting the importance of this region in AD [138]. These findings indicate that the depletion of NE in LC is an etiological factor in the development of MCI and progression to AD. The studies discussed above provide some basis for the important role of brainstem in AD. Further, an animal study has found that boosting NE transmission can lead to increased functional connectivity [139], suggesting that the reduction of NE could potentially result in lower connectivity between LC and cortical regions.

Several previous studies have suggested that OFC may be important for understanding the mechanisms for putative spreading of AD pathology in the brain [140], [141]. Robust correlation

has been found between Aβ deposition levels and volume in the orbitofrontal area [142]. In fact, the amyloid precursor protein (APP) gene contains the sequence for the Aβ peptide, which is concentrated in the senile plaques (SPs) [143]. During AD progression, the SPs appear first in the orbitofrontal and temporal cortices and later extend to the whole cortex [144]. Further, SPs and Aβ deposition has been associated with reduced connectivity at the synaptic level [145], suggesting a potential mechanism that might link SPs and Aβ deposition with directed connectivity estimated from fMRI. While we discuss the role of temporal regions later in this section, the findings presented above highlight the importance of the role of OFC in AD.

Connectivity paths from LC to the prefrontal cortex (PFC) in general, and OFC in specific (note that OFC is a region in the PFC), can be considered as an aberrant LC-PFC working memory system (Fig.3.4a). Given that many studies have referred to the PFC in general without specifying sub-regions, and hence we are going to use the same nomenclature in the ensuing discussion. Previous studies have indicated that NE is instrumental in enhancing working memory through actions within the prefrontal cortex (PFC). PFC underlies the encoding of task-relevant information in working memory [146], and it has been shown that damage to the noradrenergic innervation of the PFC impairs performance in working memory [147]. The stimulation of α_2-adrenergic receptors in the PFC of nonhuman primates has been shown to improve performance in working memory tasks [148] while α_1-adrenergic receptors impaired the working memory [149]. α_2-adrenergic receptors have a higher affinity for NE compared to α_1-adrenergic receptors, thus under normal conditions, NE facilitates working memory performance via actions at α_2-adrenergic receptors in general and also in the PFC. However, dysfunction in noradrenergic pathways emanating from LC may result in low PFC NE levels, affecting working memory [150].

The connectivity from LC to PHG can be considered as a LC-PHG emotional and spatial memory system (Fig.3.4b). The LC-NE system modulates emotional memories, and studies have suggested that emotional memories induce the activation of LC and subsequent NE release [151]. Corticotropin-releasing hormone (CRH) receptors are known play an important role in the coordination of autonomic and electrophysiological responses associated with emotional memories [152], [153]. CRH-immunoreactive fibers were observed in the LC, suggesting that CRH may modulate LC neuronal activity [154], [155]. In fact, many studies [156]–[158] have shown that CRH administered locally into the LC increases LC discharge activity and NE release in its terminal fields. Moreover, an abundant expression of CRH was found in PHG [159]. The first sign of emotional memories was also observed in PHG, and was found to then gradually spread to PFC and other cortical regions [160]. On the other hand, PHG is known to be involved in spatial memory [161]. Noradrenergic neurons within LC have widely distributed, ascending projections to the limbic system including PHG [162]. Thus, the LC-NE system may help trigger the involvement of the PHG in spatial memory. An animal study has indicated that the LC-NE system is necessary for the acquisition of spatial memories [163]. These evidence suggest that the decrease of NE in LC could likely cause dysregulation of the emotional and spatial memory system in the LC-PHG network.

Connectivity paths from LC to the frontal cortex, mediated by sensory visual regions, can be considered as a LC-visual sensory system (Fig.3.4c). Previous works in animal models have shown that the LC-NE system can alter receptive field properties such as velocity tuning, direction selectivity, etc. [164], [165]. Malfunction of the LC-visual sensory network may contribute to deficits in visual assessment [166] .

Connectivity paths from LC to the OFC mediated by MTG can be considered as a LC-MTG language system (Fig.3.4d). A previous study has shown decreased regional cerebral blood flow (rCBF) after ingestion of an α_2-adrenergic agonist drug in the MTG [167]. Given that the noradrenergic system in the brain originates from LC, this suggests that there might exist a noradrenergic pathway between LC and MTG which is impaired in AD. The malfunction of the LC-MTG language system may cause language impairments often observed in AD [168], [169].

It is evident that most of the disrupted connectivity paths emanating from the LC in the brain stem drive OFC either directly or via other systems. OFC is known to play a critical role in memory, emotions, reward, as well as decision-making mechanisms [170], [171]. Disrupted connectivity paths that converge into the OFC were observed in three of the subnetworks, and could potentially underlie behavioral deficits in these domains.

Taken together, we identified LC in the brainstem and OFC as the foci of network disruption in AD. The dysregulation of LC-NE neurotransmission likely contributes to behavioral deficits observed in AD. In corroboration, previous literature has pinpointed the same regions [136], [142] to be affected in AD. Our identification of the LC in the brain stem as the disease focus in AD supports these previous observations and suggests that functional MRI studies of AD, which have been largely cortico-centric [100], [172], must in future investigate the role of this structure in AD.

Previous studies have also identified some other regions to be crucial to AD pathology [90]–[92]. In fact, our foci-identification technique did identify some of the regions reported in these

papers. Specifically, we also identified parahippocampal gyrus, middle frontal gyrus and precuneus as foci only considering DEC networks. Further, middle temporal gyrus, lateral occipital cortex and cerebellum posterior lobe were identified as foci in SEC networks. However, these regions were not identified as foci in both DEC and SEC networks. Acknowledging that previous studies reported regions as having significantly different static connectivity between the groups, in this study we only reported the foci and the associated connectomic network that were found as having impairments in both static and dynamic EC.

Next, we report a few noteworthy limitations of this work. We have based our interpretation on the efferent projections of neurotransmitters arising out of LC. We employed this logic since functional imaging studies of the brain stem (and LC) in AD are limited, with the existing literature employing functional imaging in AD being cortico-centric. However, we have not directly measured norepinephrine in the brain, as it is difficult to do so using MRI. Therefore, our results form the basis for a hypothesis regarding dysfunction in the noradrenergic pathways in AD. Future studies must employ other modalities such as positron emission tomography for *in vivo* imaging of noradrenergic pathways (not just NE deficits) in AD. This could potentially open up possibilities for therapeutic interventions in AD. Further, the proposed methodology of combining static as well as dynamic effective connectivity analysis with probabilistic modeling for identifying dysfunctional foci and associated dysfunctional networks could provide novel insights into the pathophysiology of other brain-based disorders..

4.5 Acknowledgments

Data used in this article were obtained from the Alzheimer's Disease Neuroimaging Initiative (ADNI) database (adni.loni.usc.edu). Investigators within ADNI contributed to design and implementation of ADNI and provided data but did not participate in analysis or writing of this report. Complete listing of ADNI investigators: http://adni.loni.usc.edu/wp-content/uploads/how_to_apply/ADNI_Acknowledgement_List.pdf

Data collection and sharing for this work was funded by ADNI (National Institutes of Health Grant U01 AG024904) and DOD ADNI (Department of Defense award number W81XWH-12-2-0012). ADNI is funded by the National Institute on Aging, the National Institute of Biomedical Imaging and Bioengineering, and through generous contributions from the following: AbbVie, Alzheimer's Association; Alzheimer's Drug Discovery Foundation; Araclon Biotech; BioClinica, Inc.; Biogen; Bristol-Myers Squibb Company; CereSpir, Inc.; Eisai Inc.; Elan Pharmaceuticals, Inc.; Eli Lilly and Company; EuroImmun; F. Hoffmann-La Roche Ltd and its affiliated company Genentech, Inc.; Fujirebio; GE Healthcare; IXICO Ltd.; Janssen Alzheimer Immunotherapy Research & Development, LLC.; Johnson & Johnson Pharmaceutical Research & Development LLC.; Lumosity; Lundbeck; Merck & Co., Inc.; Meso Scale Diagnostics, LLC.; NeuroRx Research; Neurotrack Technologies; Novartis Pharmaceuticals Corporation; Pfizer Inc.; Piramal Imaging; Servier; Takeda Pharmaceutical Company; and Transition Therapeutics. The Canadian Institutes of Health Research is providing funds to support ADNI clinical sites in Canada. Private sector contributions are facilitated by the Foundation for NIH (www.fnih.org). The grantee is the Northern California Institute for Research and Education, and the study is coordinated by Alzheimer's Disease Cooperative Study at the University of California, San Diego. ADNI data are

disseminated by the Laboratory for Neuro Imaging at the University of Southern California, Los Angeles, USA.

CHAPTER 4

Two Separate Brain Networks for Predicting Trainability and Tracking Training-related Plasticity in Working Dogs

4.1 INTRODUCTION

Dogs have been mankind's faithful friends for tens of thousands of years [173] and have been trained by humans for various tasks. For example, sniffer dogs have been trained for detecting explosives, hearing dogs for alerting people who are deaf to important sounds [174], therapy dogs for supporting language-impaired children [175] and those with stress- and anxiety-related disorders [176], etc. Consequently, the ease with which dogs can be trained to perform various tasks, as well as their general behavioral capabilities such as hunting and retrieving, become critical parameters for selecting dogs for training. Despite the importance of canine capabilities to human society and the capital costs incurred in training dogs [177], [178], research into the neural basis of behavior of dogs and their trainability is sparse. Such a research endeavor is important for the following reasons. First, it could potentially lead to procedures involving non-invasive measurement of canine neural function as a criterion for selecting dogs to be trained, thereby limiting capital expenditure on less trainable dogs or dogs with less favorable behavioral capabilities. Second, a scientific account of the neural structures/processes supporting behavior in dogs could be evaluated with respect to similar literature in humans and other species for understanding the evolutionary role of brain-behavior relationships. This comparative evaluation

is particularly relevant for dogs since they are a unique species because they have socially co-evolved with humans for thousands of years [179].

One of the most widely used non-invasive tools for investigating the neural basis of behavior in humans is functional magnetic resonance imaging (fMRI), which is based on the principle that changes in the local concentration of the paramagnetic deoxygenated hemoglobin due to neural activity leads to enhancement in the magnetic resonance signal. Of particular interest to brain-behavioral relationships is the fMRI signal in the absence of a goal-directed task, known as resting state fMRI (RS-fMRI), which displays spatially correlated structure forming distributed brain networks [34]. In humans, the functional connectivity (FC) between brain regions in such networks (measured through temporal correlation between fMRI time series from those regions), has been shown to co-vary with various behavioral variables (e.g., cognitive abilities, attention, working memory, cognitive control) [180]–[184]. In our work, we extend this concept from humans to dogs, and surmised that fMRI-based resting state functional connectivity in brain networks obtained from the dog brain would correlate with canine behavior.

The methodological challenges involved in measuring fMRI-based functional connectivity in the dog brain are quite daunting. First, head movement poses a big problem for fMRI since the displacement of the head from one acquisition to the next, if not corrected for, can appear like a change in image intensity which is unrelated to underlying neural activity. Therefore, fMRI studies employing animals have either immobilized them [185], [186] or anesthetized them. The former reduces the comparative validity of the experiment (e.g., humans are not immobilized) and may make the experiment less ethologically valid, while the latter has been proved to alter neural

activity and connectivity [187], [188]. Therefore, imaging awake dogs is the best workable option. Recent studies have made strides in this regard. Both our group [179], [189]–[191] and three other groups [192]–[204] have been successful in training dogs to keep their head still inside the MRI scanner while fMRI data is acquired. Specifically, we showed the existence of resting state brain networks in dogs by scanning them in a fully conscious and unrestrained state. Critically, we employed optical head motion tracking with an external camera device to record and account for head motion, which is inevitable even if the dog is trained to keep its head still. Using this paradigm enabled us to non-invasively measure whole brain functional connectivity in awake dogs.

The objectives of the current study were twofold. First, we wanted to discover the resting state brain networks whose change in the strength of connectivity during a canine training regimen mirrored corresponding changes in their behavior. Second, we were interested in investigating whether resting state brain networks estimated from fMRI data acquired before the commencement of the training regimen were able to predict whether a given dog would eventually graduate to become a detector dog or not. In order to achieve these objectives, we designed a longitudinal experimental paradigm where fMRI data and behavioral assessments were acquired at multiple time points (TPs) across the time of participation of dogs in this study. The first time point (TP1) was prior to the dogs entering formal working detector dog training, but after 1-3 months of MRI training [189], [191] to keep their head still inside the scanner. The second time point (TP2) was soon after formal detector dog training which lasted about 3 months. The third time point (TP3) was three months post detector dog training while the dogs were engaged in a program of maintenance training for detector dog work. We hypothesized that the correlation between resting state FC in the dog brain and behavior measures would significantly change during their detection

training process (from TP1 to TP2), and would maintain for the subsequent several months of detection work (from TP2 to TP3). This was based on the premise that detection training would lead to strengthening of certain functional connectivities from TP1 to TP2, which would then maintain those FC levels from TP2 to TP3 during maintenance training. Further, the identified paths would also mirror corresponding behavioral improvements from TP1 to TP3 and subsequent maintenance till TP3.

4.2 MATERIALS AND METHODS

Ethical approval for the study was obtained from the Auburn University Institutional Animal Care and Use Committee. We recruited forty dogs (24 males/16 females) with ages in the range of 12 to 36 months from the Auburn University Canine Detection Research Institute and iK9 LLC (www.ik9.com).

4.2.1 Dog Training and Preparation

The dogs for this study came from a working dog acquisition process intended to select dogs that have the potential to be trained successfully for working tasks. A standardized assessment test was used for judging the workability of candidate dogs, and that assessment was also used as a behavioral measure for comparison with fMRI imaging metrics.

Once acquired, the dogs began training for being scanned in the MRI while fully awake and unrestrained. For this purpose, a full-scale MRI simulator was fabricated. Additionally, a couple of simulated human knee coils, into which the dog must learn to place and hold the head, were fabricated for use in training the MRI routine (Fig.4.1).

Fig.4.1 Mock MRI scanner and mock head coil for training dogs.

The training process was separated into two stages. Throughout the first stage of the training process, a recording of the MRI operation sound was played, and the volume of the sound gradually increased until it was similar to an actual scan. Once a dog put its head within the knee coil (Fig.4.2), remained relatively motionless for approximately 5 minutes, and repeated this performance several times across the course of an approximately 30 minutes training session, they were ready for the next stage.

Fig.4.2 A German shepherd dog in the MRI simulator being prompted to place his head in the

mock coil.

The second stage of training was performed inside the real MRI scanner with the running of a functional sequence. Transitioning to the actual MRI went smoothly for some dogs but was more difficult for others. The final target performance for the training was for a dog to voluntarily enter the MRI scanner, position its head into the knee coil and remain relatively motionless for an approximately hour-long session. The time to train the dogs from initial training to successful scan in the actual MRI ranged from 12 hours to 30 hours (on average, about 18 hours), which was divided into several one-hour sessions across days.

4.2.2 Longitudinal Experimental Design

To track the changes in functional imaging metrics with time, all of the fMRI scans and behavioral measures were acquired at multiple time points (TPs) across the time of participation of dogs in this study (Fig.4.3). The first time point (TP1) was prior to the dogs entering formal working detector dog training, but after 1-3 months of MRI training to keep their head still inside the scanner. The second time point (TP2) was soon after formal detector dog training which lasted about 3 months. The third time point (TP3) was three months post detector dog training while the dogs were engaged in a program of maintenance training for detector dog work.

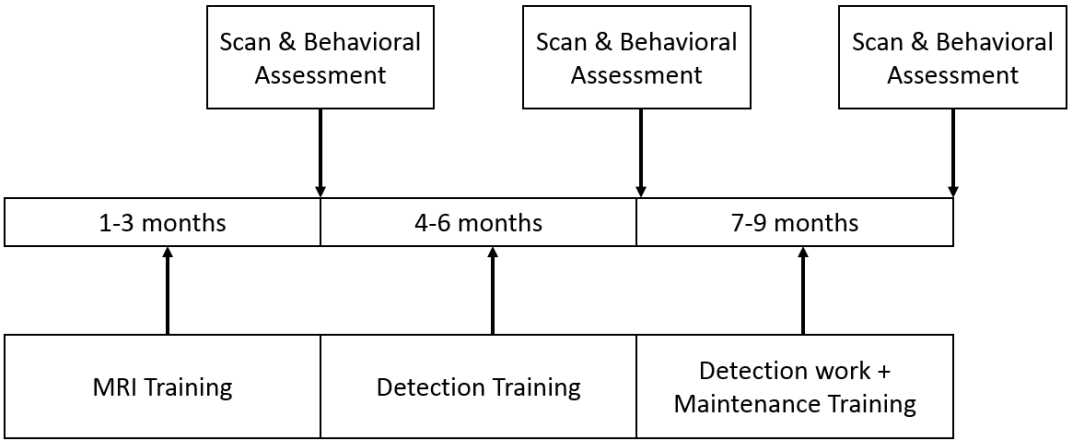

Fig.4.3 A schematic of the longitudinal experimental design.

4.2.3 Working Dog Assessments

All of the dogs in this project were assessed for their potential to be successfully trained and employed for working detector dog tasks. The assessment we employed is a variation of those widely used across many operational agencies (e.g., U.S. Military, Homeland Security agencies, law enforcement agencies) for assessing candidate working dogs. The assessment has two components, performance and environmental soundness [205], [206]. The performance element assessed the propensity of the dog to retrieve a thrown object; interest, focus, and desire to possess a toy reward; the propensity of the dog to use its nose in hunting for a desired object; the amount of effort and degree of distractibility during retrieving and hunting games. The environmental soundness element assessed the extent of startle and ability to recover from sudden loud noises; comfortableness with and ability to overcome initial difficulty with novel surfaces (such as slick floors), obstacles (such as open stairs), and surroundings; reaction to strange/new persons, places, and busy urban settings. A composite score from 1 (low proficiency) to 5 (high proficiency) was assigned for each of the measures: retrieve, hunt and environmental soundness. The scores from all the three measures were aggregated to provide one integrated working dog assessment score

named “Integrated Behavioral Score”. This measure was then used for correlation with imaging metrics.

4.2.4 Data Acquisition

Functional MRI data were acquired using a T_2^*-weighted single shot echo planar imaging (EPI) sequence on a Siemens 3 Tesla Verio scanner (Erlangen, Germany) with 16 axial slices, slice thickness = 3mm, repetition time (TR) = 1000 ms, echo time (TE) = 29 ms, field of view (FOV) = 150×150 mm^2, flip angle (FA) = 90 degree, in-plane resolution 2.3×2.3 mm, in-plane matrix = 64 × 64 and 200 temporal volumes in each run. Two resting state runs were acquired for each dog at each time point. A 15-channel human knee coil was used as a head coil for the dog brain, and all dogs were trained to keep their heads in the coil as still as possible (with eyes open) during the scanning. Anatomical images were acquired using T1-weighted, 3-dimension magnetization-prepared rapid gradient echo (3D-MPRAGE) sequence for overlay and localization (TR = 1990 ms, TE = 2.85 ms, FA = 9 deg, FOV = 152×152×104 mm^3, in-plane matrix = 192×192, number of partitions = 104, for voxel size = 0.8×0.8×1.0 mm^3). All MRI scans included Generalized Autocalibrating Partially Parallel Acquisitions (GRAPPA) with acceleration factor = 2.

The longitudinal training and assessment process (Fig.4.3) was performed in 40 dogs. However, due to the relatively long period of time that the dogs were expected to be in the longitudinal training and assessment process, 10 dogs were released from imaging for behavioral reasons in TP1, 14 dogs were released in TP2, and 16 dogs were released in TP3. Thus, data acquired from all the time points included a total of 154 scans/runs from 30 dogs, with 60 scans

from 30 dogs (17 males/13 females) at TP1, 49 scans from 26 dogs (14 males/12 females) at TP2, and 45 scans from 24 dogs (14 males/10 females) at TP3.

4.2.5 Image Preprocessing

The preprocessing of raw RS-fMRI data was performed using SPM12 and DPARSF tool box [9], [59]. The preprocessing steps included slice-timing correction, realignment to the first functional image (i.e. image-based correction for head motion by aligning 3D volumes acquired at different time-points), spatial normalization, spatial smoothing with a Gaussian kernel of 4×4×4 mm^3 full width at half maximum (FWHM), detrending and temporal band-pass filtering (in the range 0.01-0.1 Hz) for removing low and high frequency sources of noise. Further, variance due to nuisance factors such as the six head motion parameters (3 translations and 3 rotation), as well as white matter and cerebrospinal fluid signals were regressed out from each voxel time series inside the dog brain. Unlike human experiments, spatial normalization in dogs is not straightforward due to lack of a general template such as the MNI template in humans. Existing templates for dogs are derived from less than ten dogs and thus may not capture the head size variability across different breeds (Datta, 2012). Therefore, we used a relatively more accurate two-step spatial normalization method, which was employed in our previous dog fMRI studies [179], [189]–[191].

4.2.6 Characterization of Resting State Brain Networks

Resting state networks are defined as the collection of regions temporally correlated with an anchor or seed region. Consequently, many networks can be defined based on different seed regions and these networks have shown to be correlated with human personality and behavior

[207]–[209]. For example, the Default Mode Network (DMN) has been shown to correlate with traits and capabilities [15], [16], and the Reward Network (RN) has been shown to be correlated with reward and reinforcement learning in humans [207]. However, seed-based connectivity obtained from predefined ROIs is limited by the fact that they do not capture interactions between all brain regions. On the other hand, whole brain voxel-wise functional connectivity provides a more holistic measure and captures functional associations between all voxels in the brain. Therefore, voxel-wise resting state FC was obtained using Pearson's correlation between voxels taken pair wise across the entire brain. For example, if there were N voxels inside the brain of a given dog, then this would result in an $N^2 \times N^2$ voxel-wise connectivity matrix for that dog.

4.2.7 Connectivity-Behavior Correlations across Time-points

Considering that the data acquisition is longitudinal, the dogs were scanned prior to undergoing training for the detection work (TP1), at the conclusion of a standard 3-month course of training for detection work (TP2), and after 3 subsequent months of intermittent detection work and maintenance training (TP3). We hypothesized that the correlation between resting state FC in the dog brain and behavior measures would significantly change during their detection training process (from TP1 to TP2), and would maintain for the subsequent several months of detection work (from TP2 to TP3). This was achieved by two steps (Fig.4.4): 1) the difference of the FC for each subject and path between TP1 and other TPs were correlated with the difference of the corresponding behavioral measures between TP1 and other TPs, respectively. This yielded paths whose resting state connectivity differences $FC_{TP2\text{-}TP1}$ and $FC_{TP3\text{-}TP1}$ significantly correlated ($p<0.05$, uncorrected) with corresponding differences in the integrated behavioral score $IBS_{TP2\text{-}TP1}$ and $IBS_{TP3\text{-}TP1}$, respectively. 2) Among paths satisfying this condition, we retained those paths

whose FC significantly increased ($p<0.05$, uncorrected) from TP1 to TP2, and TP1 to TP3, but did not change significantly from TP2 to TP3. This was based on the premise that detection training would lead to strengthening of certain functional connectivities from TP1 to TP2, which would then maintain those FC levels from TP2 to TP3 during maintenance training. Further, the identified paths would also mirror corresponding behavioral improvements from TP1 to TP3 and subsequent maintenance till TP3. The resting state brain network resulting from this analysis represents the flexible networks which change with the detection training process.

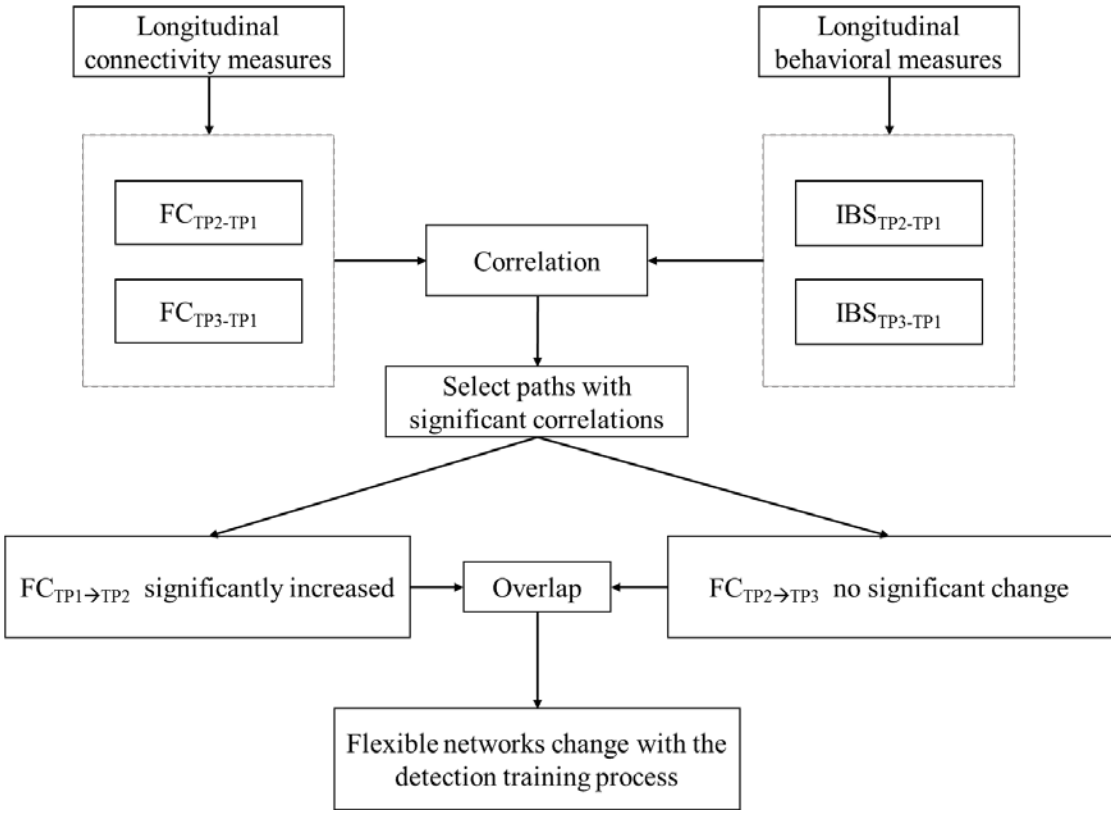

Fig.4.4 A schematic of the two steps connectivity-behavior correlation analysis

4.2.8 Brain Networks Predictive of Dogs' Suitability for Detection Work

Networks that statistically correlate with behavioral changes across time do not necessarily guarantee their ability to predict which dogs are suitable for detection work using pre-training data at TP1. To further study the resting state FC features that can predict the success of training, dogs at TP1 were divided it two groups: the successful group consisting of 13 dogs which were eventually deemed suitable for detection work at the end of the longitudinal training and assessment process (7-9 months post-recruitment, Fig.4.3) and a failure group consisting of 17 dogs which were eventually deemed unsuitable for detection work. FC paths that were significantly stronger ($p<0.01$) in the successful group compared to failure group at TP1 were determined and used as input features to the classifier. This could enhance the quality of classification and ensure that non-discriminatory features are not fed into the classifier.

In order to determine classification accuracy, i.e. the ability of FC features from TP1 identified above to predict whether a given dog would eventually fail or succeed, logistic regression was used as the training kernel since it performed consistently well. Also, using this classifier allowed us to compare our results with a previous study which is similar to ours [196]. The receiver operating characteristic (ROC), which plots the true positive rate (TPR) against false positive rate (FPR) and thus does not depend on a specific threshold, was generated and the area under the curve (AUC) for the ROC was used as a metric for performance evaluation. Four-fold cross validation was employed so that the model could be built using training data and then be tested using validation data. This minimizes the chances of model overfitting.

4.2.9 Identification of Homologous Brain Networks in Humans

In order to better understand the functional roles of paths (and corresponding regions) that correlated with behavioral changes due to detection training, we identified the homologous regions between dogs and humans by comparing the similarity of connectivity fingerprints of these regions using a permutation testing framework (readers are referred to the following papers for details regarding this method: [210], [211]). Connectivity studies often yield high-dimensional profiles that can be hard to summarize. For example, a connectivity fingerprint obtained from a whole brain voxel wise seed based map can have dimensionality equal to the number of voxels in the brain. On the contrary, the connectivity fingerprints proposed by [211] characterize the connections between the 'seed' region with a selected set of other 'target' regions which are important. In this way, connectivity profiles of a seed region can be characterized in a lower dimension which is also useful in avoiding overfitting. We have utilized this concept in our work. Comparing connectivity profiles obtained from data acquired with different scanning parameters for humans and dogs was achieved by normalizing the data to the maximum connection strength in the brain, such that functional connectivity becomes a metric of relative connection strength. Then, a single mean connectivity profile for both the dog and human samples were obtained separately. Using the Manhattan distance measure, we determined the similarity of different fingerprints. Subsequently, the homology between dog and human "seed" region was examined as described below.

Resting state functional connectivity in humans was determined using preprocessed RS-fMRI data from the Human Connectome Projection (HCP) (HCP 500 Subjects + MEG2 Data Release). This dataset included 3T MRI scans from young healthy adults (age range: 22~35 years). We manually selected 154 human subjects to match the number of scans, gender, and age in dog year equivalents (Table.4.1) based on Lebeau's model [212] with our dog group. The raw functional

data obtained from HCP were collected on a Siemens Skyra 3T scanner using multiplexed gradient-echo EPI sequence with slice thickness = 3mm, TR = 720ms, TE = 33.1ms, FA = 52^{o}, FOV = 208×180 mm^{2}, in-plane matrix = 104 × 90 and 1200 temporal volumes in each run. For more details about data acquisition and preprocessing of the data, please see "HCP 500 Subjects + MEG2 Data Release" reference manual (http://www.humanconnectome.org.documentation/S500/HCP_S500+MEG2_Release_Reference_Manual.pdf).

Table.4.1 Matched age for dogs and human subjects

Dogs (months)	Human subjects (years)
12-20	22-25
20-28	25-30
28-36	30-35

To establish connectivity fingerprints for each subject, we predefined 19 "targets" which were ROIs covering most of the cortical regions as well as several subcortical regions (Fig.4.5, Table.4.2) that are known to play a crucial role in guiding canine behavior as borne out by previous dog fMRI studies [189], [191], [199]. The selected "target" regions were: anterior cingulate cortex (ACC), ventromedial prefrontal cortex (vmPFC), bilateral dorsolateral prefrontal cortex (dlPFC), bilateral ventrolateral prefrontal cortex (vlPFC), posterior cingulate cortex (PCC), bilateral inferior parietal lobule (IPL), visual cortex, bilateral caudate, bilateral amygdala, olfactory bulb, bilateral hippocampus and bilateral temporal cortex. The MNI coordinates for these "target" regions in humans are listed in Table.4.2.

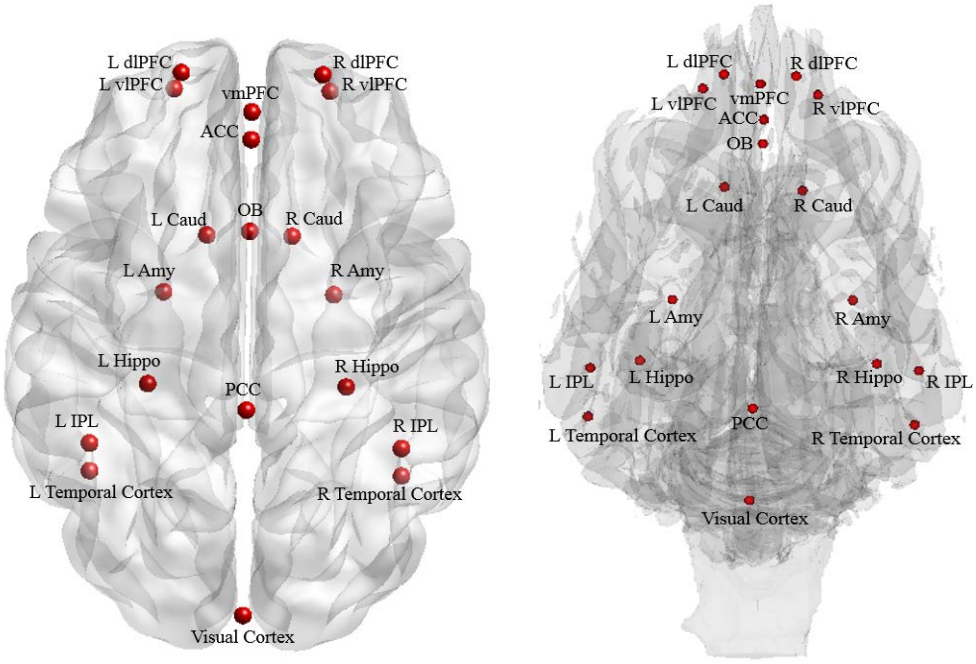

(a) (b)

Fig.4.5 A pictorial spatial representation of "target" regions in human brain (a) and dog brain (b). ROI abbreviations: anterior cingulate cortex (ACC), ventromedial prefrontal cortex (vmPFC), bilateral dorsolateral prefrontal cortex (dlPFC), bilateral ventrolateral prefrontal cortex (vlPFC), posterior cingulate cortex (PCC), bilateral inferior parietal lobule (IPL), bilateral Hippocampus (Hippo), bilateral amygdala (Amy), bilateral caudate (Caud), olfactory bulb (OB)

Table.4.2 Montreal Neurological Institute (MNI) coordinates of "target" regions in humans. ROI abbreviations as in Fig.4.2

	MNI coordinates (x, y, z)		
	X	**Y**	**Z**
ACC	0	40	8
vmPFC	0	50	-7
dlPFC	+/-20	56	28
vlPFC	+/-22	57	-12
PCC	0	-40	27

IPL	+/-44	-52	40
Visual Cortex	0	-94	-6
Caudate	+/-12	12	12
Amygdala	+/-24	0	-20
Olfactory bulb	0	16	-8
Hippocampus	+/-28	-28	-8
Temporal cortex	+/-44	-52	-16

Seed regions in the dog brain were defined as regions involving paths whose changes in connectivity with time correlated with corresponding behavioral changes due to detection training (more on this in the results section). The seed regions in the human brain included every voxel in the human brain. The connectivity fingerprints of "seed" regions for each subject were determined based on the correlation of time series of seed regions (mean time series of seed ROIs in dogs and just the voxel time series in humans) with those of "target" regions. It is noteworthy that the number of "targets" should be sufficient enough to capture the diversity of the connectivity from the seed regions, but should not be too many that might cause overfitting.

Then the Manhattan distance between the averaged connectivity fingerprint of each dog seed and each human seed (averaged over the dog and human samples, respectively) were calculated to determine voxels in the human brain that share the same pattern or fingerprint of connectivity with "seed" regions in dogs (Fig.4.6). Permutation testing was used to test the significant of the match between each of voxels in the human brain and the dog "seed" regions ($p < 0.01$).

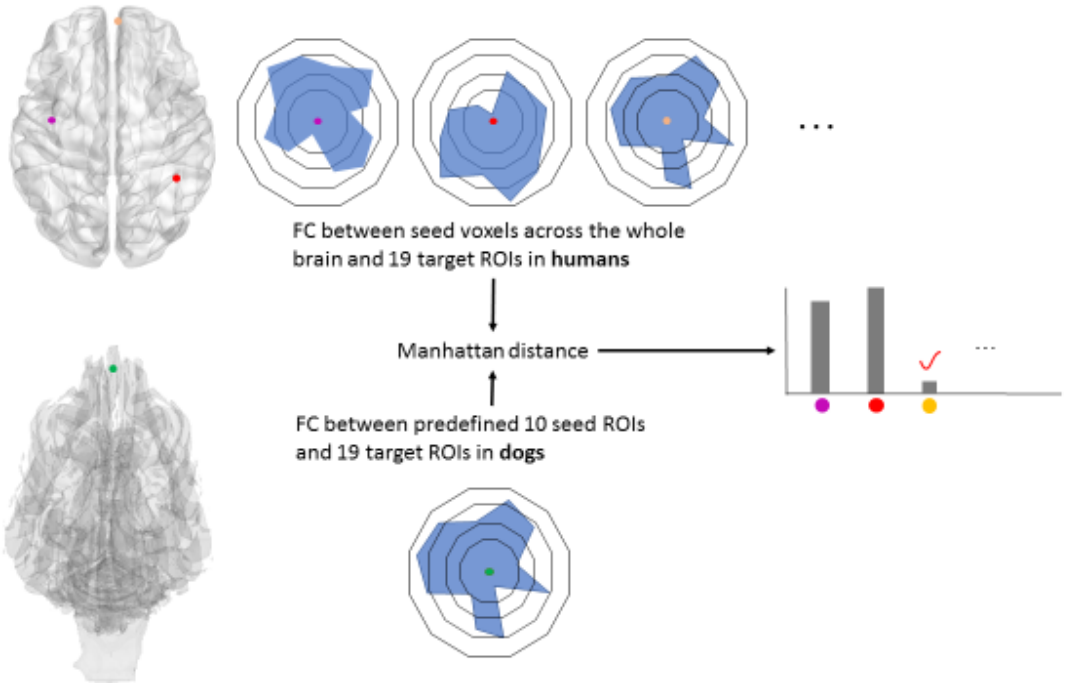

Fig.4.6 A schematic illustration of the connectivity fingerprint matching approach in our study. Each vertex of the polygon indicates individual "target" regions. A connectivity fingerprint of a dog "seed" region (in *green*) is compared to connectivity fingerprints obtained from human "seed" voxels picked from across the entire human brain (here we randomly selected three voxels shown in *yellow*, *purple* and *red* for illustration). The connectivity fingerprints were calculated by estimating resting state functional connectivity between the seed regions and 19 pre-selected target regions. Manhattan distance measure was used to determine the similarity of different fingerprints. In this case, the yellow area in human brain has a connectivity fingerprint with target regions that are most similar to that obtained by the dog "seed" region. Therefore, the yellow voxel in the human brain could potentially be the region homologous to the green seed voxel in the dog brain.

4.3 RESULTS

We identified ten paths in accordance with our hypotheses (Fig.4.7 and Table.4.3). These paths satisfied two different criteria. First, resting state connectivity differences $FC_{TP2\text{-}TP1}$ and $FC_{TP3\text{-}TP1}$

significantly correlated ($p<0.05$, uncorrected) with corresponding differences in the integrated behavioral score $IBS_{TP2-TP1}$ and $IBS_{TP3-TP1}$, respectively (Fig.4.8 and Fig.4.9). Second, the strength of these paths significantly increased ($p<0.05$, uncorrected) due to detection training (from TP1 to TP2) and then maintained from TP2 to TP3 ($p>0.05$) (Fig.4.10 and Table.4.4). This demonstrates that that detection training would lead to strengthening of certain functional connectivities from TP1 to TP2, which would then maintain those FC levels from TP2 to TP3 during maintenance training. Further, the identified paths would mirrored corresponding behavioral improvements from TP1 to TP3 and subsequent maintenance till TP3.

Table.4.3 Functional connectivity paths in the dog brain whose FC values satisfied our hypotheses. *Pyri = pyriform lobe, IPL = inferior parietal lobe, Hippo = hippocampus, Amy = amygdala, Hypo = hypothalamus, MFG = middle frontal gyrus, Caud = caudate, OB = olfactory bulb, DLPFC = dorsolateral prefrontal cortex, IFG = inferior frontal gyrus*

Path No.	Path
1	R Pyri ↔ R IPL
2	L Pyri↔ L IPL
3	L Claustrum/Insula↔ R IPL
4	L Hippo↔ L Amy
5	L Hippo↔ Hypo
6	Brainstem↔ L MFG
7	R Caud↔ L Hippo
8	R Claustrum/Insula↔ OB
9	R DLPFC↔ L IPL
10	OB↔ R IFG

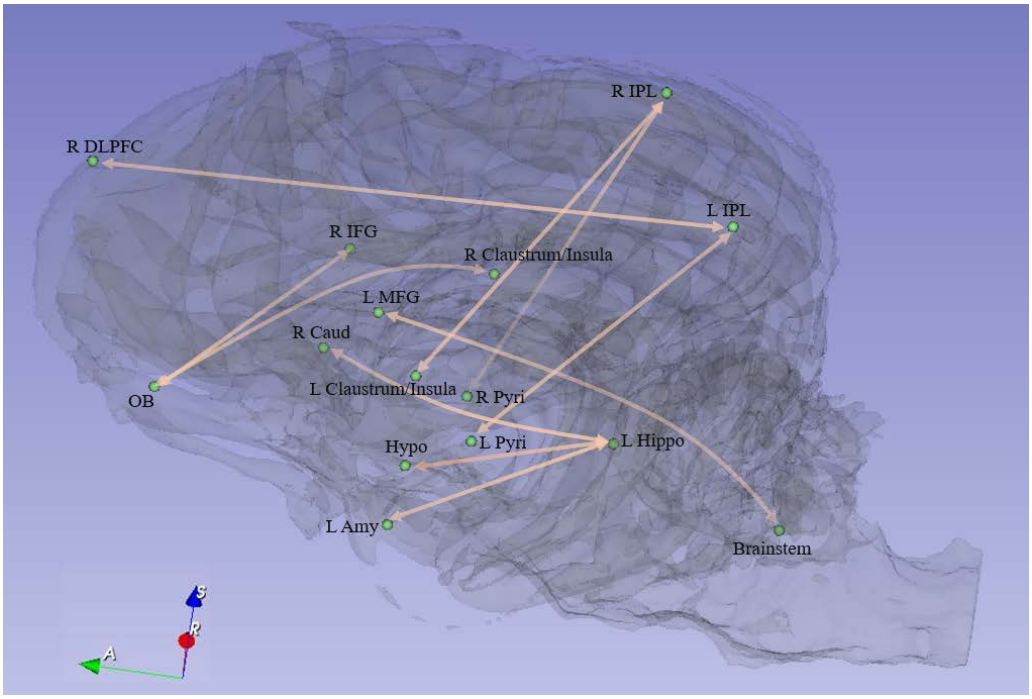

Fig.4.7 Functional connectivity paths in the dog brain whose FC values satisfied our hypotheses. *Pyri = pyriform lobe, IPL = inferior parietal lobe, Hippo = hippocampus, Amy = amygdala, Hypo = hypothalamus, MFG = middle frontal gyrus, Caud = caudate, OB = olfactory bulb, DLPFC = dorsolateral prefrontal cortex, IFG = inferior frontal gyrus.*

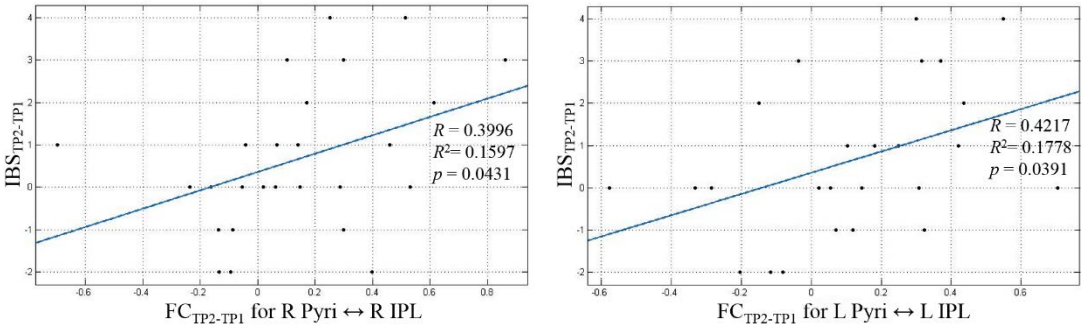

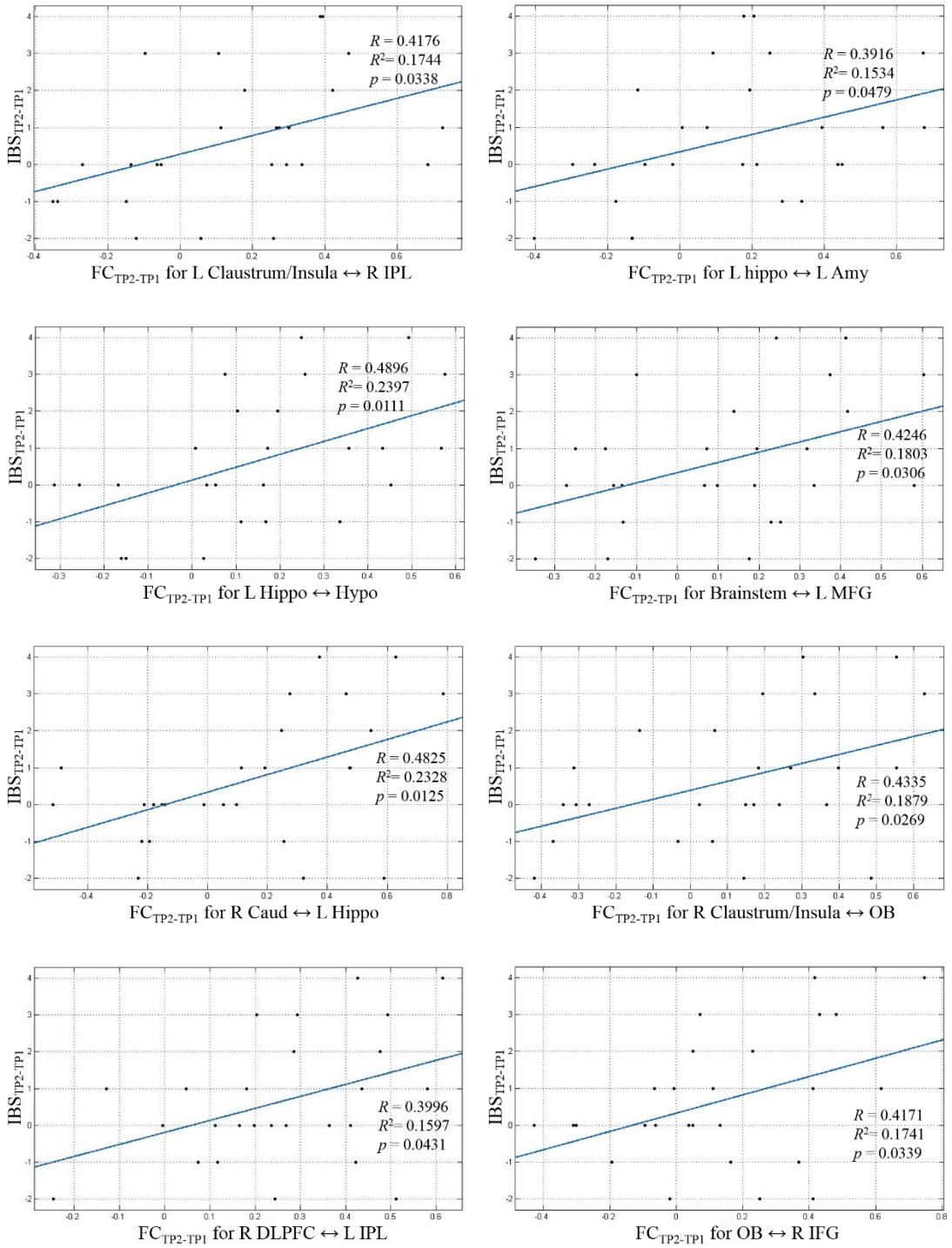

Fig.4.8 Resting state connectivity differences between TP2 and TP1 ($FC_{TP2\text{-}TP1}$) in the dog brain significantly correlated ($p<0.05$, uncorrected) with corresponding differences in the integrated behavioral score $IBS_{TP2\text{-}TP1}$.

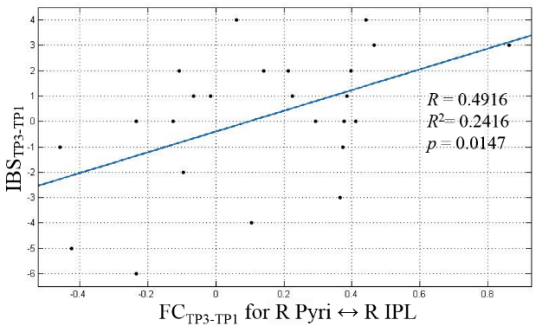
IBS$_{TP3-TP1}$
R = 0.4916
R^2= 0.2416
p = 0.0147
FC$_{TP3-TP1}$ for R Pyri ↔ R IPL

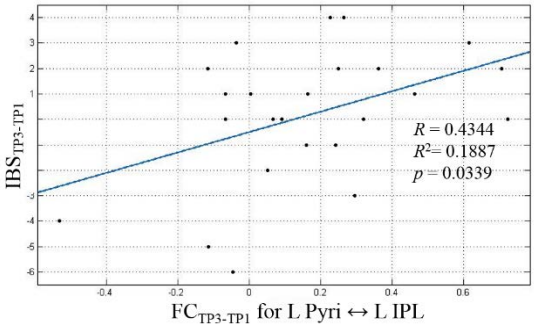
IBS$_{TP3-TP1}$
R = 0.4344
R^2= 0.1887
p = 0.0339
FC$_{TP3-TP1}$ for L Pyri ↔ L IPL

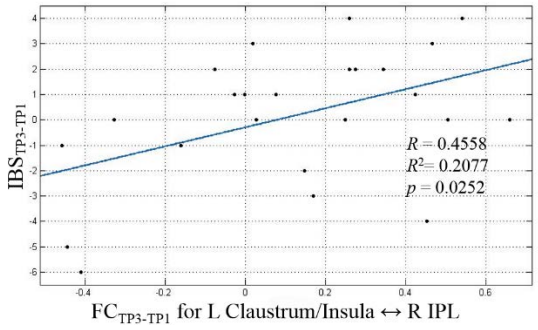
IBS$_{TP3-TP1}$
R = 0.4558
R^2= 0.2077
p = 0.0252
FC$_{TP3-TP1}$ for L Claustrum/Insula ↔ R IPL

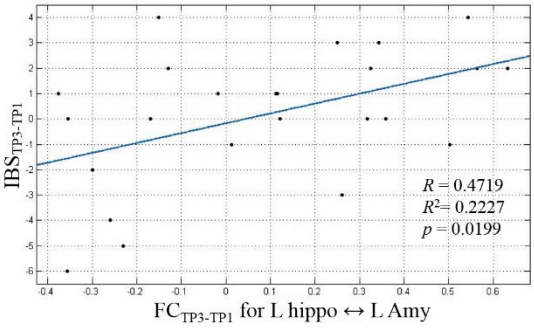
IBS$_{TP3-TP1}$
R = 0.4719
R^2= 0.2227
p = 0.0199
FC$_{TP3-TP1}$ for L hippo ↔ L Amy

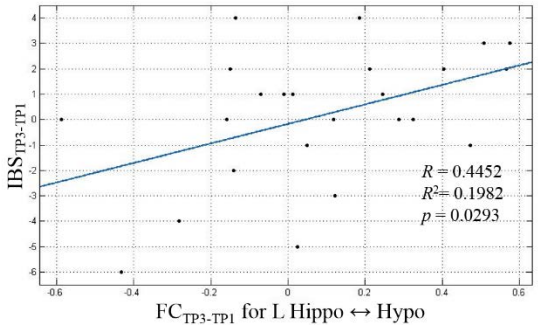
IBS$_{TP3-TP1}$
R = 0.4452
R^2= 0.1982
p = 0.0293
FC$_{TP3-TP1}$ for L Hippo ↔ Hypo

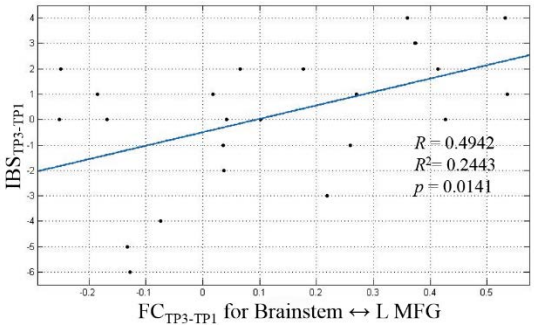
IBS$_{TP3-TP1}$
R = 0.4942
R^2= 0.2443
p = 0.0141
FC$_{TP3-TP1}$ for Brainstem ↔ L MFG

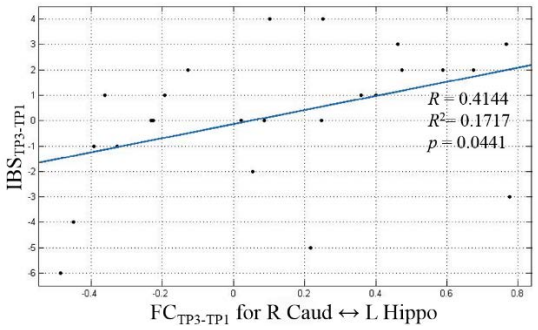
IBS$_{TP3-TP1}$
R = 0.4144
R^2= 0.1717
p = 0.0441
FC$_{TP3-TP1}$ for R Caud ↔ L Hippo

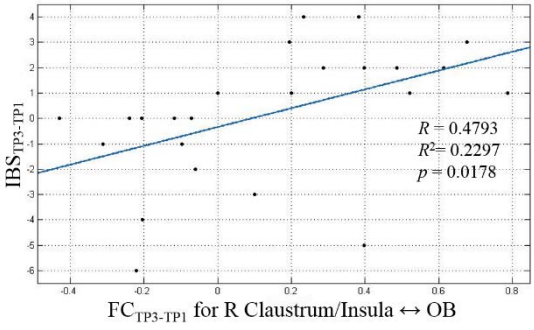
IBS$_{TP3-TP1}$
R = 0.4793
R^2= 0.2297
p = 0.0178
FC$_{TP3-TP1}$ for R Claustrum/Insula ↔ OB

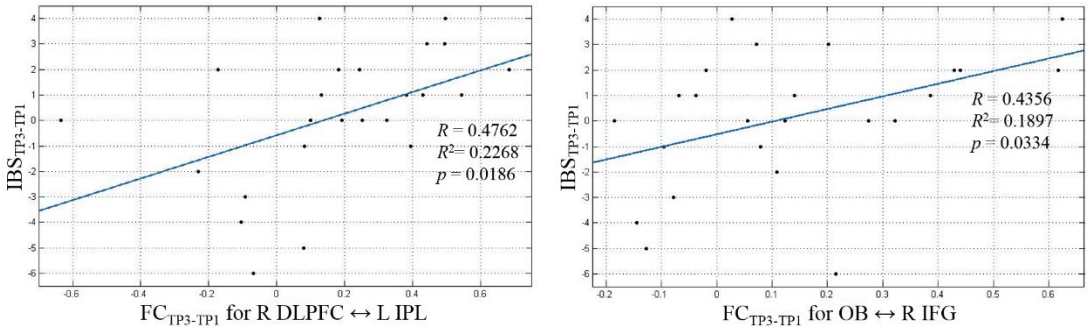

Fig.4.9 Resting state connectivity differences between TP3 and TP1 ($FC_{TP3-TP1}$) in the dog brain significantly correlated ($p<0.05$, uncorrected) with corresponding differences in the integrated behavioral score $IBS_{TP3-TP1}$..

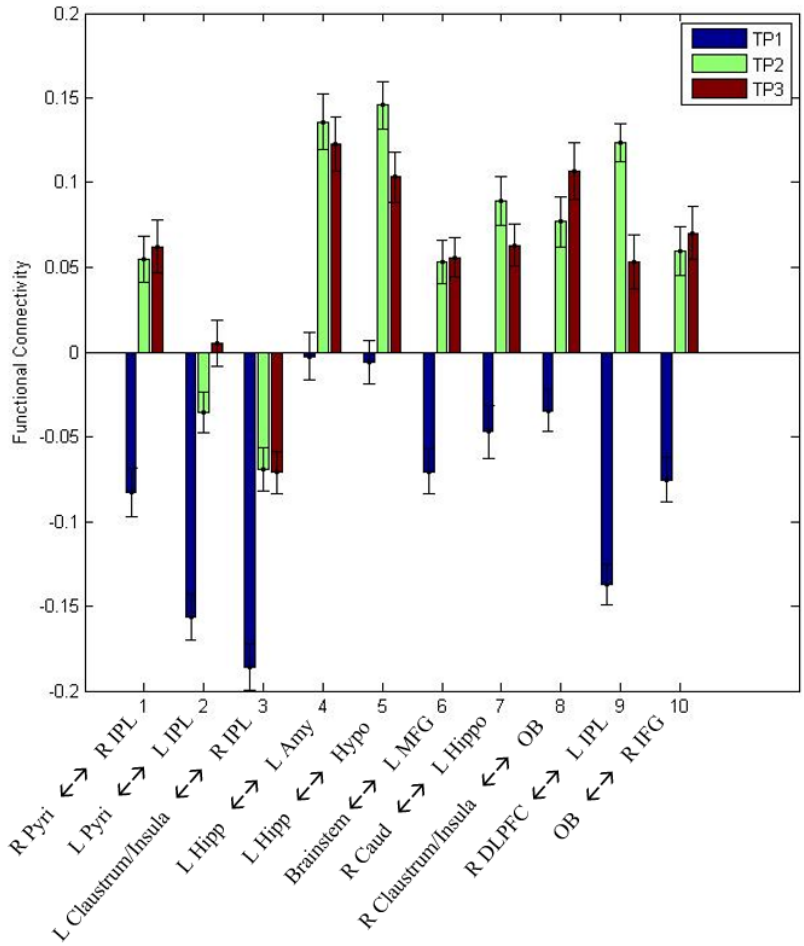

Fig.4.10 FC paths in the dog brain at each time point whose strength significantly increased ($p<0.05$, uncorrected) due to detection training (from TP1 to TP2) and then maintained from TP2

to TP3 ($p>0.05$).

Table.4.4 P-values for differences in the strength of FC across time points for paths shown in Fig.4.10.

	TP2 > TP1	TP3 > TP1	TP2 ≠ TP3
R Pyri ↔ R IPL	1.49×10^{-2}	1.76×10^{-2}	9.12×10^{-1}
L Pyri↔ L IPL	1.83×10^{-2}	5.52×10^{-3}	4.58×10^{-1}
L Claustrum/Insula↔ R IPL	2.66×10^{-2}	3.06×10^{-2}	9.75×10^{-1}
L Hippo↔ L Amy	2.23×10^{-2}	3.53×10^{-2}	8.54×10^{-1}
L Hippo↔ Hypo	7.71×10^{-3}	4.39×10^{-2}	5.18×10^{-1}
Brainstem↔ L MFG	1.69×10^{-2}	1.42×10^{-2}	9.65×10^{-1}
R Caud↔ L Hippo	2.29×10^{-2}	4.61×10^{-2}	6.69×10^{-1}
R Claustrum/Insula↔ OB	3.73×10^{-2}	1.92×10^{-2}	6.79×10^{-1}
R DLPFC↔ L IPL	2.75×10^{-6}	2.17×10^{-3}	2.62×10^{-1}
OB↔ R IFG	1.57×10^{-2}	1.51×10^{-2}	8.72×10^{-1}

To better understand the functional roles of regions in the dog brain connected by paths identified above, corresponding homologous regions in the human brain were determined. This was done because there is a lot more literature about the functional roles of brain regions in the human brain than in the dog brain. We selected 10 “seed” regions from the dog brain based on regions that were connected in the paths identified above (R Pyri, R IPL, L Pyri, L IPL, L Claustrum/Insula, Brainstem, L MFG, R Claustrum/Insula, R DLPFC, and R IFG). The role of many of these regions in canine cognition is unclear due to lack of corresponding literature. After identified the homologous regions in the human brain (Table.4.5), corresponding paths connecting them in the human brain were mapped on a brain surface (Fig.4.11) using BrainNet Viewer software [78].

Table.4.5 Regions of the dog brain connected by paths identified above (in Table.4.3) and

corresponding homologous regions in the human brain with their MNI coordinates

Dog region	Human region	Peak MNI coordinate in human brain		
		x	y	z
R pyriform lobe	R parahippocampal gyrus	14	-8	-22
R inferior parietal lobe	R inferior parietal lobe	36	-46	39
L pyriform	L parahippocampal gyrus	-16	-4	-14
L inferior parietal lobe	L inferior parietal lobe	-38	-44	50
L Claustrum/Insula	L Claustrum/Insula	-38	6	4
Brainstem	Locus Coeruleus in Brainstem	2	-40	-36
L middle frontal gyrus	L middle frontal gyrus	-40	48	14
R Claustrum/Insula	R Insula	40	6	2
R dorsolateral prefrontal cortex	R superior frontal gyrus	16	46	30
R inferior frontal gyrus	R inferior frontal gyrus	60	10	22

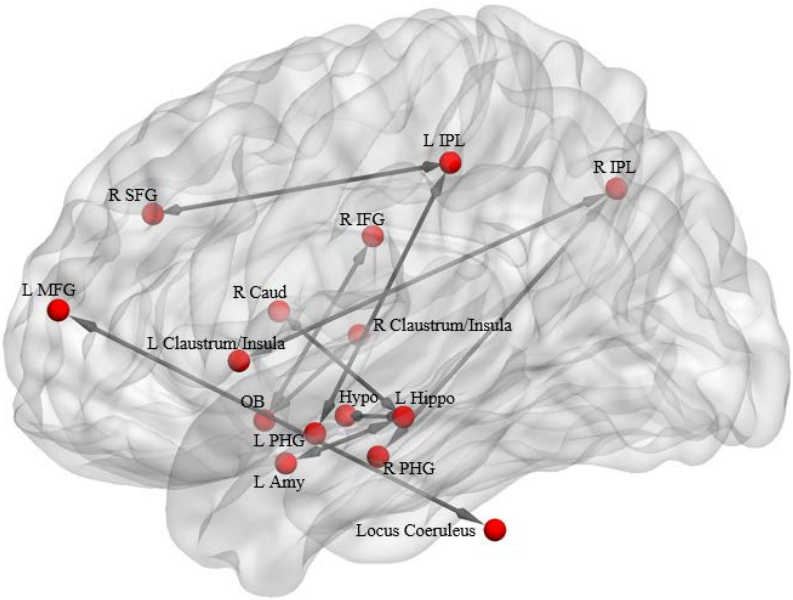

Fig.4.11 A pictorial spatial representation of homologous regions in the human brain identified in Table.4.4. *PHG = parahippocampal gyrus, IPL = inferior parietal lobe, Hippo = hippocampus, Amy = amygdala, Hypo = hypothalamus, MFG = middle frontal gyrus, Caud = caudate, OB =*

olfactory bulb, SFG = superior frontal gyrus, IFG = inferior frontal gyrus

Further, we identified seven paths in the dog brain (Fig.4.12) whose FCs were significantly stronger in the successful group (n = 13) as compared to the failure group (n = 17) at TP1 as well as other time points (Table.4.6, Fig.4.13), but did not change with training (Table.4.7). Among them, six paths were located between Caudate and L MTG. The corresponding homologous regions (Table.4.8) in the human brain and corresponding paths were then mapped on a human brain surface (Fig.4.14).

Table.4.6 Paths in the dog brain whose FC values were significantly stronger ($p<0.01$) in the successful group as compared to the failure group at each time point. *Caud = Caudate, MTG = middle temporal gyrus, STG = superior temporal gyrus*

	P-value of $FC_{successful} > FC_{failure}$		
Path	TP1	TP2	TP3
1-6. Caudate ↔ L MTG	3.38×10^{-4}	2.9×10^{-3}	1.9×10^{-3}
	7.97×10^{-4}	2.1×10^{-3}	1.6×10^{-3}
	8.55×10^{-5}	1.6×10^{-3}	4.1×10^{-3}
	9.91×10^{-5}	9.4×10^{-4}	1.7×10^{-3}
	2.8×10^{-3}	1.6×10^{-3}	1.9×10^{-3}
	3.7×10^{-3}	4.2×10^{-3}	1.8×10^{-3}
7. L Caud ↔ R STG	3.8×10^{-6}	1.9×10^{-3}	4.8×10^{-3}

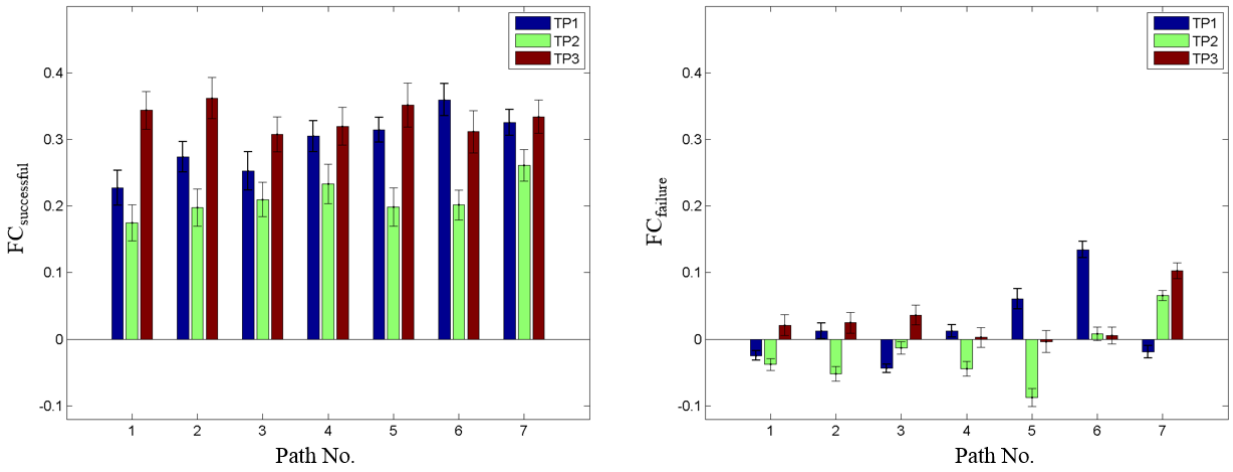

(a) (b)

Fig.4.12 FC paths in the dog brain whose strength was significantly stronger in the successful group (a) as compared to the failure group (b) specifically at TP2, but also at other time points.

Table.4.7 P-values for differences in the strength of FC across time points for paths shown in Fig.4.12. None of them were significant

	P-value of successful group			P-value of failure group		
Path No.	TP1≠TP2	TP1≠TP3	TP2≠TP3	TP1≠TP2	TP1≠TP3	TP2≠TP3
1	5.6×10^{-1}	2.3×10^{-1}	9.5×10^{-2}	7.8×10^{-1}	5.2×10^{-1}	4.4×10^{-1}
2	3.8×10^{-1}	3.5×10^{-1}	1.2×10^{-1}	3.4×10^{-1}	8.7×10^{-1}	3.3×10^{-1}
3	6.4×10^{-1}	5.7×10^{-1}	2.9×10^{-1}	5.1×10^{-1}	2.4×10^{-1}	5.1×10^{-1}
4	4.3×10^{-1}	8.7×10^{-1}	4.1×10^{-1}	3.5×10^{-1}	8.9×10^{-1}	5.4×10^{-1}
5	1.7×10^{-1}	6.9×10^{-1}	1.7×10^{-1}	8.8×10^{-2}	5.1×10^{-1}	3.5×10^{-1}
6	6.2×10^{-2}	6.2×10^{-1}	2.6×10^{-1}	6.3×10^{-2}	9.3×10^{-2}	9.6×10^{-1}
7	3.9×10^{-1}	9.1×10^{-1}	4.1×10^{-1}	1.1×10^{-1}	6.6×10^{-2}	5.4×10^{-1}

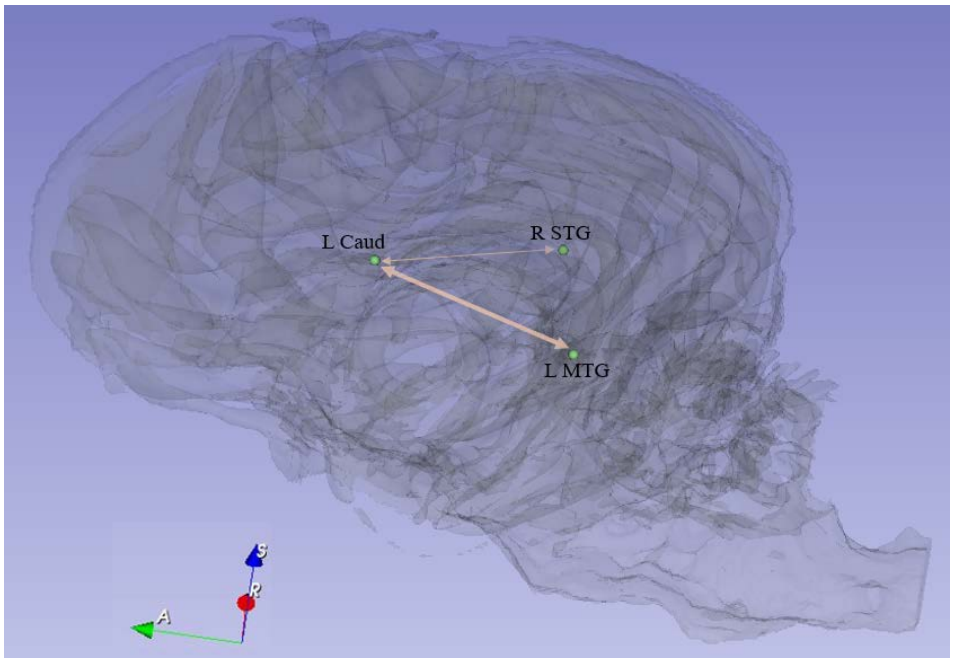

Fig.4.13 A pictorial spatial representation of the paths shown in Table.4.6. The thick line corresponds to multiple paths between L Caud and L MTG while the thin line corresponds to the single connection between L Caud and R STG. *Caud = Caudate, MTG = middle temporal gyrus, STG = superior temporal gyrus*

Table.4.8. Regions of the dog brain connected by paths identified above (in Table.4.6) and corresponding homologous regions in the human brain with their MNI coordinates

Dog region	Human region	Peak MNI coordinate in human brain		
		x	y	z
L caudate	L caudate	-12	2	20
L middle temporal gyrus	L middle temporal gyrus	-58	-46	6
R superior temporal gyrus	R superior temporal gyrus	54	-40	12

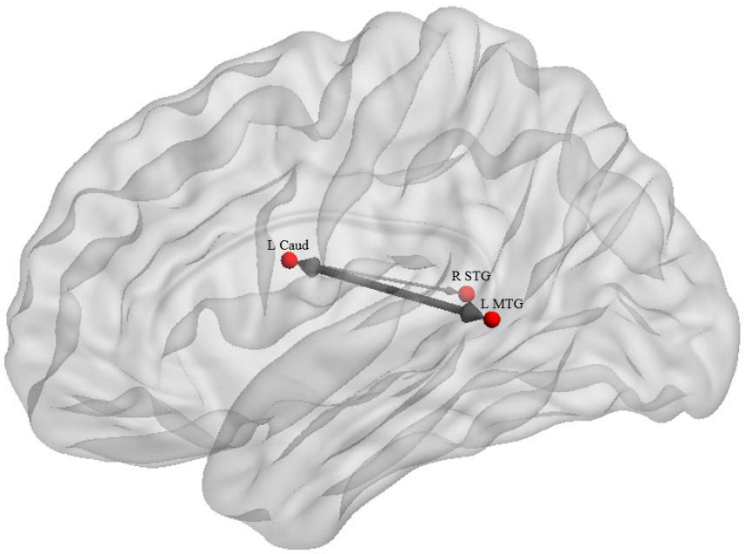

Fig.4.14 A pictorial spatial representation of homologous regions in the human brain identified in Table.4.6. The thick line corresponds to multiple paths between L Caud and L MTG while the thin line corresponds to the single connection between L Caud and R STG. *Caud = Caudate, MTG = middle temporal gyrus, STG = superior temporal gyrus*

Considering that the sample size was relatively small, we performed classification analyses using 1000 iterations of stratified random shuffling with a test size of 25% of the data (4 folds cross-validation). Classifiers with behavior (integrated behavioral score) performed above chance with AUC equal to 0.62 (Fig.4.15, *blue*). Classifiers using functional connections in a flexible neural network in the dog brain which changed with detection training and correlated with corresponding behavioral changes (Table.4.3) also performed above chance with AUC=0.68 (Fig.4.15, *red*). However, best classification performance was achieved using functional connections in a predictive neural network in the dog brain which was significantly stronger in the successful group as compared to the failure group (Table.4.6), but did not change with training (Table 4.7). This network gave an AUC equal to 0.90 (Fig.4.15, *green*).

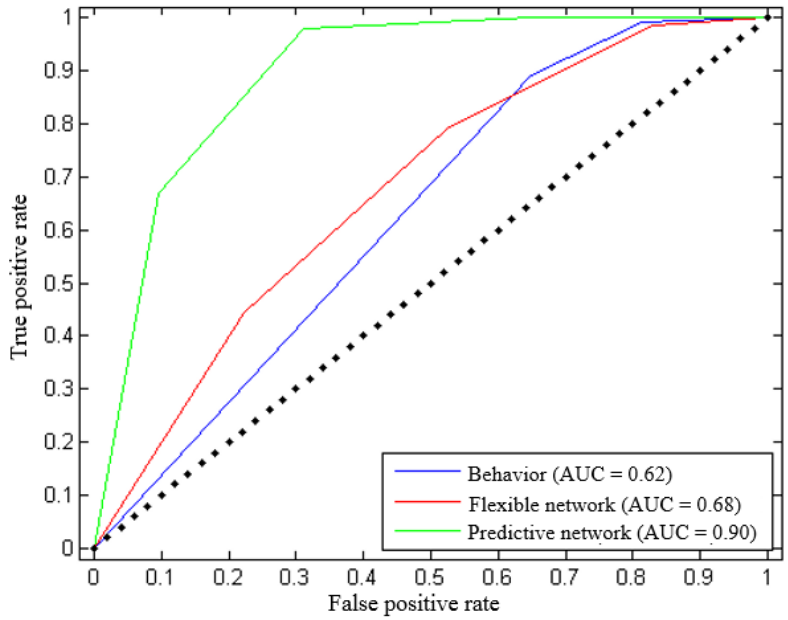

Fig.4.15 ROC plot for the three classifier models used to predict, using data at TP1, whether a dog would eventually be suitable for detection work.

4.4 DISCUSSION

Dogs have a unique ability to interact with humans and this ability has led to dogs working with and assisting humans for various tasks. Therefore, investigations on their general behavioral capabilities and their related neural bases can inform us about critical parameters for selecting dogs for training. However, research into the neural basis of the behavior of dogs, specifically longitudinal investigations, is sparse. This study is the first to our knowledge to explore the neural processes across different training time points at *in vivo* level using resting state fMRI.

Previous studies have shown reconfiguration of brain networks during task learning in humans [213]–[216]. Such regional network dynamics are consistent with a core-periphery model wherein certain brain regions show relatively stable (with respect to time) patterns of interaction that are

necessary for the task performance, while others display relatively flexible patterns that support the learning and changes in task performance [216]. In our work, we extended this concept to the dogs training process and hypothesized that such a core-periphery network may not only mirror changes in behavior with training, but also predict the success of dog training and could potentially be used for selecting dogs to be trained.

We identified two systems, one system (periphery system) consisting of a brain network which strengthened its connectivity with improvements in canine behavior scores after detection training. We believe that this is a flexible system which supports learning related plasticity during the training process. However, the periphery system is not predictive, and its connectivity at the baseline first time point prior to training could not predict whether a given dog could eventually be trained to become a good detector dog. The other system we identified did not show significant changes in its connectivity strength during the training process. However, the strength of connectivity of this core network predicted, with 90% accuracy, whether a given dog would eventually graduate as a detector dog from the training regimen. We speculate that the core stable network may be an endophenotype that is inherited and mainly controlled by genes while the flexible periphery network may be amended by environmental influences [217], [218]. Below, we discuss this core-periphery model in greater detail.

4.4.1 Flexible Periphery Network underlying Detection Training

We found significant correlations between behavioral changes and connectivity changes between the following ROIs: L Amy and L Hippo, L Hippo and Hypo, L Hippo and R Caud (Fig.4.16). Previous human studies [219]–[221] as well as dog studies [189], [191] have implicated

these set of regions during olfactory processing. Further, previous studies have shown that functional connectivity of olfactory-related networks may be reinforced by training, and training-induced behavioral improvement in olfactory performance has been observed in healthy humans [222]. Therefore, this sub-network may be related to improvement in olfactory processing capabilities of dogs during detection training. Additionally, in a meta-analysis study on food-cue neuroimaging, the insula and inferior frontal gyrus were commonly activated by visual and odor food-cue stimulation in humans [223]. Considering that during the training process, dogs were reinforced for successful performance with treats, the increase of FC between the OB and R insula, as well as between the OB and IFG (Fig.4.17) might reflect neural plasticity of conditioning for food-related stimuli.

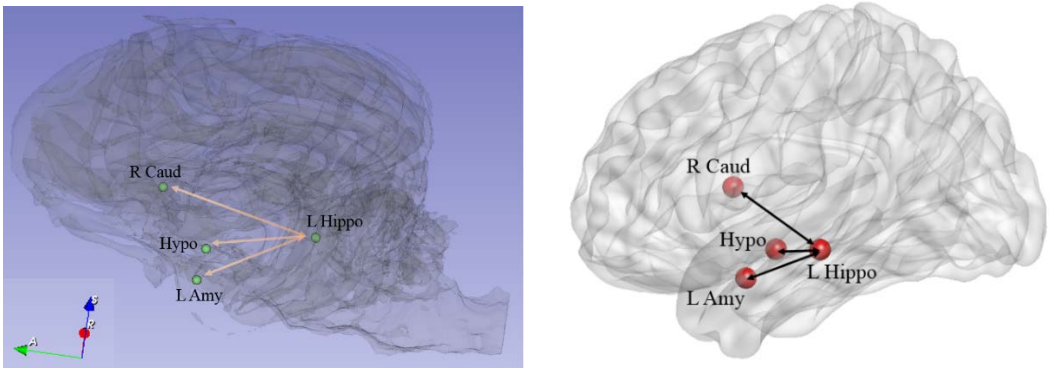

(a) (b)

Fig.4.16 Olfaction-related network in the dog brain (a) and homologous regions in the human brain (b) which showed significant correlations between behavioral changes and connectivity changes. *Hippo = hippocampus, Amy = amygdala, Hypo = hypothalamus, Caud = caudate*

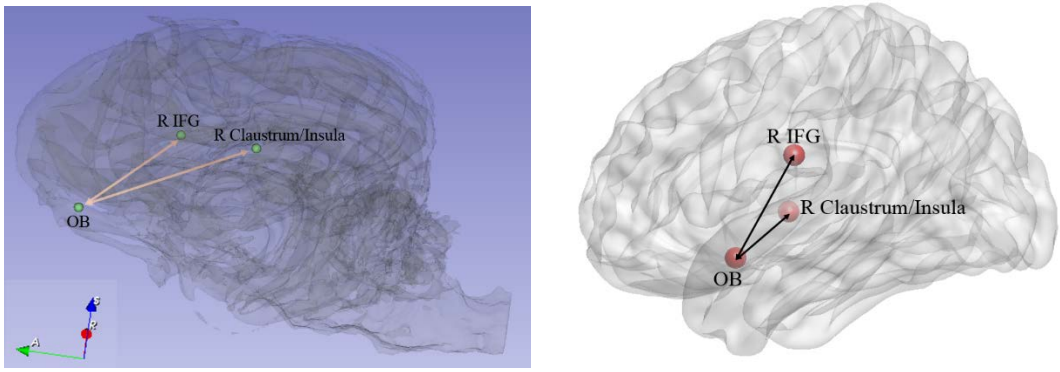

(a) (b)

Fig.4.17 Positive reinforcement network in the dog brain (a) and homologous regions in the human brain (b) which showed significant correlations between behavioral changes and connectivity changes. *OB = olfactory bulb, IFG = inferior frontal gyrus*

Paths from the R SFG to L IPL in the periphery network may be considered to be part of the fronto-parietal network (Fig.4.18). This is consistent with human studies that have shown behavioral variables co-vary with connectivity in frontal-parietal networks (FPN) [180], [181]. Previous human studies have suggested that brain regions in the frontal and parietal cortices played an important role in cognitive control processes and connectivity within the FPN directly relates to attention [224]–[226]. An ICA study has shown greatly overlapped frontal-parietal network in macaque and human brains, suggesting an evolutionary preserved frontal-parietal system [227]. Moreover, studies related to individual human intelligence found that greater connectivity, especially during task performance, within the frontal-parietal network was associated with higher intelligence scores [228], [229].

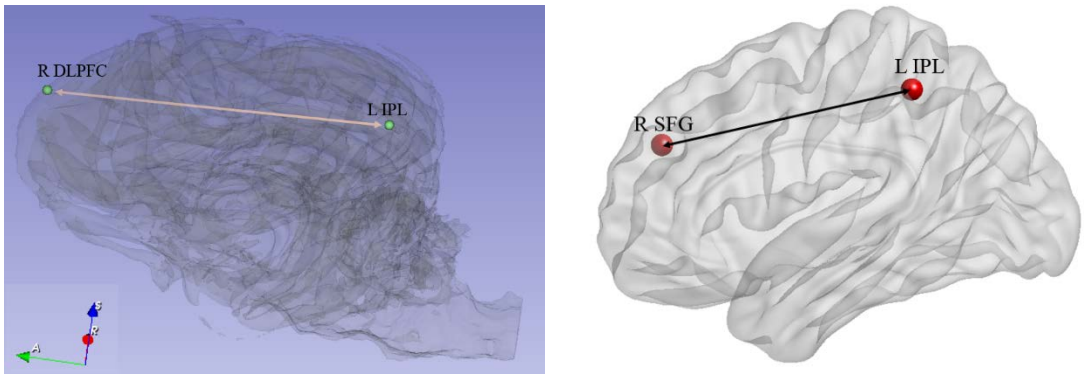

(a) (b)

Fig.4.18 The fronto-parietal network in the dog brain (a) and homologous regions in the human brain (b) which showed significant correlations between behavioral changes and connectivity changes. *DLPFC = dorsolateral prefrontal cortex, IPL = inferior parietal lobe, SFG = superior frontal grrus*

The IPL is known to be associated with familiarity and recollection-related judgments [230]. Also, the PHG and insula are also known to be involved in familiarity-related judgments [231]–[233]. The increase of the FC within the FPN, and between the L insula and IPL, as well as between the PHG and IPL (Fig.4.19) might suggest improved understanding and reaction towards the trainer's gestures and commands through the learning process.

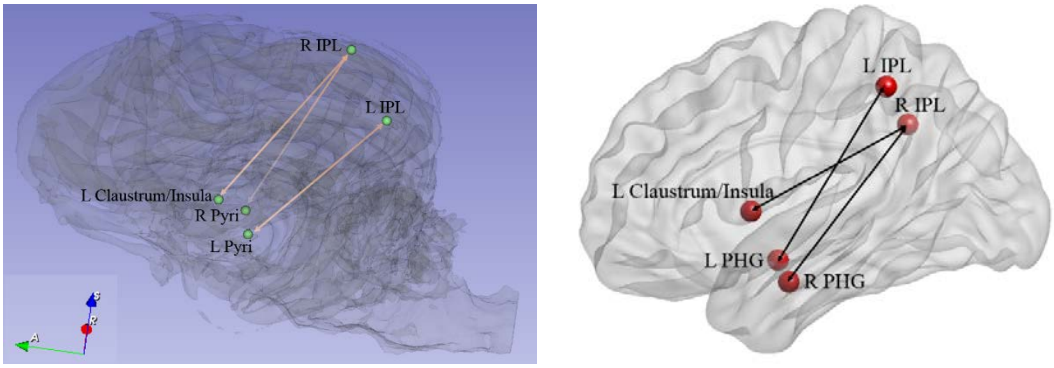

(a) (b)

Fig.4.19 The fronto-parietal network in the dog brain (a) and homologous regions in the human brain (b) which showed significant correlations between behavioral changes and connectivity

changes. *PHG = parahippocampal gyrus, IPL = inferior parietal lobe, Pyri = pyriform lobe*

The Locus coeruleus (LC) in the brain stem is the largest repository of Norepinephrine (NE) in the human brain [133]. Noradrenergic neurons within LC are widely distributed, and one of the main ascending pathways from the LC projects to the prefrontal cortex [134], [135]. It has been shown that NE projections from the LC to the cortex support learning and memory retrieval [234], [235]. An animal study has further found that boosting NE transmission can lead to increased functional connectivity [139]. Thus, the significantly increased FC (from baseline time point to other TPs post detection training) between the LC in the brainstem and L MFG might correspond to the mechanisms of learning of odors and retrieval of such memory.

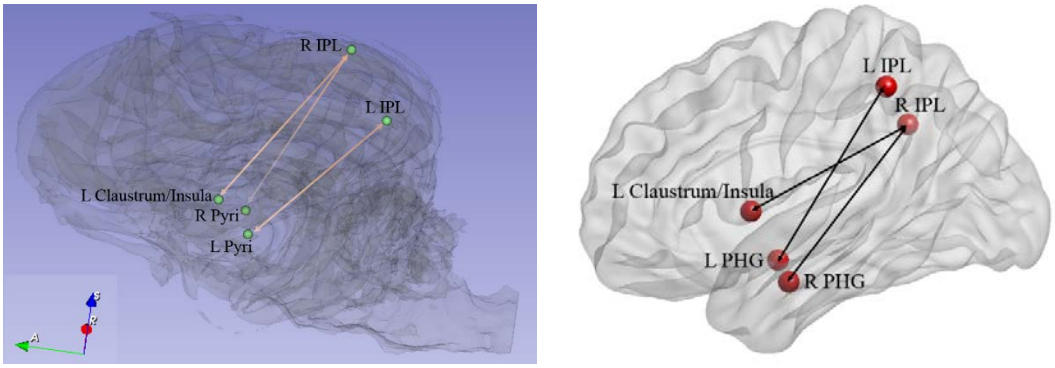

(a) (b)

Fig.4.20 The fronto-parietal network in the dog brain (a) and homologous regions in the human brain (b) which showed significant correlations between behavioral changes and connectivity changes. *MFG = middle frontal gyrus*

4.4.2 Stable Core Network for Predicting Training Outcome

It can be noted that a majority of the paths in the stable core network involved the caudate. Previous studies have considered the caudate as a part of reward system and may reinforce learning

in humans as well as dogs [191], [194], [207]. Studies in humans and monkeys have indicated that regions in the temporal cortex respond preferentially to face recognition [236]. Further, a recent canine study has shown that using fMRI activations from the caudate, amygdala, and a specialized region in the temporal cortex for face processing (known as the dog face area or DFA), the authors were able to predict (with cross-validation) a given dog's suitability for assistance work with an accuracy of 80% [196]. Thus, it is not surprising that we found multiple paths between the L Caud and L MTG in the stable core network that were stronger in the successful group at TP1. Further, the strength of connectivity of these paths at TP1 was able to predict the success of training with an accuracy of 90% using a classifier with cross-validation comparable to the one used by Berns et al, 2016.

The main role of the STG is to process sound stimuli [237]. During the training process, dogs were reinforced for successful performance with treats and verbal reward (trainer praised the dog – "Good dog" or "Yes"). Stronger connectivity between the L Caud and R STG in the successful group might suggest that dogs that were able to associate human verbal praise with reward might have a better chance to be trained as detection dogs.

It should be noted that the caudate was found to be a part of both the core and periphery networks (L Caud in the stable core network and R Caud in flexible periphery network). The factor that prohibits dogs from successful training is believed to be their fearfulness/anxiety towards novel/complex environments [238]. Previous studies have suggested that dopamine D4 receptors influence canine fearfulness, anxiety and impulsivity related traits [239], [240]. Dopamine D4 receptors have been found to be concentrated in the caudate [241]. Since the expression of D4

receptors in the caudate is controlled by specific genes, they might influence fearfulness, anxiety and impulsivity related traits in dogs, thereby influencing baseline neural connectivity between the caudate and other brain regions. This might be a potential mechanism by which the caudate may be involved in the stable core network that predicts whether dogs can be trained to become successful working dogs. On the other hand, the role played by the caudate in reinforcement-based learning in humans is known [242], [243]. Specifically in dogs, Berns et al found that the caudate was significantly more active when the dogs were exposed to different types of reward stimuli [194], [196], [197], [199], [200]. We found an increase in FC between the R caudate and L hippo in periphery network with detection training. Therefore, our findings also support the role of the caudate in learning, reward and training-related neural plasticity.

Taken together, we identified a core-periphery organization in the dog brain and these systems responded differently to the detection training process, which appear to represent ontogeny and phylogeny. The flexible periphery network is ontological, as it changed with corresponding behavioral changes due to training/learning that were mainly located in regions implicated in odor processing. Biologically, the network flexibility might be driven by physiological processes that facilitate the participation of corresponding regions in multiple functional communities while learning new tasks. On the other hand, the caudate based core network is driven more by phylogeny because of its stability across detection training. Such a stable network may contain information about intrinsic learning ability for individuals that can successfully predict the outcome of training. Our result suggests that, upon replication and refinement, fMRI-based resting state brain connectivity may assist in choosing dogs that are more easily trainable for performing detection tasks before they enter the training regimen.

4.4.3 Insights from Human Homology

A basic challenge in animal neuroimaging is to compare and explain brain functions across species, especially at the voxel level. Interpretation often relies on the assumption that putative homologous areas are functionally similar [244]. However, this assumption is not always valid [245] since putative homology is generally not established on any rigorous statistical premise. Previous studies have suggested that specific functions in an area of one species may be shifted to other regions in other species [246]. In this study, we sought to identify the homologous areas by comparing the connectivity fingerprints of regions between humans and dogs [211], [210]. This was done because there is a relatively abundant literature about the functional roles of brain regions in the human brain than in the dog brain. The approach of matching connectivity fingerprints is a viable technique and has been used in a number of studies previously [247], [248].

We identified several regions that do not functionally correspond to their putative homologous regions. For example, the R pyriform lobe, L pyriform lobe and R dorsolateral prefrontal cortex in dogs shared similar connectivity profiles as the R parahippocampal gyrus, L parahippocampal gyrus and R superior frontal gyrus in humans. Moreover, the LC in the human brainstem was identified to be homologous to a specific region of the dog brainstem. With the help of previous human literature, and based on the homology established using the connectivity fingerprint matching procedure, we speculated that the connectivity between the brain stem and the frontal cortex in dogs corresponded to that between the LC and L MFG in humans and this might underlie mechanisms of learning of odors and retrieval of such memory. Despite the lack of abundant literature into the neural basis of behaviors of dogs and their trainability, projecting dog brain

regions identified here onto the human brain, and evaluating similar literature in humans may help us better understand the evolutionary role of brain-behavior relationships. This comparative evaluation is particularly relevant for dogs since they are a rare species which has socially co-evolved with humans for thousands of years.

4.5 Limitations

A few limitations of this work are noteworthy. Although the number of dogs is comparatively large, the sample size is still considered small which did not allow us to use stringent p-value thresholds. However, the identified dog core-periphery model could provide a window into the evolutionary role of brain-behavior relationships and provides great potential in answering questions about phylogeny and ontogeny. It should be noted that no significant gender differences were found in the identified two systems in our study; however, future studies should aim to replicate our findings in different breeds of dog. Further, we have compared our classification results with that from a previous study [194]. However, here we studied detection dogs while they focused on service dogs. Therefore, comparison of our results with those reported by Berns et al is qualitative at best.

4.6 Acknowledgments

Funding from Auburn University's Intramural Grant and from the Defense Advanced Research Projects Agency (government contract/grant number W911QX-13-C-0123) is gratefully acknowledged. The views, opinions, and/or findings contained in this article are those of the authors and should not be interpreted as representing the official views or policies, either expressed

or implied, of the Defense Advanced Research Projects Agency, US Department of Defense or the federal Government of the United States.

CHAPTER 5

Conclusions

The main purpose of this work was to characterize brain functions based on connectivity analysis in human and dogs. We employed multiple approaches to identify brain-based biomarkers of Alzheimer's disease. Further, considering that functional brain connectivity based on resting state fMRI had been shown to be correlated with human personality and behavior, we sought to identify whether capabilities and traits in dogs can be predicted from their resting state connectivity as in humans. The main contributions of this work are:

1. Using Middlemen Power and effective connectivity modeling, we identified Lateral Occipital Cortex and Left Orbitofrontal Cortex that significantly decreased with the deterioration of the disease. Betweenness Centrality only found Lateral Occipital Cortex. We showed that the Middlemen Power of LOC and L OFC, and Betweenness Centrality of LOC also correlated significantly with behavioral scores, indicating their relevance to underlying pathology. We suggested that Middlemen Power might be a better local nodal characteristic compared to BC and, directed networks seem to be more sensitive than undirected networks.
2. Using static and dynamic effective connectivity modeling, we identified focal directed connectivity deficits in AD compared to healthy controls. We characterized group differences using a (between-subject) generative model of pathology, which generates

latent connectivity variables that best explain the (within-subject) directed connectivity. Crucially, our generative model at the second (between-subject) level explains connectivity in terms of local or regionally specific abnormalities. This allows us to explain disconnections among multiple regions in terms of regionally specific pathology; thereby offering a target for therapeutic intervention. We identified two foci, locus coeruleus in the brain stem and right orbitofrontal cortex. We further partitioned the aberrant connectomic network into four unique sub-networks and explained how the dysfunction of foci cause symptoms commonly observed in AD.

3. We designed a longitudinal experimental paradigm where fMRI data and behavioral assessments were acquired at multiple time points (TPs) across the time of participation of dogs in this study. We discovered the resting state brain networks whose change in the strength of connectivity during a canine training regimen mirrored corresponding changes in their behavior. We also investigated whether resting state brain networks estimated from fMRI data acquired before the commencement of the training regimen were able to predict whether a given dog would eventually graduate to become a detector dog or not. We identified the homologous areas by comparing the connectivity fingerprints of regions between humans and dogs. Despite the lack of abundant literature into the neural basis of behaviors of dogs and their trainability, projecting dog brain regions identified here onto the human brain, and evaluating similar literature in humans may help us better understand the evolutionary role of brain-behavior relationships. This study is the first to our knowledge to explore the neural processes across different training time points at in vivo level using resting state fMRI.

CHAPTER 6

Information on Peer-Reviewed Publications

6.1 Peer-reviewed Journal publications

For review:

S Zhao, P Liang, G Deshpande, "Deterioration from Healthy to Mild Cognitive Impairment and Alzheimer's Disease Mirrored in Corresponding Loss of Centrality in Directed Brain Networks", ***IEEE Transactions on Neural Systems and Rehabilitation Engineering***, 2017 (revisions awaited)

(From Chapter-2)

S Zhao, B Ramaiahgai, A Thompkins, P Waggoner, R Beyers, E Morrison, V Vodynaoy, TS Denney Jr., JS Katz, G Deshpande, "Two Separate Brain Networks for Predicting Trainability and Tracking Training-related Plasticity in Working Dogs", ***Neuroimage*** (under preparation)

(From Chapter-4)

Accepted:

S Zhao, D Rangaprakash, A Venkataraman, P Liang, G Deshpande, "Investigating Focal Connectivity Deficits in Alzheimer's Disease using Directional Brain Networks Derived from Resting-State fMRI". ***Frontiers in Aging Neuroscience***, 2017 (in press)

(From Chapter-3)

S Lacey, R Stilla, G Deshpande, S Zhao, C Stepehsn, K McCormick, D Kemmerer, K Sathian, “Engagement of the left extrastriate body area during body-part metaphor comprehension”, ***Brain and Language***, vol. 166, pp. 1-18 2016

P Liang*, G Deshpande*, S Zhao, J Liu, X Hu, K Li, “Altered directional connectivity between emotion network and motor network in Parkinson’s disease with depression”, ***Medicine***, vol. 95(30), pp. e4222, 2016. * joint first authors

6.2 Peer-reviewed Conference proceedings

Sinan Zhao, Peipeng Liang, Gopikrishna Deshpande, “Identifying Brain Connectomic Alterations Specific to Mild Cognitive Impairment and Depression Co-morbid with Parkinson’s Disease”, *Annual Mtg of ISMRM*, 2016

S Zhao, CK Kumar, DN Dutt, P Liang, G Deshpande, "Deterioration from Healthy to Mild Cognitive Impairment and Alzheimer’s disease Mirrored in Corresponding Loss of Centrality in Directed Brain Networks", *Annual Mtg of ISMRM*, 2015
(Chapter-2)

S. Zhao, A. Venkataraman, P. Liang and G. Deshpande. Investigating the Role of Brain Stem in Alzheimers Disease using Directional Brain Networks derived from Resting State fMRI, *Annual Mtg of ISMRM*, 2015.
(Chapter-3)

T Shi, S Zhao, J Anglin, P Lanka, A Thompkins, L Lazarowski, O Pustovyy, Y Wang, P Waggoner, R Beyers, J Fleming, L Benecke, P Hammond, N Salibi, E Morrison, TS Denney, V Vodyanoy, JS Katz, G Deshpande, “Predicting Dogs’ Training Ease and Behavior using their fMRI-based Neural Responses”, *Annual Mtg of OHBM*, 2015

(Chapter-4)

Bibliography

[1] A. Filler, “The History, Development and Impact of Computed Imaging in Neurological Diagnosis and Neurosurgery: CT, MRI, and DTI,” *Nat. Preced.*, pp. 1–76, 2009.

[2] E. M. Haacke, R. W. Brown, M. R. Thompson, and R. Venkatesan, *Magnetic Resonance Imaging: Physical Principles and Sequence Design*, vol. 1st. 1999.

[3] D. B. Twieg, “The k-trajectory formulation of the NMR imaging process with applications in analysis and synthesis of imaging methods.,” *Med. Phys.*, vol. 10, no. 5, pp. 610–21, 1982.

[4] W. Golder, “Magnetic resonance spectroscopy in clinical oncology,” *Onkologie*, vol. 27, no. 3, pp. 304–309, 2004.

[5] R. B. Buxton, “Introduction to Functional Magnetic Resonance Imaging: Principles and Techniques,” *Energy*, vol. 24, no. 2, p. xi, 523 , 2002.

[6] S.-G. Kim and K. Ugurbil, “Functional magnetic resonance imaging of the human brain,” *J. Neurosci. Methods*, vol. 74, no. 2, pp. 229–243, 1997.

[7] S. Ogawa and T. Lee, “Brain magnetic resonance imaging with contrast dependent on blood oxygenation,” *Proc. …*, vol. 87, no. 24, pp. 9868–72, 1990.

[8] K. Bush and J. Cisler, “Decoding neural events from fMRI BOLD signal: a comparison of existing approaches and development of a new algorithm,” *Magn. Reson. Imaging*, vol. 31, no. 6, pp. 976–989, 2013.

[9] Y. Chao-Gan and Z. Yu-Feng, “DPARSF: A MATLAB Toolbox for ‘Pipeline’ Data Analysis of Resting-State fMRI.,” *Front. Syst. Neurosci.*, vol. 4, no. May, p. 13, 2010.

[10] K. J. Friston, *Statistical Parametric Mapping: The Analysis of Functional Brain Images*. 2006.

[11] X.-W. Song, Z.-Y. Dong, X.-Y. Long, S.-F. Li, X.-N. Zuo, C.-Z. Zhu, Y. He, C.-G. Yan, and Y.-F. Zang, “REST: a toolkit for resting-state functional magnetic resonance imaging

data processing.," *PLoS One*, vol. 6, no. 9, p. e25031, 2011.

[12] J. L. Lancaster, D. Tordesillas-Guti??rrez, M. Martinez, F. Salinas, A. Evans, K. Zilles, J. C. Mazziotta, and P. T. Fox, "Bias between MNI and talairach coordinates analyzed using the ICBM-152 brain template," *Hum. Brain Mapp.*, vol. 28, no. 11, pp. 1194–1205, 2007.

[13] G. Wu, W. Liao, S. Stramaglia, J.-R. Ding, H. Chen, and D. Marinazzo, "A blind deconvolution approach to recover effective connectivity brain networks from resting state fMRI data.," *Med. Image Anal.*, vol. 17, no. 3, pp. 365–74, 2013.

[14] C. F. Beckmann, M. DeLuca, J. T. Devlin, and S. M. Smith, "Investigations into resting-state connectivity using independent component analysis.," *Philos. Trans. R. Soc. Lond. B. Biol. Sci.*, vol. 360, no. 1457, pp. 1001–13, 2005.

[15] M. D. Fox and M. E. Raichle, "Spontaneous fluctuations in brain activity observed with functional magnetic resonance imaging," *Nat Rev Neurosci*, vol. 8, no. 9, pp. 700–711, 2007.

[16] M. E. Raichle, A. M. MacLeod, A. Z. Snyder, W. J. Powers, D. A. Gusnard, and G. L. Shulman, "A default mode of brain function.," *Proceedings of the National Academy of Sciences of the United States of America*, vol. 98, no. 2, pp. 676–82, 2001.

[17] G. Deshpande, K. Sathian, and X. Hu, "Effect of hemodynamic variability on Granger causality analysis of fMRI," *Neuroimage*, vol. 52, no. 3, pp. 884–896, 2010.

[18] O. David, I. Guillemain, S. Saillet, S. Reyt, C. Deransart, C. Segebarth, and A. Depaulis, "Identifying neural drivers with functional MRI: an electrophysiological validation.," *PLoS Biol.*, vol. 6, no. 12, pp. 2683–97, 2008.

[19] R. B. Buxton, K. Uludağ, D. J. Dubowitz, and T. T. Liu, "Modeling the hemodynamic response to brain activation," in *NeuroImage*, 2004, vol. 23, no. SUPPL. 1.

[20] A. Mechelli, C. J. Price, and K. J. Friston, "{N}onlinear coupling between evoked r{CBF} and {BOLD} signals: a simulation study of hemodynamic responses.," *Neuroimage*, vol. 14, no. 4, pp. 862–872, 2001.

[21] K. J. Friston, A. Mechelli, R. Turner, and C. J. Price, "Nonlinear responses in fMRI: the Balloon model, Volterra kernels, and other hemodynamics," *Neuroimage*, vol. 12, no. 4, pp. 466–77, 2000.

[22] S. Ryali, T. Chen, K. Supekar, and V. Menon, "Estimation of functional connectivity in fMRI data using stability selection-based sparse partial correlation with elastic net penalty,"

Neuroimage, vol. 59, no. 4, pp. 3852–3861, 2012.

[23] D. Weinshenker, "Functional consequences of locus coeruleus degeneration in Alzheimer's disease.," *Curr. Alzheimer Res.*, vol. 5, no. 3, pp. 342–5, 2008.

[24] S. Owen and G. Robert, "Critical Nodes In Directed Networks," *arXiv Prepr. arXiv1401.0655*, no. January, 2014.

[25] H. Jia, X. Hu, and G. Deshpande, "Behavioral relevance of the dynamics of the functional brain connectome.," *Brain Connect.*, vol. 4, no. 9, pp. 741–59, 2014.

[26] R. M. Hutchison, T. Womelsdorf, E. A. Allen, P. A. Bandettini, V. D. Calhoun, M. Corbetta, S. Della Penna, J. H. Duyn, G. H. Glover, J. Gonzalez-Castillo, D. A. Handwerker, S. Keilholz, V. Kiviniemi, D. A. Leopold, F. de Pasquale, O. Sporns, M. Walter, and C. Chang, "Dynamic functional connectivity: Promise, issues, and interpretations," *Neuroimage*, vol. 80, pp. 360–378, 2013.

[27] K. Blennow, M. J. de Leon, and H. Zetterberg, "Alzheimer's disease," *Lancet*, vol. 368, no. 9533, pp. 387–403, 2006.

[28] S. G. Mueller, M. W. Weiner, L. J. Thal, R. C. Petersen, C. Jack, W. Jagust, J. Q. Trojanowski, A. W. Toga, and L. Beckett, "The Alzheimer's disease neuroimaging initiative," *Neuroimaging Clinics of North America*, vol. 15, no. 4. pp. 869–877, 2005.

[29] M. W. Weiner, P. S. Aisen, C. R. Jack, W. J. Jagust, J. Q. Trojanowski, L. Shaw, A. J. Saykin, J. C. Morris, N. Cairns, L. A. Beckett, A. Toga, R. Green, S. Walter, H. Soares, P. Snyder, E. Siemers, W. Potter, P. E. Cole, and M. Schmidt, "The Alzheimer's disease neuroimaging initiative: progress report and future plans.," *Alzheimers. Dement.*, vol. 6, no. 3, p. 202–11.e7, 2010.

[30] D. Tosun, N. Schuff, C. A. Mathis, W. Jagust, and M. W. Weiner, "Spatial patterns of brain amyloid-beta burden and atrophy rate associations in mild cognitive impairment.," *Brain*, vol. 134, no. Pt 4, pp. 1077–88, 2011.

[31] R. C. Petersen, R. Doody, a Kurz, R. C. Mohs, J. C. Morris, P. V Rabins, K. Ritchie, M. Rossor, L. Thal, and B. Winblad, "Current concepts in mild cognitive impairment.," *Arch. Neurol.*, vol. 58, pp. 1985–1992, 2001.

[32] I. K. Amlien, A. M. Fjell, K. B. Walhovd, P. Selnes, V. Stenset, R. Grambaite, A. Bjørnerud, P. Due-Tønnessen, A. Skinningsrud, L. Gjerstad, I. Reinvang, and T. Fladby, "Mild cognitive impairment: cerebrospinal fluid tau biomarker pathologic levels and longitudinal

changes in white matter integrity.," *Radiology*, vol. 266, no. 1, pp. 295–303, 2013.

[33] G. Douaud, R. a L. Menke, A. Gass, A. U. Monsch, A. Rao, B. Whitcher, G. Zamboni, P. M. Matthews, M. Sollberger, and S. Smith, "Brain microstructure reveals early abnormalities more than two years prior to clinical progression from mild cognitive impairment to Alzheimer's disease.," *J. Neurosci.*, vol. 33, no. 5, pp. 2147–55, 2013.

[34] B. Biswal, F. Z. Yetkin, V. M. Haughton, and J. S. Hyde, "Functional connectivity in the motor cortex of resting human brain using echo-planar MRI.," *Magn. Reson. Med.*, vol. 34, no. 4, pp. 537–541, 1995.

[35] G. Deshpande, P. Santhanam, and X. Hu, "Instantaneous and causal connectivity in resting state brain networks derived from functional MRI data," *Neuroimage*, vol. 54, no. 2, pp. 1043–1052, 2011.

[36] P. Liang, Z. Li, G. Deshpande, Z. Wang, X. Hu, and K. Li, "Altered causal connectivity of resting state brain networks in amnesic MCI," *PLoS One*, vol. 9, no. 3, 2014.

[37] K. Supekar, V. Menon, D. Rubin, M. Musen, and M. D. Greicius, "Network analysis of intrinsic functional brain connectivity in Alzheimer's disease," *PLoS Comput. Biol.*, vol. 4, no. 6, 2008.

[38] K. Wang, M. Liang, L. Wang, L. Tian, X. Zhang, K. Li, and T. Jiang, "Altered functional connectivity in early Alzheimer's disease: A resting-state fMRI study," *Hum. Brain Mapp.*, vol. 28, no. 10, pp. 967–978, 2007.

[39] C. L. Grady, M. L. Furey, P. Pietrini, B. Horwitz, and S. I. Rapoport, "Altered brain functional connectivity and impaired short-term memory in Alzheimer's disease.," *Brain*, vol. 124, pp. 739–756, 2001.

[40] R. Heun, K. Freymann, M. Erb, D. T. Leube, F. Jessen, T. T. Kircher, and W. Grodd, "Successful verbal retrieval in elderly subjects is related to concurrent hippocampal and posterior cingulate activation," *Dement. Geriatr. Cogn. Disord.*, vol. 22, no. 2, pp. 165–172, 2006.

[41] M. D. Greicius, B. Krasnow, A. L. Reiss, and V. Menon, "Functional connectivity in the resting brain: a network analysis of the default mode hypothesis.," *Proc. Natl. Acad. Sci. U. S. A.*, vol. 100, no. 1, pp. 253–8, 2003.

[42] S. Huang, J. Li, L. Sun, J. Ye, A. Fleisher, T. Wu, K. Chen, and E. Reiman, "Learning brain connectivity of Alzheimer's disease by sparse inverse covariance estimation," *Neuroimage*,

vol. 50, no. 3, pp. 935–949, 2010.

[43] C. Sorg, V. Riedl, M. Mühlau, V. D. Calhoun, T. Eichele, L. Läer, A. Drzezga, H. Förstl, A. Kurz, C. Zimmer, and A. M. Wohlschläger, "Selective changes of resting-state networks in individuals at risk for Alzheimer's disease.," *Proc. Natl. Acad. Sci. U. S. A.*, vol. 104, no. 47, pp. 18760–18765, 2007.

[44] D. S. Bassett and E. Bullmore, "Small-world brain networks.," *Neuroscientist*, vol. 12, no. 6, pp. 512–23, 2006.

[45] Y. Gong and Z. Zhang, "Global robustness and identifiability of random, scale-free, and small-world networks," *Ann. N. Y. Acad. Sci.*, vol. 1158, pp. 82–92, 2009.

[46] B. C. M. van Wijk, C. J. Stam, and A. Daffertshofer, "Comparing brain networks of different size and connectivity density using graph theory," *PLoS One*, vol. 5, no. 10, 2010.

[47] D. Ottavia and C. Mara, "Network functional connectivity and whole-brain functional connectomics to investigate cognitive decline in neurodegenerative conditions," *Funct. Neurol.*, vol. 31, no. 4, pp. 191–203, 2016.

[48] E. J. Friedman, K. Young, D. Asif, I. Jutla, M. Liang, S. Wilson, A. S. Landsberg, and N. Schuff, "Directed progression brain networks in Alzheimer's disease: properties and classification.," *Brain Connect.*, vol. 4, no. 5, pp. 384–93, 2014.

[49] E. J. Sanz-Arigita, M. M. Schoonheim, J. S. Damoiseaux, S. A. R. B. Rombouts, E. Maris, F. Barkhof, P. Scheltens, and C. J. Stam, "Loss of 'Small-World' Networks in Alzheimer's Disease: Graph Analysis of fMRI Resting-State Functional Connectivity," *PLoS One*, vol. 5, no. 11, 2010.

[50] E. H. Seo, D. S. Y. Lee, J. Lee, J.-S. Park, B. K. Sohn, Y. M. Choe, and J. I. Woo, "Whole-brain functional networks in cognitively normal, mild cognitive impairment, and Alzheimer's disease.," *PLoS One*, vol. 8, no. 1, p. e53922, 2013.

[51] G. Deshpande, S. LaConte, G. A. James, S. Peltier, and X. Hu, "Multivariate granger causality analysis of fMRI data," *Hum. Brain Mapp.*, vol. 30, no. 4, pp. 1361–1373, 2009.

[52] G. Bellucci, S. Chernyak, M. Hoffman, G. Deshpande, O. Dal Monte, K. M. Knutson, J. Grafman, and F. Krueger, "Effective connectivity of brain regions underlying third-party punishment: Functional MRI and Granger causality evidence," *Soc Neurosci*, pp. 1–11, 2016.

[53] C. Feng, G. Deshpande, C. Liu, R. Gu, Y. J. Luo, and F. Krueger, "Diffusion of

responsibility attenuates altruistic punishment: A functional magnetic resonance imaging effective connectivity study," *Hum. Brain Mapp.*, vol. 37, no. 2, pp. 663–677, 2016.

[54] B. M. Hampstead, M. Khoshnoodi, W. Yan, G. Deshpande, and K. Sathian, "Patterns of effective connectivity during memory encoding and retrieval differ between patients with mild cognitive impairment and healthy older adults," *Neuroimage*, vol. 124, pp. 997–1008, 2016.

[55] M. M. Grant, K. Wood, K. Sreenivasan, M. Wheelock, D. White, J. Thomas, D. C. Knight, and G. Deshpande, "Influence of Early Life Stress on Intra- and Extra-Amygdaloid Causal Connectivity.," *Neuropsychopharmacology*, vol. 40, no. 7, pp. 1–12, 2015.

[56] N. L. Hutcheson, K. R. Sreenivasan, G. Deshpande, M. A. Reid, J. Hadley, D. M. White, L. Ver Hoef, and A. C. Lahti, "Effective connectivity during episodic memory retrieval in schizophrenia participants before and after antipsychotic medication," *Hum. Brain Mapp.*, vol. 36, no. 4, pp. 1442–1457, 2015.

[57] V. Chattaraman, G. Deshpande, H. Kim, and K. R. Sreenivasan, "Form 'defines' function: Neural connectivity between aesthetic perception and product purchase decisions in an fMRI study," *J. Consum. Behav.*, vol. 15, no. 4, pp. 335–347, 2016.

[58] Wang, S. Katwal, B. Rogers, J. Gore, and G. Deshpande, "Experimental Validation of Dynamic Granger Causality for Inferring Stimulus-evoked Sub-100ms Timing Differences from fMRI.," *IEEE Trans. Neural Syst. Rehabil. Eng.*, vol. 4320, no. c, 2016.

[59] K. J. Friston, A. P. Holmes, K. J. Worsley, J.-P. J. P.-. P. J. P. Poline, C. D. Frith, and R. S. J. Frackowiak, "Statistical parametric mapping in functional imaging: a general linear approach," *Hum. Brain Mapp.*, vol. 2, pp. 189–210, 1995.

[60] R. C. Craddock, G. A. James, P. E. Holtzheimer, X. P. Hu, and H. S. Mayberg, "A whole brain fMRI atlas generated via spatially constrained spectral clustering," *Hum. Brain Mapp.*, vol. 33, no. 8, pp. 1914–1928, 2012.

[61] Wang, X. Wang, M. Xia, X. Liao, A. Evans, and Y. He, "Corrigendum: GRETNA: a graph theoretical network analysis toolbox for imaging connectomics," *Front. Hum. Neurosci.*, vol. 9, 2015.

[62] M. D. Wheelock, K. R. Sreenivasan, K. H. Wood, L. W. Ver Hoef, G. Deshpande, and D. C. Knight, "Threat-related learning relies on distinct dorsal prefrontal cortex network connectivity," *Neuroimage*, vol. 102, no. P2, pp. 904–912, 2014.

[63] S. Lacey, R. Stilla, K. Sreenivasan, G. Deshpande, and K. Sathian, “Spatial imagery in haptic shape perception,” *Neuropsychologia*, vol. 60, no. 1, pp. 144–158, 2014.

[64] D. Kapogiannis, G. Deshpande, F. Krueger, M. P. Thornburg, and J. H. Grafman, “Brain networks shaping religious belief.,” *Brain Connect.*, vol. 4, no. 1, pp. 70–9, 2014.

[65] G. Deshpande, L. E. Libero, K. R. Sreenivasan, H. D. Deshpande, and R. K. Kana, “Identification of neural connectivity signatures of autism using machine learning.,” *Front. Hum. Neurosci.*, vol. 7, no. October, p. 670, 2013.

[66] M. M. Grant, D. White, J. Hadley, N. Hutcheson, R. Shelton, K. Sreenivasan, and G. Deshpande, “Early life trauma and directional brain connectivity within major depression,” *Hum. Brain Mapp.*, vol. 35, no. 9, pp. 4815–4826, 2014.

[67] P. Liang, G. Deshpande, S. Zhao, J. Liu, X. Hu, and K. Li, “Altered directional connectivity between emotion network and motor network in Parkinson’s disease with depression,” *Medicine (Baltimore).*, vol. 95, no. 30, p. e4222, 2016.

[68] K. Sathian, S. Lacey, R. Stilla, G. O. Gibson, G. Deshpande, X. Hu, S. LaConte, and C. Glielmi, “Dual pathways for haptic and visual perception of spatial and texture information,” *Neuroimage*, vol. 57, no. 2, pp. 462–475, 2011.

[69] F. Preusse, van der Meer Elke, G. Deshpande, F. Krueger, and I. Wartenburger, “Fluid intelligence allows flexible recruitment of the parieto-frontal network in analogical reasoning.,” *Front. Hum. Neurosci.*, vol. 5, no. March, p. 22, 2011.

[70] F. Krueger, S. Landgraf, E. Van Der Meer, G. Deshpande, and X. Hu, “Effective connectivity of the multiplication network: A functional MRI and multivariate granger causality mapping study,” *Hum. Brain Mapp.*, vol. 32, no. 9, pp. 1419–1431, 2011.

[71] G. Deshpande and X. Hu, “Investigating effective brain connectivity from fMRI data: past findings and current issues with reference to Granger causality analysis.,” *Brain Connect.*, vol. 2, no. 5, pp. 235–45, 2012.

[72] G. Deshpande, X. Hu, S. Lacey, R. Stilla, and K. Sathian, “Object familiarity modulates effective connectivity during haptic shape perception,” *Neuroimage*, vol. 49, no. 3, pp. 1991–2000, 2010.

[73] O. David, I. Guillemain, S. Saillet, S. Reyt, C. Deransart, C. Segebarth, and A. Depaulis, “Identifying neural drivers with functional MRI: an electrophysiological validation.,” *PLoS Biol.*, vol. 6, no. 12, pp. 2683–2697, 2008.

[74] G. Deshpande, Z. Li, P. Santhanam, C. D. Coles, M. E. Lynch, S. Hamann, and X. Hu, "Recursive cluster elimination based support vector machine for disease state prediction using resting state functional and effective brain connectivity," *PLoS One*, vol. 5, no. 12, 2010.

[75] B. M. Hampstead, A. Y. Stringer, R. F. Stilla, G. Deshpande, X. Hu, A. B. Moore, and K. Sathian, "Activation and effective connectivity changes following explicit-memory training for face-name pairs in patients with mild cognitive impairment: a pilot study," *Neurorehabil Neural Repair*, vol. 25, no. 3, pp. 210–222, 2011.

[76] S. Kintali, "Betweenness Centrality : Algorithms and Lower Bounds," *arXiv*, vol. cs.DS, 2008.

[77] M. Rubinov and O. Sporns, "Complex network measures of brain connectivity: Uses and interpretations," *Neuroimage*, vol. 52, no. 3, pp. 1059–1069, 2010.

[78] M. Xia, J. Wang, and Y. He, "BrainNet Viewer: A Network Visualization Tool for Human Brain Connectomics," *PLoS One*, vol. 8, no. 7, 2013.

[79] G. W. Van Hoesen, J. Parvizi, and C. Chu, "Orbitofrontal Cortex Pathology in Alzheimer ' s Disease," *Cereb. cortex*, vol. 10, pp. 243–251, 2000.

[80] K. B. Walhovd, A. M. Fjell, A. M. Dale, L. K. McEvoy, J. Brewer, D. S. Karow, D. P. Salmon, and C. Fennema-Notestine, "Multi-modal imaging predicts memory performance in normal aging and cognitive decline," *Neurobiol. Aging*, vol. 31, no. 7, pp. 1107–1121, 2010.

[81] D. H. Salat, D. S. Tuch, D. N. Greve, A. J. W. Van Der Kouwe, N. D. Hevelone, A. K. Zaleta, B. R. Rosen, B. Fischl, S. Corkin, H. Diana Rosas, and A. M. Dale, "Age-related alterations in white matter microstructure measured by diffusion tensor imaging," *Neurobiol. Aging*, vol. 26, no. 8, pp. 1215–1227, 2005.

[82] C. R. McDonald, L. K. McEvoy, L. Gharapetian, C. Fennema-Notestine, D. J. Hagler, D. Holland, A. Koyama, J. B. Brewer, and A. M. Dale, "Regional rates of neocortical atrophy from normal aging to early Alzheimer disease," *Neurology*, vol. 73, no. 6, pp. 457–465, 2009.

[83] H. Yao, B. Zhou, Z. Zhang, P. Wang, Y. Guo, Y. Shang, L. Wang, X. Zhang, N. An, and Y. Liu, "Longitudinal alteration of amygdalar functional connectivity in mild cognitive impairment subjects revealed by resting-state FMRI.," *Brain Connect.*, vol. 4, no. 5, pp.

361–70, 2014.

[84] B. Zhou, Y. Liu, Z. Zhang, N. An, H. Yao, P. Wang, L. Wang, X. Zhang, and T. Jiang, “Impaired Functional Connectivity of the Thalamus in Alzheimer’ s Disease and Mild Cognitive Impairment: A Resting-State fMRI Study,” *Curr. Alzheimer Res.*, vol. 10, no. 7, pp. 754–766, 2013.

[85] F. Bai, D. R. Watson, H. Yu, Y. Shi, Y. Yuan, and Z. Zhang, “Abnormal resting-state functional connectivity of posterior cingulate cortex in amnestic type mild cognitive impairment,” *Brain Res.*, vol. 1302, pp. 167–174, 2009.

[86] R. L. Buckner, “Molecular, Structural, and Functional Characterization of Alzheimer’s Disease: Evidence for a Relationship between Default Activity, Amyloid, and Memory,” *J. Neurosci.*, vol. 25, no. 34, pp. 7709–7717, 2005.

[87] T. Hedden, K. R. a Van Dijk, J. A. Becker, A. Mehta, R. a Sperling, K. a Johnson, and R. L. Buckner, “Disruption of functional connectivity in clinically normal older adults harboring amyloid burden.,” *J. Neurosci.*, vol. 29, no. 40, pp. 12686–94, 2009.

[88] D. J. Selkoe, “Alzheimer’s disease is a synaptic failure.,” *Science*, vol. 298, no. 5594, pp. 789–791, 2002.

[89] D. R. Thal, U. Rüb, M. Orantes, and H. Braak, “Phases of A beta-deposition in the human brain and its relevance for the development of AD.,” *Neurology*, vol. 58, no. 12, pp. 1791–800, 2002.

[90] Z. Dai, C. Yan, K. Li, Z. Wang, J. Wang, M. Cao, Q. Lin, N. Shu, M. Xia, Y. Bi, and Y. He, “Identifying and mapping connectivity patterns of brain network hubs in Alzheimer’s disease,” *Cereb. Cortex*, vol. 25, no. 10, pp. 3723–3742, 2015.

[91] M. R. Brier, J. B. Thomas, A. M. Fagan, J. Hassenstab, D. M. Holtzman, T. L. Benzinger, J. C. Morris, and B. M. Ances, “Functional connectivity and graph theory in preclinical Alzheimer’s disease,” *Neurobiol. Aging*, vol. 35, no. 4, pp. 757–768, 2014.

[92] J. Mutlu, B. Landeau, C. Tomadesso, R. de Flores, F. Mézenge, V. de La Sayette, F. Eustache, and G. Chételat, “Connectivity Disruption, Atrophy, and Hypometabolism within Posterior Cingulate Networks in Alzheimer’s Disease,” *Front. Neurosci.*, vol. 10, no. December, pp. 1–10, 2016.

[93] R. J. Caselli, E. M. Reiman, D. Osborne, J. G. Hentz, L. C. Baxter, J. L. Hernandez, and G. G. Alexander, “Longitudinal changes in cognition and behavior in asymptomatic carriers of

the APOE e4 allele," *Neurology*, vol. 62, no. 11, pp. 1990–1995, 2004.

[94] K. Buerger, M. Ewers, T. Pirttil??, R. Zinkowski, I. Alafuzoff, S. J. Teipel, J. DeBernardis, D. Kerkman, C. McCulloch, H. Soininen, and H. Hampel, "CSF phosphorylated tau protein correlates with neocortical neurofibrillary pathology in Alzheimer's disease," *Brain*, vol. 129, no. 11, pp. 3035–3041, 2006.

[95] X. Sui, M. Zhu, Y. Cui, C. Yu, J. Sui, X. Zhang, J. Liu, Y. Duan, Z. Zhang, L. Wang, X. Zhang, and T. Jiang, "Functional Connectivity Hubs Could Serve as a Potential Biomarker in Alzheimer's Disease: A Reproducible Study.," *Curr. Alzheimer Res.*, vol. 12, no. 10, pp. 974–83, 2015.

[96] F. Agosta, M. Pievani, C. Geroldi, M. Copetti, G. B. Frisoni, and M. Filippi, "Resting state fMRI in Alzheimer's disease: Beyond the default mode network," *Neurobiol. Aging*, vol. 33, no. 8, pp. 1564–1578, 2012.

[97] M. D. Fox, D. Zhang, A. Z. Snyder, and M. E. Raichle, "The global signal and observed anticorrelated resting state brain networks.," *J. Neurophysiol.*, vol. 101, no. 6, pp. 3270–83, 2009.

[98] Y.-B. Lee, J. Lee, S. Tak, K. Lee, D. L. Na, S. Seo, Y. Jeong, and J. C. Ye, "Sparse SPM: Sparse-dictionary learning for resting-state functional connectivity {MRI} analysis," *Neuroimage*, p. , 2015.

[99] T. Zhang, J. Wang, Y. Yang, Q. Wu, B. Li, L. Chen, Q. Yue, H. Tang, C. Yan, S. Lui, X. Huang, R. C. K. Chan, Y. Zang, Y. He, and Q. Gong, "Abnormal small-world architecture of top-down control networks in obsessive-compulsive disorder," *J. Psychiatry Neurosci.*, vol. 36, no. 1, pp. 23–31, 2011.

[100] E. L. Dennis and P. M. Thompson, "Functional brain connectivity using fMRI in aging and Alzheimer's disease," *Neuropsychology Review*, vol. 24, no. 1. pp. 49–62, 2014.

[101] H. Y. Zhang, S. J. Wang, J. Xing, B. Liu, Z. L. Ma, M. Yang, Z. J. Zhang, and G. J. Teng, "Detection of PCC functional connectivity characteristics in resting-state fMRI in mild Alzheimer's disease," *Behav. Brain Res.*, vol. 197, no. 1, pp. 103–108, 2009.

[102] J. S. Damoiseaux, K. E. Prater, B. L. Miller, and M. D. Greicius, "Functional connectivity tracks clinical deterioration in Alzheimer's disease," *Neurobiol. Aging*, vol. 33, no. 4, 2012.

[103] K. J. Friston, "Functional and effective connectivity: a review," *Brain Connect.*, vol. 1, no. 1, pp. 13–36, 2011.

[104] C. W. J. Granger, “Investigating Causal Relations by Econometric Models and Cross-spectral Methods,” *Econometrica*, vol. 37, no. 3, pp. 424–438, 1969.

[105] G. Deshpande, X. Hu, R. Stilla, and K. Sathian, “Effective connectivity during haptic perception: A study using Granger causality analysis of functional magnetic resonance imaging data,” *Neuroimage*, vol. 40, no. 4, pp. 1807–1814, 2008.

[106] K. J. Friston, L. Harrison, and W. Penny, “Dynamic causal modelling,” *Neuroimage*, vol. 19, no. 4, pp. 1273–1302, 2003.

[107] G. Deshpande, K. Sathian, X. Hu, and J. a Buckhalt, “A rigorous approach for testing the constructionist hypotheses of brain function.,” *Behav. Brain Sci.*, vol. 35, no. 3, pp. 148–9, 2012.

[108] K. Sathian, G. Deshpande, and R. Stilla, “Neural changes with tactile learning reflect decision-level reweighting of perceptual readout.,” *J. Neurosci.*, vol. 33, no. 12, pp. 5387–98, 2013.

[109] S. B. Katwal, J. C. Gore, J. C. Gatenby, and B. P. Rogers, “Measuring relative timings of brain activities using fMRI,” *Neuroimage*, vol. 66, pp. 436–448, 2013.

[110] X. Wen, G. Rangarajan, and M. Ding, “Is Granger Causality a Viable Technique for Analyzing fMRI Data?,” *PLoS One*, vol. 8, no. 7, 2013.

[111] K. Friston, R. Moran, and A. K. Seth, “Analysing connectivity with Granger causality and dynamic causal modelling,” *Current Opinion in Neurobiology*, vol. 23, no. 2. pp. 172–178, 2013.

[112] Z. Liu, Y. Zhang, L. Bai, H. Yan, R. Dai, C. Zhong, H. Wang, W. Wei, T. Xue, Y. Feng, Y. You, and J. Tian, “Investigation of the effective connectivity of resting state networks in Alzheimer’s disease: A functional MRI study combining independent components analysis and multivariate Granger causality analysis,” *NMR Biomed.*, vol. 25, no. 12, pp. 1311–1320, 2012.

[113] R. Li, X. Wu, K. Chen, A. S. Fleisher, E. M. Reiman, and L. Yao, “Alterations of directional connectivity among resting-state networks in Alzheimer disease,” *Am. J. Neuroradiol.*, vol. 34, no. 2, pp. 340–345, 2013.

[114] G. Chen, B. D. Ward, G. Chen, and S. J. Li, “Decreased effective connectivity from cortices to the right parahippocampal gyrus in Alzheimer’s disease subjects,” *Brain Connect*, vol. 4, no. 9, pp. 702–708, 2014.

[115] Y. Zhong, L. Huang, S. Cai, Y. Zhang, K. M. von Deneen, A. Ren, and J. Ren, “Altered effective connectivity patterns of the default mode network in Alzheimer’s disease: An fMRI study,” *Neurosci. Lett.*, vol. 578, pp. 171–175, 2014.

[116] S. Lacey, H. Hagtvedt, V. M. Patrick, A. Anderson, R. Stilla, G. Deshpande, X. Hu, J. R. Sato, S. Reddy, and K. Sathian, “Art for reward’s sake: Visual art recruits the ventral striatum,” *Neuroimage*, vol. 55, no. 1, pp. 420–433, 2011.

[117] M. Strenziok, F. Krueger, G. Deshpande, R. K. Lenroot, E. Van der meer, and J. Grafman, “Fronto-parietal regulation of media violence exposure in adolescents: A multi-method study,” *Soc. Cogn. Affect. Neurosci.*, vol. 6, no. 5, pp. 537–547, 2011.

[118] C. Chang and G. H. Glover, “Time-frequency dynamics of resting-state brain connectivity measured with fMRI,” *Neuroimage*, vol. 50, no. 1, pp. 81–98, 2010.

[119] B. Rashid, M. R. Arbabshirani, E. Damaraju, M. S. Cetin, R. Miller, G. D. Pearlson, and V. D. Calhoun, “Classification Of Schizophrenia And Bipolar Patients Using Static And Dynamic Resting-State Fmri Brain Connectivity.,” *Neuroimage*, 2016.

[120] D. D. Garrett, G. R. Samanez-Larkin, S. W. S. MacDonald, U. Lindenberger, A. R. McIntosh, and C. L. Grady, “Moment-to-moment brain signal variability: A next frontier in human brain mapping?,” *Neuroscience and Biobehavioral Reviews*, vol. 37, no. 4. pp. 610–624, 2013.

[121] D. Rangaprakash, G. Deshpande, T. A. Daniel, A. Goodman, J. Robinson, N. Salibi, J. S. Katz, T. S. Denney, and M. N. Dretsch, “Compromised Hippocampus-Striatum Pathway as a Potential Imaging Biomarker of Mild Traumatic Brain Injury and Posttraumatic Stress Disorder,” *Hum. Brain Mapp.*, vol. In press, 2017.

[122] A. Venkataraman, M. Kubicki, and P. Golland, “From connectivity models to region labels: Identifying foci of a neurological disorder,” *IEEE Trans. Med. Imaging*, vol. 32, no. 11, pp. 2078–2098, 2013.

[123] R. L. Miller, M. Yaesoubi, J. A. Turner, D. Mathalon, A. Preda, G. Pearlson, T. Adali, and V. D. Calhoun, “Higher Dimensional Meta-State Analysis Reveals Reduced Resting fMRI Connectivity Dynamism in Schizophrenia Patients.,” *PLoS One*, vol. 11, no. 3, p. e0149849, 2016.

[124] D. A. Handwerker, J. M. Ollinger, and M. D’Esposito, “Variation of BOLD hemodynamic responses across subjects and brain regions and their effects on statistical analyses,”

Neuroimage, vol. 21, no. 4, pp. 1639–1651, 2004.

[125] G. Deshpande, K. Sathian, and X. Hu, "Assessing and compensating for zero-lag correlation effects in time-lagged granger causality analysis of fMRI," *IEEE Trans. Biomed. Eng.*, vol. 57, no. 6, pp. 1446–1456, 2010.

[126] E. Tagliazucchi, P. Balenzuela, D. Fraiman, and D. R. Chialvo, "Criticality in large-scale brain fmri dynamics unveiled by a novel point process analysis," *Front. Physiol.*, vol. 3 FEB, no. February, pp. 1–12, 2012.

[127] G. H. Glover, "Deconvolution of Impulse Response in Event-Related BOLD fMRI," *Neuroimage*, vol. 9, no. 4, pp. 416–429, 1999.

[128] M. Arnold, W. H. R. Miltner, H. Witte, R. Bauer, and C. Braun, "Adaptive AR modeling of nonstationary time series by means of kaiman filtering," *IEEE Trans. Biomed. Eng.*, vol. 45, no. 5, pp. 545–552, 1998.

[129] C. Büchel and K. J. Friston, "Dynamic changes in effective connectivity characterized by variable parameter regression and Kalman filtering," in *Human Brain Mapping*, 1998, vol. 6, no. 5–6, pp. 403–408.

[130] M. Havlicek, J. Jan, M. Brazdil, and V. D. Calhoun, "Dynamic Granger causality based on Kalman filter for evaluation of functional network connectivity in fMRI data," *Neuroimage*, vol. 53, no. 1, pp. 65–77, 2010.

[131] A. P. Dempster, N. M. Laird, and D. B. Rubin, "Maximum likelihood from incomplete data via the EM algorithm," *J. R. Stat. Soc. Ser. B*, vol. 39, no. 1, pp. 1–38, 1977.

[132] E. Kienzl, K. Jellinger, H. Stachelberger, and W. Linert, "Iron as catalyst for oxidative stress in the pathogenesis of Parkinson's disease?," in *Life Sciences*, 1999, vol. 65, no. 18–19, pp. 1973–1976.

[133] P. Herregodts, G. Ebinger, and Y. Michotte, "Distribution of monoamines in human brain: evidence for neurochemical heterogeneity in subcortical as well as in cortical areas," *Brain Res.*, vol. 542, no. 2, pp. 300–306, 1991.

[134] S. J. Sara and S. Bouret, "Orienting and Reorienting: The Locus Coeruleus Mediates Cognition through Arousal," *Neuron*, vol. 76, no. 1. pp. 130–141, 2012.

[135] S. J. Sara, "The locus coeruleus and noradrenergic modulation of cognition.," *Nat. Rev. Neurosci.*, vol. 10, no. 3, pp. 211–223, 2009.

[136] M. T. Heneka, F. Nadrigny, T. Regen, A. Martinez-Hernandez, L. Dumitrescu-Ozimek, D.

Terwel, D. Jardanhazi-Kurutz, J. Walter, F. Kirchhoff, U.-K. Hanisch, and M. P. Kummer, “Locus ceruleus controls Alzheimer’s disease pathology by modulating microglial functions through norepinephrine.,” *Proc. Natl. Acad. Sci. U. S. A.*, vol. 107, no. 13, pp. 6058–63, 2010.

[137] S. C. Kelly, B. He, S. E. Perez, S. D. Ginsberg, E. J. Mufson, and S. E. Counts, “Locus coeruleus cellular and molecular pathology during the progression of Alzheimer’s disease,” *Acta Neuropathol. Commun.*, vol. 5, no. 1, p. 8, 2017.

[138] P. Theofilas, A. J. Ehrenberg, S. Dunlop, A. T. Di Lorenzo Alho, A. Nguy, R. E. P. Leite, R. D. Rodriguez, M. B. Mejia, C. K. Suemoto, R. E. D. L. Ferretti-Rebustini, L. Polichiso, C. F. Nascimento, W. W. Seeley, R. Nitrini, C. A. Pasqualucci, W. Jacob Filho, U. Rueb, J. Neuhaus, H. Heinsen, and L. T. Grinberg, “Locus coeruleus volume and cell population changes during Alzheimer’s disease progression: A stereological study in human postmortem brains with potential implication for early-stage biomarker discovery,” *Alzheimer’s and Dementia*, 2016.

[139] C. Guedj, E. Monfardini, A. J. Reynaud, A. Farnè, M. Meunier, and F. Hadj-Bouziane, “Boosting Norepinephrine Transmission Triggers Flexible Reconfiguration of Brain Networks at Rest.,” *Cereb. Cortex*, p. bhw262-, 2016.

[140] J. Sepulcre, M. R. Sabuncu, A. Becker, R. Sperling, and K. A. Johnson, “In vivo characterization of the early states of the amyloid-beta network,” *Brain*, vol. 136, no. 7, pp. 2239–2252, 2013.

[141] G. W. Van Hoesen, J. Parvizi, and C. C. Chu, “Orbitofrontal cortex pathology in Alzheimer’s disease,” *Cereb. Cortex*, vol. 10, no. 3, pp. 243–251, 2000.

[142] K. Ishibashi, K. Ishiwata, J. Toyohara, S. Murayama, and K. Ishii, “Regional analysis of striatal and cortical amyloid deposition in patients with Alzheimer’s disease,” *Eur. J. Neurosci.*, vol. 40, no. 4, pp. 2701–2706, 2014.

[143] P. Cras, M. Kawai, D. Lowery, P. Gonzalez-DeWhitt, B. Greenberg, and G. Perry, “Senile plaque neurites in Alzheimer disease accumulate amyloid precursor protein.,” *Proc. Natl. Acad. Sci. U. S. A.*, vol. 88, no. 17, pp. 7552–6, 1991.

[144] H. Braak and E. Braak, “Temporal Sequence of Alzheimer’s Disease-Related Pathology,” *Cereb. Cortex*, vol. 14, pp. 475–512, 1999.

[145] C. Yeh, B. Vadhwana, A. Verkhratsky, and J. J. Rodríguez, “Early astrocytic atrophy in the

entorhinal cortex of a triple transgenic animal model of Alzheimer's disease," *ASN Neuro*, vol. 3, no. 5, pp. 271–279, 2011.

[146] A. Baddeley, "Working memory: Looking back and looking forward," *Nat. Rev. Neurosci.*, vol. 4, no. 10, pp. 829–839, 2003.

[147] T. J. Brozoski, R. M. Brown, H. E. Rosvold, and P. S. Goldman, "Cognitive deficit caused by regional depletion of dopamine in prefrontal cortex of rhesus monkey.," *Science*, vol. 205, no. 4409, pp. 929–32, 1979.

[148] B. M. Li, Z. M. Mao, M. Wang, and Z. T. Mei, "Alpha-2 adrenergic modulation of prefrontal cortical neuronal activity related to spatial working memory in monkeys.," *Neuropsychopharmacology*, vol. 21, no. 99, pp. 601–610, 1999.

[149] A. F. T. Arnsten and J. D. Jentsch, "The alpha-1 adrenergic agonist, cirazoline, impairs spatial working memory performance in aged monkeys," *Pharmacol. Biochem. Behav.*, vol. 58, no. 1, pp. 55–59, 1997.

[150] M. F. O'Rourke, H. S. Blaxall, L. J. Iversen, and D. B. Bylund, "Characterization of [3H]RX821002 binding to alpha-2 adrenergic receptor subtypes," *J. Pharmacol. Exp. Ther.*, vol. 268, no. 3, pp. 1362–1367, 1994.

[151] J. M. Weiss, W. H. Bailey, L. A. Pohorecky, D. Korzeniowski, and G. Grillione, "Stress-induced depression of motor activity correlates with regional changes in brain norepinephrine but not in dopamine," *Neurochem. Res.*, vol. 5, no. 1, pp. 9–22, 1980.

[152] A. J. Dunn and C. W. Berridge, "Physiological and behavioral responses to corticotropin-releasing factor administration: is CRF a mediator of anxiety or stress responses?," *Brain Research Reviews*, vol. 15, no. 2. pp. 71–100, 1990.

[153] G. F. Koob and F. E. Bloom, "Corticotropin-releasing factor and behavior.," *Fed. Proc.*, vol. 44, no. 1 Pt 2, pp. 259–63, 1985.

[154] S. Cummings, R. Elde, J. Ells, and a Lindall, "Corticotropin-releasing factor immunoreactivity is widely distributed within the central nervous system of the rat: an immunohistochemical study.," *J. Neurosci.*, vol. 3, no. 7, pp. 1355–1368, 1983.

[155] I. Merchenthaler, S. Vigh, P. Petrusz, and A. V Schally, "Immunocytochemical localization of corticotropin-releasing factor (CRF) in the rat brain," *Am J Anat*, vol. 165, no. 4, pp. 385–396, 1982.

[156] R. J. Valentino, S. L. Foote, and G. Aston-Jones, "Corticotropin-releasing factor activates

noradrenergic neurons of the locus coeruleus," *Brain Res.*, vol. 270, no. 2, pp. 363–367, 1983.

[157] J. M. Finlay, H. P. Jedema, a D. Rabinovic, M. J. Mana, M. J. Zigmond, and a F. Sved, "Impact of corticotropin-releasing hormone on extracellular norepinephrine in prefrontal cortex after chronic cold stress.," *J. Neurochem.*, vol. 69, no. 1, pp. 144–50, 1997.

[158] H. P. Jedema, J. M. Finlay, A. F. Sved, and A. A. Grace, "Chronic cold exposure potentiates CRH-evoked increases in electrophysiologic activity of locus coeruleus neurons," *Biol. Psychiatry*, vol. 49, no. 4, pp. 351–359, 2001.

[159] M. L. Wong, J. Licinio, K. I. Pasternak, and P. W. Gold, "Localization of corticotropin-releasing hormone (CRH) receptor mRNA in adult rat brain by in situ hybridization histochemistry," *Endocrinology*, vol. 135, no. 5, pp. 2275–2278, 1994.

[160] I. Sotiropoulos, C. Catania, L. G. Pinto, R. Silva, G. E. Pollerberg, A. Takashima, N. Sousa, and O. F. X. Almeida, "Stress acts cumulatively to precipitate Alzheimer's disease-like tau pathology and cognitive deficits.," *J. Neurosci.*, vol. 31, no. 21, pp. 7840–7847, 2011.

[161] V. D. Bohbot, M. Kalina, K. Stepankova, N. Spackova, M. Petrides, and L. Nadel, "Spatial memory deficits in patients with lesions to the right hippocampus and to the right parahippocampal cortex," *Neuropsychologia*, vol. 36, no. 11, pp. 1217–1238, 1998.

[162] E. Szabadi, "Functional neuroanatomy of the central noradrenergic system.," *J. Psychopharmacol.*, vol. 27, no. 8, pp. 659–93, 2013.

[163] M. J. Gertner and S. A. Thomas, "The role of norepinephrine in spatial reference and spatial working memory," *CUREJ-College Undergrad. Res. Electron. J.*, p. 18, 2006.

[164] J. McLean and B. D. Waterhouse, "Noradrenergic modulation of cat area 17 neuronal responses to moving visual stimuli," *Brain Res.*, vol. 667, no. 1, pp. 83–97, 1994.

[165] B. D. Waterhouse, S. Ausim Azizi, R. A. Burne, and D. J. Woodward, "Modulation of rat cortical area 17 neuronal responses to moving visual stimuli during norepinephrine and serotonin microiontophoresis," *Brain Res.*, vol. 514, no. 2, pp. 276–292, 1990.

[166] K. A. Johnson, N. C. Fox, R. A. Sperling, and W. E. Klunk, "Brain imaging in Alzheimer disease," *Cold Spring Harb. Perspect. Med.*, vol. 2, no. 4, 2012.

[167] B. E. Swartz, E. Kovalik, K. Thomas, D. Torgersen, and M. A. Mandelkern, "The effects of an alpha-2 adrenergic agonist, guanfacine, on rCBF in human cortex in normal controls and subjects with focal epilepsy," *Neuropsychopharmacology*, vol. 23, no. 3. pp. 263–275,

2000.

[168] S. H. Ferris and M. Farlow, “Language impairment in alzheimer’s disease and benefits of acetylcholinesterase inhibitors,” *Clinical Interventions in Aging*, vol. 8. pp. 1007–1014, 2013.

[169] G. Szatloczki, I. Hoffmann, V. Vincze, J. Kalman, and M. Pakaski, “Speaking in Alzheimer’s disease, is that an early sign? Importance of changes in language abilities in Alzheimer’s disease,” *Frontiers in Aging Neuroscience*, vol. 7, no. OCT. 2015.

[170] N. L. Rempel-Clower, “Role of orbitofrontal cortex connections in emotion,” in *Annals of the New York Academy of Sciences*, 2007, vol. 1121, pp. 72–86.

[171] E. T. Rolls, “The functions of the orbitofrontal cortex,” *Brain and Cognition*, vol. 55, no. 1. pp. 11–29, 2004.

[172] H.-J. Li, X.-H. Hou, H.-H. Liu, C.-L. Yue, Y. He, and X.-N. Zuo, “Toward systems neuroscience in mild cognitive impairment and Alzheimer’s disease: A meta-analysis of 75 fMRI studies.,” *Hum. Brain Mapp.*, 2014.

[173] K. Miyadera, G. M. Acland, and G. D. Aguirre, “Genetic and phenotypic variations of inherited retinal diseases in dogs: The power of within- and across-breed studies,” *Mammalian Genome*, vol. 23, no. 1–2. pp. 40–61, 2012.

[174] N. Sachs-Ericsson, N. K. Hansen, and S. G. Fitzgerald, “Benefits of assistance dogs: A review.,” *Rehabil. Psychol.*, vol. 47, no. 3, pp. 251–277, 2002.

[175] N. R. Gee, S. L. Harris, and K. L. Johnson, “The role of therapy dogs in speed and accuracy to complete motor skills tasks for preschool children,” *Anthrozoos*, vol. 20, no. 4, pp. 375–386, 2007.

[176] R. a Yount, M. D. Olmert, and M. R. Lee, “Service dog training program for treatment of posttraumatic stress in service members.,” *US. Army Med. Dep. J.*, no. June, pp. 63–9, 2012.

[177] J. M. Slabbert and J. S. J. Odendaal, “Early prediction of adult police dog efficiency - A longitudinal study,” *Appl. Anim. Behav. Sci.*, vol. 64, no. 4, pp. 269–288, 1999.

[178] M. Cobb, N. Branson, P. McGreevy, A. Lill, and P. Bennett, “The advent of canine performance science: Offering a sustainable future for working dogs,” *Behav. Processes*, vol. 110, pp. 96–104, 2015.

[179] A. M. Thompkins, G. Deshpande, P. Waggoner, and J. S. Katz, “Functional Magnetic Resonance Imaging of the Domestic Dog: Research, Methodology, and Conceptual Issues,”

Comp. Cogn. Behav. Rev., vol. 11, no. January, pp. 63–82, 2016.

[180] W. W. Seeley, V. Menon, A. F. Schatzberg, J. Keller, G. H. Glover, H. Kenna, A. L. Reiss, and M. D. Greicius, "Dissociable intrinsic connectivity networks for salience processing and executive control.," *J. Neurosci.*, vol. 27, no. 9, pp. 2349–2356, 2007.

[181] M. Hampson, N. R. Driesen, P. Skudlarski, J. C. Gore, and R. T. Constable, "Brain connectivity related to working memory performance.," *J. Neurosci.*, vol. 26, no. 51, pp. 13338–43, 2006.

[182] R. Leech, S. Kamourieh, C. F. Beckmann, and D. J. Sharp, "Fractionating the default mode network: distinct contributions of the ventral and dorsal posterior cingulate cortex to cognitive control.," *J. Neurosci.*, vol. 31, no. 9, pp. 3217–24, 2011.

[183] R. L. Buckner, J. R. Andrews-Hanna, and D. L. Schacter, "The brain's default network: Anatomy, function, and relevance to disease," *Annals of the New York Academy of Sciences*, vol. 1124. pp. 1–38, 2008.

[184] D. T. Gilbert and T. D. Wilson, "Prospection: experiencing the future.," *Science*, vol. 317, no. 5843, pp. 1351–1354, 2007.

[185] P. Kulkarni, T. Stolberg, J. M. Sullivan, and C. F. Ferris, "Imaging evolutionarily conserved neural networks: Preferential activation of the olfactory system by food-related odor," *Behav. Brain Res.*, vol. 230, no. 1, pp. 201–207, 2012.

[186] G. Chen, F. Wang, B. C. Dillenburger, R. M. Friedman, L. M. Chen, J. C. Gore, M. J. Avison, and A. W. Roe, "Functional magnetic resonance imaging of awake monkeys: Some approaches for improving imaging quality," *Magn. Reson. Imaging*, vol. 30, no. 1, pp. 36–47, 2012.

[187] H. Lu, Y. Zuo, H. Gu, J. a Waltz, W. Zhan, C. a Scholl, W. Rea, Y. Yang, and E. a Stein, "Synchronized delta oscillations correlate with the resting-state functional MRI signal.," *Proc. Natl. Acad. Sci. U. S. A.*, vol. 104, no. 46, pp. 18265–18269, 2007.

[188] K. Wang, M. P. A. Van Meer, K. Van Der Marel, A. Van Der Toorn, L. Xu, Y. Liu, M. A. Viergever, T. Jiang, and R. M. Dijkhuizen, "Temporal scaling properties and spatial synchronization of spontaneous blood oxygenation level-dependent (BOLD) signal fluctuations in rat sensorimotor network at different levels of isoflurane anesthesia," *NMR Biomed.*, vol. 24, no. 1, pp. 61–67, 2011.

[189] H. Jia, O. M. Pustovyy, P. Waggoner, R. J. Beyers, J. Schumacher, C. Wildey, J. Barrett, E.

Morrison, N. Salibi, T. S. Denney, V. J. Vodyanoy, and G. Deshpande, “Functional MRI of the olfactory system in conscious dogs,” *PLoS One*, vol. 9, no. 1, 2014.

[190] S. P. Kyathanahally, H. Jia, O. M. Pustovyy, P. Waggoner, R. Beyers, J. Schumacher, J. Barrett, E. E. Morrison, N. Salibi, T. S. Denney, V. J. Vodyanoy, and G. Deshpande, “Anterior-posterior dissociation of the default mode network in dogs,” *Brain Struct. Funct.*, vol. 220, no. 2, pp. 1063–1076, 2015.

[191] H. Jia, O. M. Pustovyy, Y. Wang, P. Waggoner, R. J. Beyers, J. Schumacher, C. Wildey, E. Morrison, N. Salibi, T. S. Denney, V. J. Vodyanoy, and G. Deshpande, “Enhancement of odor-induced activity in the canine brain by zinc nanoparticles: A functional MRI study in fully unrestrained conscious dogs,” *Chem. Senses*, vol. 41, no. 1, pp. 53–67, 2016.

[192] Andics, A. Gábor, M. Gácsi, T. Faragó, D. Szabó, Á. Miklósi, E. F. Briefer, S. Frühholz, W. Trost, S. A. Kotz, M. J. Yip, K. Collier, B. Bickel, C. P. van Schaik, M. B. Manser, S. W. Townsend, R. M. Seyfarth, D. L. Cheney, P. Marler, I. M. Pepperberg, H. R. Shive, J. R. Binder, R. H. Desai, W. W. Graves, L. L. Conant, D. Poeppel, W. Wetzel, F. W. Ohl, H. Scheich, Y. Shtyrov, E. Pihko, F. Pulvermüller, A. Poremba, M. Malloy, R. C. Saunders, R. E. Carson, P. Herscovitch, M. Mishkin, G. Ehret, H. U. Voss, K. Tabelow, J. Polzehl, O. Tchernichovski, K. K. Maul, D. Salgado-Commissariat, D. Ballon, S. A. Helekar, P. Pongrácz, C. Molnár, A. Miklósi, J. M. Gibson, S. A. Scavelli, C. J. Udell, M. A. R. Udell, Á. Miklósi, J. Topál, V. Csányi, J. Topál, G. Gergely, A. Erdőhegyi, G. Csibra, A. Miklósi, J. Kaminski, J. Call, J. Fischer, A. Andics, M. Gácsi, T. Faragó, A. Kis, A. Miklósi, V. F. Ratcliffe, D. Reby, A. Fernald, W. Schultz, P. Dayan, P. R. Montague, J. P. O’Doherty, S. N. Haber, B. Knutson, S. J. Russo, E. J. Nestler, G. S. Berns, A. Brooks, M. Spivak, A. Kerepesi, A. Dóka, Á. Miklósi, M. Wilke, V. J. Schmithorst, S. Norman-Haignere, N. Kanwisher, J. H. McDermott, D. Bendor, X. Wang, D. Wildgruber, H. Ackermann, B. Kreifelts, T. Ethofer, V. N. Salimpoor, I. van den Bosch, N. Kovacevic, A. R. McIntosh, A. Dagher, R. J. Zatorre, D. A. Sauter, F. Eisner, P. Ekman, S. K. Scott, T. Faragó, A. Andics, V. Devecseri, A. Kis, M. Gácsi, A. Miklósi, P. Belin, S. Fecteau, I. Charest, N. Nicastro, M. D. Hauser, J. L. Armony, S. A. Kotz, S. Paulmann, M. C. Corballis, M. Kleiner, D. Brainard, D. Pelli, A. Ingling, M. Wilke, K. Lidzba, S. Whitfield-Gabrieli, and A. Nieto-Castanon, “Neural mechanisms for lexical processing in dogs.,” *Science*, vol. 353, no. 6303, pp. 1–20, 2016.

[193] Andics, M. Gácsi, T. Faragó, A. Kis, and Á. Miklósi, “Voice-sensitive regions in the dog and human brain are revealed by comparative fMRI,” *Curr. Biol.*, vol. 24, no. 5, pp. 574–578, 2014.

[194] P. F. Cook, A. Prichard, M. Spivak, and G. S. Berns, “Awake Canine fMRI Predicts Dogs’ Preference for Praise Versus Food,” *bioRxiv*, pp. 1–28, 2016.

[195] D. D. Dilks, P. Cook, S. K. Weiller, H. P. Berns, M. Spivak, and G. S. Berns, “Awake fMRI reveals a specialized region in dog temporal cortex for face processing.,” *PeerJ*, vol. 3, p. e1115, 2015.

[196] G. S. Berns, A. M. Brooks, M. Spivak, and K. Levy, “Functional Mri in Awake Dogs Predicts Suitability for Assistance Work,” vol. 90, pp. 1–13, 2016.

[197] G. S. Berns, A. M. Brooks, and M. Spivak, “Functional MRI in awake unrestrained dogs,” *PLoS One*, vol. 7, no. 5, 2012.

[198] P. F. Cook, M. Spivak, and G. Berns, “Neurobehavioral evidence for individual differences in canine cognitive control: an awake fMRI study,” *Anim. Cogn.*, vol. 19, no. 5, pp. 867–878, 2016.

[199] P. F. Cook, M. Spivak, and G. S. Berns, “One pair of hands is not like another: caudate BOLD response in dogs depends on signal source and canine temperament.,” *PeerJ*, vol. 2, p. e596, 2014.

[200] G. S. Berns, A. M. Brooks, and M. Spivak, “Scent of the familiar: An fMRI study of canine brain responses to familiar and unfamiliar human and dog odors,” *Behav. Processes*, vol. 110, pp. 37–46, 2015.

[201] L. V. Cuaya, R. Hernández-Pérez, and L. Concha, “Our faces in the dog’s brain: Functional imaging reveals temporal cortex activation during perception of human faces,” *PLoS One*, vol. 11, no. 3, 2016.

[202] L. Huber and C. Lamm, “Understanding dog cognition by functional magnetic resonance imaging,” *Learn Behav*, 2017.

[203] G. S. Berns and P. F. Cook, “Why Did the Dog Walk Into the MRI?,” *Curr. Dir. Psychol. Sci.*, vol. 25, no. 5, pp. 363–369, 2016.

[204] N. Bunford, A. Andics, A. Kis, Á. Miklósi, and M. Gácsi, “Canis familiaris as model for non-invasive comparative neuroscience,” *Trends Neurosci.*, no. May, 2017.

[205] D. Rocznik, D. L. Sinn, S. Thomas, and S. D. Gosling, “Criterion analysis and content

validity for standardized behavioral tests in a detector-dog breeding program," *J. Forensic Sci.*, vol. 60, no. s1, pp. S213–S221, 2015.

[206] D. L. Sinn, S. D. Gosling, and S. Hilliard, "Personality and performance in military working dogs: Reliability and predictive validity of behavioral tests," *Appl. Anim. Behav. Sci.*, vol. 127, no. 1–2, pp. 51–65, 2010.

[207] R. Bluhm, P. Williamson, R. Lanius, J. Théberge, M. Densmore, R. Bartha, R. Neufeld, and E. Osuch, "Resting state default-mode network connectivity in early depression using a seed region-of-interest analysis: Decreased connectivity with caudate nucleus," *Psychiatry Clin. Neurosci.*, vol. 63, no. 6, pp. 754–761, 2009.

[208] D. a Fair, A. L. Cohen, N. U. F. Dosenbach, J. a Church, F. M. Miezin, D. M. Barch, M. E. Raichle, S. E. Petersen, and B. L. Schlaggar, "The maturing architecture of the brain's default network.," *Proc. Natl. Acad. Sci. U. S. A.*, vol. 105, no. 10, pp. 4028–4032, 2008.

[209] Y. I. Sheline, M. E. Raichle, A. Z. Snyder, J. C. Morris, D. Head, S. Wang, and M. A. Mintun, "Amyloid Plaques Disrupt Resting State Default Mode Network Connectivity in Cognitively Normal Elderly," *Biol. Psychiatry*, vol. 67, no. 6, pp. 584–587, 2010.

[210] R. B. Mars, L. Verhagen, T. E. Gladwin, F. X. Neubert, J. Sallet, and M. F. S. Rushworth, "Comparing brains by matching connectivity profiles," *Neuroscience and Biobehavioral Reviews*, vol. 60. pp. 90–97, 2016.

[211] R. E. Passingham, K. E. Stephan, and R. Kotter, "The anatomical basis of functional localization in the cortex," *Nat Rev Neurosci*, vol. 3, no. 8, p. 606–16., 2002.

[212] G. J. Patronek, D. J. Waters, and L. T. Glickman, "Comparative longevity of pet dpgs and humans: Implication for gerontology research," *J. Gerontol. Biol. Sci.*, vol. 52A, no. 3, pp. B171–B178, 1997.

[213] Bassett, N. F. Wymbs, M. A. Porter, P. J. Mucha, J. M. Carlson, and S. T. Grafton, "Dynamic reconfiguration of human brain networks during learning.," *Proc. Natl. Acad. Sci. U. S. A.*, vol. 108, no. 18, pp. 7641–7646, 2011.

[214] U. Braun, A. Schäfer, H. Walter, S. Erk, N. Romanczuk-Seiferth, L. Haddad, J. I. Schweiger, O. Grimm, A. Heinz, H. Tost, A. Meyer-Lindenberg, and D. S. Bassett, "Dynamic reconfiguration of frontal brain networks during executive cognition in humans.," *Proc. Natl. Acad. Sci. U. S. A.*, vol. 112, no. 37, pp. 11678–83, 2015.

[215] L. R. Chai, M. G. Mattar, I. A. Blank, E. Fedorenko, and D. S. Bassett, "Functional Network

Dynamics of the Language System," *Cereb. Cortex*, vol. 26, no. 11, pp. 4148–4159, 2016.

[216] Bassett, N. F. Wymbs, M. P. Rombach, M. A. Porter, P. J. Mucha, and S. T. Grafton, "Task-Based Core-Periphery Organization of Human Brain Dynamics," *PLoS Comput. Biol.*, vol. 9, no. 9, p. 16, 2013.

[217] L. L. Gollo, J. A. Roberts, and L. Cocchi, "Mapping how local perturbations influence systems-level brain dynamics," *Neuroimage*, no. January, p. 41, 2016.

[218] M. Ekman, J. Derrfuss, M. Tittgemeyer, and C. J. Fiebach, "Predicting errors from reconfiguration patterns in human brain networks," *Proc Natl Acad Sci USA*, vol. 109, pp. 16714–16719, 2012.

[219] I. Savic, B. Gulyas, M. Larsson, and P. Roland, "Olfactory functions are mediated by parallel and hierarchical processing.," *Neuron*, vol. 26, no. 3, pp. 735–745, 2000.

[220] F. Vedaei, M. A. Oghabian, K. Firouznia, M. H. Harirchian, Y. Lotfi, and M. Fakhri, "The Human Olfactory System: Cortical Brain Mapping Using fMRI," *Iran. J. Radiol.*, vol. In Press, no. In Press, 2016.

[221] A. Poellinger, R. Thomas, P. Lio, A. Lee, N. Makris, B. R. Rosen, and K. K. Kwong, "Activation and habituation in olfaction--an fMRI study.," *Neuroimage*, vol. 13, no. 4, pp. 547–60, 2001.

[222] K. Kollndorfer, F. P. S. Fischmeister, K. Kowalczyk, E. Hoche, C. A. Mueller, S. Trattnig, and V. Sch??pf, "Olfactory training induces changes in regional functional connectivity in patients with long-term smell loss," *NeuroImage Clin.*, vol. 9, pp. 401–410, 2015.

[223] C. I. Huerta, P. R. Sarkar, T. Q. Duong, A. R. Laird, and P. T. Fox, "Neural bases of food perception: Coordinate-based meta-analyses of neuroimaging studies in multiple modalities," *Obesity*, vol. 22, no. 6, pp. 1439–1446, 2014.

[224] N. U. F. Dosenbach, D. A. Fair, A. L. Cohen, B. L. Schlaggar, and S. E. Petersen, "A dual-networks architecture of top-down control," *Trends Cogn. Sci.*, vol. 12, no. 3, pp. 99–105, 2008.

[225] A. Olsson and K. N. Ochsner, "The role of social cognition in emotion," *Trends in Cognitive Sciences*, vol. 12, no. 2. pp. 65–71, 2008.

[226] S. Markett, M. Reuter, C. Montag, G. Voigt, B. Lachmann, S. Rudorf, C. E. Elger, and B. Weber, "Assessing the function of the fronto-parietal attention network: Insights from resting-state fMRI and the attentional network test," *Hum. Brain Mapp.*, vol. 35, no. 4, pp.

1700–1709, 2014.

[227] M. Ghahremani, R. M. Hutchison, R. S. Menon, and S. Everling, “Frontoparietal Functional Connectivity in the Common Marmoset,” *Cereb. Cortex*, no. 1, pp. 1–16, 2016.

[228] M. Song, Y. Zhou, J. Li, Y. Liu, L. Tian, C. Yu, and T. Jiang, “Brain spontaneous functional connectivity and intelligence,” *Neuroimage*, vol. 41, no. 3, pp. 1168–1176, 2008.

[229] L. J. Hearne, J. B. Mattingley, and L. Cocchi, “Functional brain networks related to individual differences in human intelligence at rest,” *Sci. Rep.*, vol. 6, no. August, p. 32328, 2016.

[230] K. L. Vilberg and M. D. Rugg, “Memory retrieval and the parietal cortex: A review of evidence from a dual-process perspective,” *Neuropsychologia*, vol. 46, no. 7. pp. 1787–1799, 2008.

[231] D. Montaldi, T. J. Spencer, N. Roberts, and A. R. Mayes, “The neural system that mediates familiarity memory,” *Hippocampus*, vol. 16, no. 5, pp. 504–520, 2006.

[232] K. L. Vilberg and M. D. Rugg, “Dissociation of the neural correlates of recognition memory according to familiarity, recollection, and amount of recollected information,” *Neuropsychologia*, vol. 45, no. 10, pp. 2216–2225, 2007.

[233] C. C. Woodruff, J. D. Johnson, M. R. Uncapher, and M. D. Rugg, “Content-specificity of the neural correlates of recollection,” *Neuropsychologia*, vol. 43, no. 7, pp. 1022–1032, 2005.

[234] C. W. Harley, “Norepinephrine and dopamine as learning signals,” *Neural Plasticity*, vol. 11, no. 3–4. pp. 191–204, 2004.

[235] C. F. Murchison, X.-Y. Zhang, W.-P. Zhang, M. Ouyang, A. Lee, and S. a Thomas, “A distinct role for norephinephrine in memory retrieval,” *Cell*, vol. 117, pp. 131–142, 2004.

[236] M. a Pinsk, M. Arcaro, K. S. Weiner, J. F. Kalkus, S. J. Inati, C. G. Gross, and S. Kastner, “Neural representations of faces and body parts in macaque and human cortex: a comparative FMRI study.,” *J. Neurophysiol.*, vol. 101, no. 5, pp. 2581–2600, 2009.

[237] D. R. Langers, P. van Dijk, and W. H. Backes, “Lateralization, connectivity and plasticity in the human central auditory system,” *Neuroimage*, vol. 28, pp. 490–9, 2005.

[238] K. L. Overall, “That Dog Is Smarter Than You Know: Advances in Understanding Canine Learning, Memory, and Cognition,” *Topics in Companion Animal Medicine*, vol. 26, no. 1. pp. 2–9, 2011.

[239] M. Wan, K. Hejjas, Z. Ronai, Z. Elek, M. Sasvari-Szekely, F. A. Champagne, Á. Miklõsi, and E. Kubinyi, “DRD4 and TH gene polymorphisms are associated with activity, impulsivity and inattention in Siberian Husky dogs,” *Anim. Genet.*, vol. 44, no. 6, pp. 717–727, 2013.

[240] L. ChaeYoung, K. ChangHoon, S. SooAn, S. DaeSung, K. JooHyun, and P. ChanKyu, “The dopamine D4 receptor polymorphism affects the canine fearfulness,” *Animal Cells Syst. (Seoul).*, vol. 12, no. 2, pp. 77–83, 2008.

[241] R. J. Primus, A. Thurkauf, J. Xu, E. Yevich, S. Mcinerney, K. Shaw, J. F. Tallman, and D. W. Gallager, “II. Localization and Characterization of Dopamine D4 Binding Sites in Rat and Human Brain by Use of the Novel, D4 Receptor-Selective Ligand [3H] NGD 94-1,” *J. Pharmacol. Exp. Ther.*, vol. 282, no. 2, pp. 1020–1027, 1997.

[242] M. Haruno, “A Neural Correlate of Reward-Based Behavioral Learning in Caudate Nucleus: A Functional Magnetic Resonance Imaging Study of a Stochastic Decision Task,” *J. Neurosci.*, vol. 24, no. 7, pp. 1660–1665, 2004.

[243] M. Haruno and M. Kawato, “Heterarchical reinforcement-learning model for integration of multiple cortico-striatal loops: fMRI examination in stimulus-action-reward association learning,” *Neural Networks*, vol. 19, no. 8, pp. 1242–1254, 2006.

[244] D. C. Van Essen and D. L. Dierker, “Surface-based and probabilistic atlases of primate cerebral cortex,” *Neuron*, vol. 56, no. 2, pp. 209–225, 2007.

[245] G. A. Orban, K. Claeys, K. Nelissen, R. Smans, S. Sunaert, J. T. Todd, C. Wardak, J. B. Durand, and W. Vanduffel, “Mapping the parietal cortex of human and non-human primates,” *Neuropsychologia*, vol. 44, no. 13, pp. 2647–2667, 2006.

[246] G. F. Striedter, “Brain homology and function: An uneasy alliance,” in *Brain Research Bulletin*, 2002, vol. 57, no. 3–4, pp. 239–242.

[247] J. Sallet, R. B. Mars, M. P. Noonan, F.-X. Neubert, S. Jbabdi, J. X. O’Reilly, N. Filippini, A. G. Thomas, and M. F. Rushworth, “The organization of dorsal frontal cortex in humans and macaques.,” *J. Neurosci.*, vol. 33, no. 30, pp. 12255–74, 2013.

[248] R. M. Hutchison and J. P. Gallivan, “Functional coupling between frontoparietal and occipitotemporal pathways during action and perception,” *Cortex*, pp. 1–20, 2016.